Electronic Supplementary Material (ESI) for Chemical Communications.

Supporting Information

Reduction chemistry yields stable and soluble divalent lanthanide tris(pyrazolyl)borate complexes

Tajrian Chowdhury,[a] Matthew J. Evans,[b] Martyn P. Coles,[b] Anna G. Bailey,[a] William J. Peveler,[a] Claire Wilson,[a] and Joy H. Farnaby*[a]

[a] School of Chemistry, Joseph Black Building, University of Glasgow, Glasgow, G12 8QQ, UK.
[b] School of Chemical and Physical Sciences, Victoria University of Wellington, PO Box 600, Wellington 6140, New Zealand.

* Corresponding author: Joy.Farnaby@glasgow.ac.uk.

Contents

Experimental

General Experimental Considerations

All air-sensitive manipulations were carried out in an MBraun glovebox (O_2 <0.1 ppm and H_2O <0.1 ppm) or by using standard Schlenk techniques under N_2. All glassware was dried at 130-135 °C overnight, in a Binder ED53 Drying Oven/Hot Air Steriliser, prior to use. Filter cannulas were prepared using Whatman 25 mm glass microfiber filters and were pre-dried at 130-135 °C overnight. An Innovative Technology Inc. Pure Solv 400-5-MD solvent purification system (activated alumina columns) was used to obtain anhydrous toluene, tetrahydrofuran (THF), and acetonitrile (MeCN). Anhydrous hexane (95%) and 1,2-dimethoxyethane (DME, 99.5%) were purchased from Merck. Anhydrous solvents were degassed, sparged with N_2, and stored in ampoules over activated 3.0 Å molecular sieves (25-35% weight by volume) under N_2. Absence of water/levels of residual water in bulk solvents were confirmed by using a sodium benzophenone ketyl solution in THF after 24-48 hours. Deuterated benzene (d_6-benzene) was dried by directly transferring from sealed glass ampoules onto activated 3.0 Å molecular sieves and stored in ampoules in a N_2 atmosphere glovebox. Absence of water was confirmed by ^{1}H NMR after 48 hours. High purity potassium (99.95% metal basis) was obtained in break seal ampoules from Alfa Aesar and stored/handled in a N_2 atmosphere glovebox. Graphite powder (<20 μM synthetic grade) was obtained from Merck and degassed at 150 °C *in vacuo*, prior to use. KC_8 was prepared by reacting 8 equivalents of degassed graphite powder with an equivalent of high purity K by heating with heat gun in a Schlenk flask under static vacuum. Potassium hydrotris(1-pyrazolyl)borate K(Tp), lanthanide triflates $Ln(OTf)_3$ and $[Ln(Tp)_2(OTf)]$ (Ln = Y, Eu, Yb) were synthesised according to literature procedures.[1] The Al(I) reducing agent $[\{K[Al(NON^{Dipp})]\}_2]$ (NON^{Dipp} = $\{O(SiMe_2N(2,6\text{-}^iPr_2\text{-}C_6H_3))_2\}^{2-}$) was obtained in collaboration with the Coles research group, where it was synthesised according to literature procedures.[2] The following starting materials were purchased from Merck: triphenylphosphine oxide, 18-crown-6 and 2.2.2-cryptand (4,7,13,16,21,24-hexaoxa-1,10-diazabicyclo[8.8.8]hexacosane) and dried under vacuum prior to use.

Physical Methods

NMR data were recorded on an AVIII 400 MHz spectrometer operating at frequencies 400.1 MHz (^{1}H), 100.6 MHz (^{13}C{^{1}H}), 376.5 MHz (^{19}F), 162.0 MHz (^{31}P), 128.4 MHz (^{11}B and ^{11}B{^{1}H}). The NMR data were referenced internally to the appropriate residual proteo-solvent and reported relative to tetramethylsilane (δ = 0 ppm) for ^{1}H and ^{13}C{^{1}H} NMR. ^{19}F NMR data were reported relative to $CFCl_3$ (δ = 0 ppm), ^{31}P NMR data were reported relative to 85% H_3PO_4 in aqueous solution (δ = 0 ppm), and ^{11}B and ^{11}B{^{1}H} NMR data were reported relative to 15% BF_3•OEt_2 in $CDCl_3$ (δ = 0 ppm). All spectra were recorded at a constant temperature of 25 °C (298 K). Coupling constants (*J*) are reported in hertz (Hz). Standard abbreviations for multiplicity were used as follows: m = multiplet, t = triplet, d = doublet, s = singlet. For broad intensities, abbreviated as br, the full width at half-maximum intensity (FWHM) is provided in Hz. UV/vis/NIR absorption spectra and excitation-

emission spectral matrices (EEM) were collected using a Horiba Duetta Bio fluorimeter in anhydrous solvents (acetonitrile, toluene, hexane), which were filtered through Celite® prior to use. The Duetta instrument uses monochromated emission from a 75 W Xe arc lamp as the excitation source and diffractive optics with a Si charge coupled device (CCD) spectrograph to collect emitted light between 250 and 1100 nm simultaneously. The UV/vis/NIR absorption and EEM data were collected at ambient temperature in 1 cm path-length cuvettes, fitted with either a screw-cap containing a silicone gasket or J. Young's (JY) Teflon seal (see **Section B S3** for details of protocol of sample preparation, data procurement, cuvette cleaning, checking cuvettes for cross-contamination). ATR-IR spectra were collected in air at ambient temperature using ThermoFisher Scientific Nicolet Summit LITE FTIR Spectrometer (containing a $LiTaO_3$ detector) equipped with Everest ATR. Abbreviations for the intensity of stretching frequencies were used as follows: s = strong, m = medium, w = weak. Single-crystal X-ray diffraction data were collected at 150 K using Mo-K_α radiation (λ = 0.71073 Å) on a Bruker D8 VENTURE diffractometer equipped with a Photon II CPAD detector, with Oxford Cryosystems n-Helix device mounted on an IμS 3.0 (dual Cu and Mo) microfocus sealed tube generator. CCDC numbers 2161063-2161071 and 2195976 contain the crystallographic information for this paper. Elemental analyses were performed by Orla McCullough at the London Metropolitan University, using a Flash 2000 Organic Elemental Analyzer, Thermo Scientific analyser. The samples for the measurements were prepared using V_2O_5 (to ensure complete combustion of all complexes) in tin capsules inside an inert argon glovebox atmosphere.

A. Synthesis of complexes 1-Ln and 1-Ln$(OPPh_3)_2$

S I Reduction chemistry of $[Eu(Tp)_2(OTf)]$ and synthesis of $[\{Eu(Tp)_2\}_2]$ 1-Eu

S I a NMR-scale reaction between $[Eu(Tp)_2(OTf)]$ with $[\{K[Al(NON^{Dipp})]\}_2]$

The white powder of $[Eu(Tp)_2(OTf)]$ (2.7 mg, 3.30 μmol, 1.0 eq) was weighed into a JY NMR tube and then a yellow d_6-benzene solution (0.15 mL) of $[\{K[Al(NON^{Dipp})]\}_2]$ (1.8 mg, 1.60 μmol, 0.5 eq) was added to it by pipette and the resultant yellow suspension was analysed *via* multinuclear NMR. The data were consistent with immediate consumption of $[Eu(Tp)_2(OTf)]$ and $[\{K[Al(NON^{Dipp})]\}_2]$ and the formation of the paramagnetic $4f^7$ Eu(II) ion (see **Figures S 32** to **S 34**).

S I b Synthesis of $[\{Eu(Tp)_2\}_2]$ 1-Eu by reaction of $[Eu(Tp)_2(OTf)]$ with KC_8

In the glovebox, a 20 mL scintillation vial was charged with a stirrer bar, and then the white powder $[Eu(Tp)_2(OTf)]$ (70.1 mg, 0.096 mmol, 1.0 eq) was added and suspended in toluene (8 mL) with stirring. To this suspension, the bronze powder KC_8 (40.8 mg, 0.302 mmol, 3.1 eq) was added by a spatula in small portions over two minutes, with stirring at ambient temperature. The resultant yellow and bronze suspension was stirred at ambient temperature for 3.25 h, after which the brown suspension was filtered across a frit into a Büchner flask, to exclude excess KC_8, graphite and K(OTf). The residue on the frit was further extracted using toluene (3 x 1 mL) and filtered. Toluene (11 mL) was removed *in vacuo* from the combined orange-yellow filtrate, to yield an orange-yellow

oil. Hexane (1 mL) was added to precipitate neon-yellow solids and all solvents removed *in vacuo*. The resultant neon-yellow powder (**Figure 1(a)**) was dried *in vacuo* (10^{-2} mbar, 1.5 h) yielding [{Eu(Tp)$_2$}$_2$] **1-Eu** (52.5 mg, 0.045 mmol, 94%). Tablet-shaped yellow single-crystals of **1-Eu** (**Figure 1(c)**) suitable for X-ray diffraction were grown from a saturated toluene solution with a hexane antisolvent at -35 °C over several weeks. Yellow block-like single-crystals of **1-Eu(THF)$_2$** suitable for X-ray diffraction were grown from a saturated THF:hexane (1:2) solution with a hexane antisolvent at -35 °C overnight. Structures with and without lattice solvent were obtained for **1-Eu(THF)$_2$**, under these crystallisation conditions. **1-Eu** is paramagnetic ($4f^7$) and no resonances were observed by ^{1}H or ^{11}B NMR spectroscopy; Evans' Method (d_6-benzene) magnetic moment (μ_{eff}): 7.62-7.78 μ_B (see **Table 1** below) The magnetic moment was calculated per Eu metal centre, using the molecular weight of half of **1-Eu**. Anal. Calcd. for $C_{36}H_{40}B_4N_{24}Eu_2$: C, 37.40%; H, 3.49%; N, 29.08%. Found: C, 37.56-37.62%; H, 3.55-3.57%; N, 27.16-27.44%. IR (ATR): 3130 (w, $\upsilon_{sp^2\text{-}CH}$), 2456 (w, υ_{BH}), 2412 (w, υ_{BH}), 2379 (w, υ_{BH}), 1728 (w), 1631 (w), 1502 (m, $\upsilon_{C=C}$), 1401 (m), 1382 (m), 1291 (m), 1212 (m), 1113 (s), 1041 (s), 972 (m), 750 (s), 721 (s), 666 (m), 619 (s), 455 (w) cm^{-1}. λ_{max} MeCN (0.26 mM)/nm (ε/M^{-1}cm^{-1}): 269 (2394), 298 (2564), 333 (1862), 401 (1138), 465 (579). λ_{max} toluene (0.18 mM)/nm (ε/M^{-1}cm^{-1}): 290 (1449), 395 (3191). λ_{max} hexane (0.18 mM)/nm (ε/M^{-1}cm^{-1}): 398 (3668). The concentrations for UV-vis spectroscopy and therefore the ε values were calculated using the dimeric molecular weight for **1-Eu**.

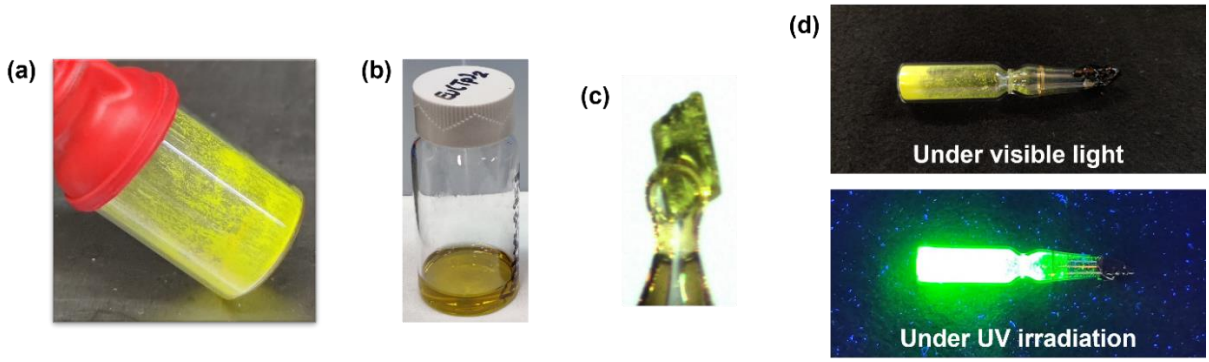

Figure 1. (a) Neon-yellow solid of **1-Eu** obtained after synthesis. (b) Toluene solution of **1-Eu**. (c) Single-crystal of **1-Eu**. (d) Bright photoluminescence of a solid sample of **1-Eu** under UV irradiation.

Table 1. Corrected magnetic moment data for [{Eu(Tp)$_2$}$_2$] **1-Eu**. Measurements were obtained in d_6-benzene at ambient temperature and magnetic moments calculated according to Evans' Method.[3]

Complex	Concentration of solution of the compound in d_6-benzene (moldm^{-3} or M)	Average shift in d_6-benzene resonance of solution relative to a sealed d_6-benzene capillary Δf (Hz)	Calculated Evans' Method magnetic moment μ_{eff} (μ_B)	Expected spin-only magnetic moment μ_{SO} (μ_B)
[{Eu(Tp)$_2$}$_2$] **1-Eu**	0.00760	304.1	7.62	7.94
	0.00683	280.1	7.72	
	0.00891	372.1	7.78	

S II Reduction chemistry of [Yb(Tp)$_2$(OTf)] and synthesis of [Yb(Tp)$_2$] 1-Yb

S II a Synthesis of [Yb(Tp)$_2$] 1-Yb by reduction of [Yb(Tp)$_2$(OTf)] using [{K[Al(NON^{Dipp})]}$_2$]

In the glovebox, a 20 mL scintillation vial was charged with a stirrer bar, and then the white powder [Yb(Tp)$_2$(OTf)] (106.5 mg, 0.142 mmol, 1.0 eq) was added and suspended in toluene (1.5 mL) with stirring. To this suspension, a toluene solution (0.5 mL) of the yellow powder [{K[Al(NON^{Dipp})]}$_2$] (78.3 mg, 0.071 mmol, 0.5 eq) was added, by pipette dropwise over two minutes, with stirring at ambient temperature. An immediate dark wine-red suspension was obtained, which was stirred at ambient temperature for 1.25 h, after which the suspension turned dark violet. The violet suspension was filtered across a frit into a Büchner flask, to exclude pale-yellow solids, predominantly K(OTf). The residue on the frit was further extracted using toluene (3 x 0.5 mL) and filtered. Toluene (3.5 mL) was removed *in vacuo* from the combined dark purple filtrate, to yield black-violet crystalline and gum-like solids, which were dried *in vacuo* (10^{-2} mbar, 1 h). These solids were washed with hexane (2 x 3 mL) at ambient temperature to remove by-products. The resultant dark-pink powder (**Figure 2(a)**) was dried *in vacuo* (10^{-2} mbar, 1 h) yielding [Yb(Tp)$_2$] **1-Yb** (50.8 mg, 0.085 mmol, 60%). Plate-shaped red single-crystals of **1-Yb** (**Figure 2(c)**) suitable for X-ray diffraction were grown from a saturated toluene solution with a hexane antisolvent at -35 °C over several weeks. Tablet-shaped red single-crystals of **1-Yb(THF)** suitable for X-ray diffraction were grown from a saturated THF solution with a hexane antisolvent at -35 °C over several weeks. ^{1}H NMR (d_6-benzene): δ 4.96 (very br m, FWHM = 278.3 Hz, Tp-B**H**) 5.97 (6H, t, $^3J_{H\text{-}H}$ = 2.0 Hz, Tp-C^4**H**) 7.42 (6H, d, $^3J_{H\text{-}H}$ = 1.8 Hz, Tp-C^3**H**) 7.67 (6H, dd, $^3J_{H\text{-}H}$ = 2.2 Hz, $^4J_{H\text{-}H}$ = 0.6 Hz, Tp-C^5**H**) ppm (see **Figure 2(d)** for numbering of the pyrazolyl carbon atoms of Tp ligand); ^{13}C{^{1}H} NMR (d_6-benzene): δ 104.61 (s, Tp-**C^4**) 136.46 (s, Tp-**C^5**) 140.57 (s, Tp-**C^3**) ppm; ^{11}B NMR (d_6-benzene): δ -1.85 (d, $^1J_{B\text{-}H}$ = 79.8 Hz, Tp-**B**) ppm; ^{11}B{^{1}H} NMR (d_6-benzene): δ -1.75 (s, Tp-**B**) ppm. Anal. Calcd. for $C_{18}H_{20}B_2N_{12}Yb$: C, 36.09%; H, 3.36%; N, 28.06%. Found: C, 36.05-36.84%; H, 3.30-3.39%; N, 25.31-25.84%. IR (ATR): 3141 (w, $\upsilon_{sp^2\text{-}CH}$), 2457 (w, υ_{BH}), 2417 (w, υ_{BH}), 2383 (w, υ_{BH}), 1737 (w), 1627 (w), 1500 (m, $\upsilon_{C=C}$), 1405 (m), 1388 (m), 1299 (m), 1208 (m), 1116 (s), 1045 (s), 971 (m), 749 (s), 717 (s), 662 (m), 628 (s), 477 (w) cm^{-1}. λ_{max} MeCN (0.42 mM)/nm (ε/M^{-1}cm^{-1}): 288 (1944), 337 (2180), 410 (877), 519 (1052). λ_{max} toluene (0.33 mM)/nm (ε/M^{-1}cm^{-1}): 341 (1708), 461 (682), 520 (1035). λ_{max} hexane (0.33 mM)/nm (ε/M^{-1}cm^{-1}): 339 (1927), 467 (908), 516 (1158).

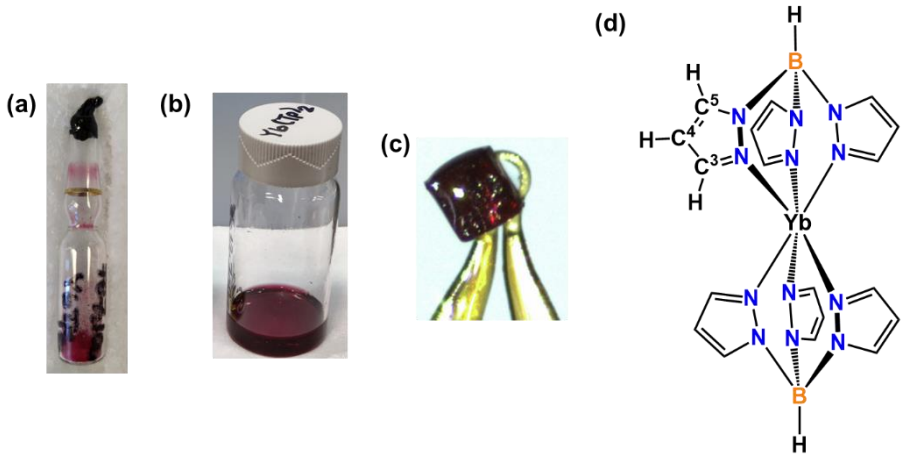

Figure 2. (a) Dark-pink solid of **1-Yb**. (b) Toluene solution of **1-Yb**. (c) Single-crystal of **1-Yb**. (d) Structural diagram of **1-Yb**, showing numbering of the pyrazolyl carbon atoms of Tp ligand.

S II b Synthesis of $[Yb(Tp)_2]$ 1-Yb by reaction of $[Yb(Tp)_2(OTf)]$ with KC_8

In the glovebox, a 20 mL scintillation vial was charged with a stirrer bar, and then the white powder $[Yb(Tp)_2(OTf)]$ (75.1 mg, 0.100 mmol, 1.0 eq) was added and suspended in toluene (8 mL) with stirring. To this suspension, the bronze powder KC_8 (38.5 mg, 0.285 mmol, 2.8 eq) was added by a spatula in small portions over two minutes, with stirring at ambient temperature. The resultant red and bronze suspension was stirred at ambient temperature for 20 h, after which the brown suspension was filtered across a frit into a Büchner flask, to exclude excess KC_8, graphite and K(OTf). The residue on the frit was further extracted using toluene (3 x 1.5 mL) and filtered. Toluene (12.5 mL) was removed *in vacuo* from the combined dark-pink filtrate, to yield a dark-pink oil. Hexane (1 mL) was added to precipitate dark-pink solids and all solvents removed *in vacuo*. The resultant dark-pink powder (**Figure 2(a)**) was dried *in vacuo* (10^{-2} mbar, 3.25 h) yielding $[Yb(Tp)_2]$ **1-Yb** (52.0 mg, 0.087 mmol, 87%).

S III Reaction of $[Ln(Tp)_2]$ 1-Ln (Ln = Eu, Yb) with two equivalents of Ph_3PO to synthesise the adduct complexes $[Ln(Tp)_2(OPPh_3)_2]$ 1-Ln$(OPPh_3)_2$ (Ln = Eu, Yb)

S III a Synthesis of $[Eu(Tp)_2(OPPh_3)_2]$ 1-Eu$(OPPh_3)_2$

In the glovebox, a 20 mL scintillation vial was charged with a stirrer bar, and then the neon-yellow powder $[\{Eu(Tp)_2\}_2]$ (15.6 mg, 0.014 mmol, 1.0 eq) was added and dissolved in toluene (1 mL) with stirring. To this solution, a colourless solution of Ph_3PO (15.2 mg, 0.055 mmol, 4.0 eq) in toluene (2 mL) was added by pipette dropwise over two minutes, with stirring at ambient temperature. The resultant orange solution was stirred at ambient temperature for 0.5 h after which toluene was removed *in vacuo*, yielding an orange oil. Hexane (0.5 mL) was added to precipitate pale orange solids and all solvents removed *in vacuo*. The resultant pale orange powder was dried *in vacuo* (10^{-2} mbar, 2.75 h) yielding $[Eu(Tp)_2(OPPh_3)_2]$ **1-Eu$(OPPh_3)_2$** (27.7 mg, 0.024 mmol, 91%). Tablet-shaped yellow single-crystals of **1-Eu$(OPPh_3)_2$** suitable for X-ray diffraction were grown from a saturated toluene solution with a hexane antisolvent at -35 °C over several weeks. **1-Eu$(OPPh_3)_2$** does not exhibit ^{1}H, ^{31}P or ^{11}B NMR. Evans' Method (d_6-benzene) magnetic moment (μ_{eff}): 7.19-7.46

μ_B (see **Table 2** below). Anal. Calcd. for $C_{54}H_{50}B_2N_{12}O_2P_2Eu$: C, 57.16%; H, 4.44%; N, 14.81%. Found: C, 58.99-59.33%; H, 4.67-4.77%; N, 13.20-13.48%. IR (ATR): 3056 (w, $\upsilon_{sp^2\text{-}CH}$), 2455 (w, υ_{BH}), 2409 (w, υ_{BH}), 2372 (w, υ_{BH}), 1590 (w), 1503 (m, $\upsilon_{C=C}$), 1434 (m), 1386 (m), 1300 (m), 1182 (s), 1117 (s, $\upsilon_{P=O}$), 1044 (s), 967 (m), 750 (s), 721 (s), 691 (s), 626 (s), 535 (s), 447 (m) cm^{-1}. λ_{max} MeCN (0.18 mM)/nm ($\varepsilon/M^{-1}cm^{-1}$): 265 (3254), 272 (2617), 298 (1196), 338 (904), 399 (676), 467 (378).

Table 2. Corrected magnetic moment data for $[Eu(Tp)_2(OPPh_3)_2]$ **1-Eu(OPPh$_3$)$_2$**. Measurements were obtained in d_6-benzene at ambient temperature and magnetic moments calculated according to Evans' Method.[3]

Complex	Concentration of solution of the compound in d_6-benzene ($moldm^{-3}$ or M)	Average shift in d_6-benzene resonance of solution relative to a sealed d_6-benzene capillary Δf (Hz)	Calculated Evans' Method magnetic moment μ_{eff} (μ_B)	Expected spin-only magnetic moment μ_{SO} (μ_B)
$[Eu(Tp)_2(OPPh_3)_2]$ **1-Eu(OPPh$_3$)$_2$**	0.00342	120.0	7.19	7.94
	0.00193	72.0	7.41	
	0.00222	84.0	7.46	

S III b Synthesis of $[Yb(Tp)_2(OPPh_3)_2]$ 1-Yb(OPPh$_3$)$_2$

In the glovebox, a 20 mL scintillation vial was charged with a stirrer bar, and then the dark-pink powder $[Yb(Tp)_2]$ (17.3 mg, 0.029 mmol, 1.0 eq) was added and dissolved in toluene (1 mL) with stirring. To this solution, a colourless solution of Ph_3PO (16.1 mg, 0.058 mmol, 2.0 eq) in toluene (2 mL) was added by pipette dropwise over two minutes, with stirring at ambient temperature. The resultant black-violet solution was stirred at ambient temperature for 0.5 h after which toluene was removed *in vacuo*, yielding a purple oil. Hexane (0.5 mL) was added to precipitate purple solids and all solvents removed *in vacuo*. The resultant purple powder was dried *in vacuo* (10^{-2} mbar, 2.5 h) yielding $[Yb(Tp)_2(OPPh_3)_2]$ **1-Yb(OPPh$_3$)$_2$** (29.0 mg, 0.025 mmol, 87%). Rod-shaped red single-crystals of **1-Yb(OPPh$_3$)$_2$** suitable for X-ray diffraction were grown from a saturated toluene solution with a hexane antisolvent at -35 °C over several days. ^{1}H NMR (d_6-benzene): δ 5.07 (very br m, FWHM = 234.8 Hz, Tp-B**H**) 5.87 (6H, t, $^3J_{H\text{-}H}$ = 1.9 Hz, Tp-C^4**H**) 6.92 (12H, td, $^3J_{H\text{-}H}$ = 7.5 Hz, $^4J_{H\text{-}H}$ = 2.6 Hz, *ortho*-Ph-C**H**) 7.02 (6H, td, $^3J_{H\text{-}H}$ = 7.4 Hz, $^4J_{H\text{-}H}$ = 1.0 Hz, *para*-Ph-C**H**) 7.24 (6H, d, $^3J_{H\text{-}H}$ = 1.6 Hz, Tp-C^3**H**) 7.49 (12H, dd, $^3J_{H\text{-}H}$ = 11.7 Hz, 7.7 Hz, *meta*-Ph-C**H**) 7.74 (6H, d, $^3J_{H\text{-}H}$ = 1.9 Hz, Tp-C^5**H**) ppm; ^{13}C{^{1}H} NMR (d_6-benzene): δ 103.83 (s, Tp-**C^4**) 128.62 (d, $^2J_{C\text{-}P}$ = 11.4 Hz, *ortho*-Ph-**C**H) 131.77 (s, *para*-Ph-**C**H) 132.43 (d, $^3J_{C\text{-}P}$ = 9.0 Hz, *meta*-Ph-**C**H) 134.94 (s, Tp-**C^5**) 140.60 (s, Tp-**C^3**) ppm (Note: The *ipso*-Ph-**C** resonance could not be observed); ^{31}P NMR (d_6-benzene): δ 27.63 (s, FWHM = 17.9 Hz, Ph_3**P**O) ppm; ^{11}B NMR (d_6-benzene): δ -1.84 (d, $^1J_{B\text{-}H}$ = 78.4 Hz, Tp-**B**) ppm; ^{11}B{^{1}H} NMR (d_6-benzene): δ -1.75 (s, Tp-**B**) ppm. Anal. Calcd. for $C_{54}H_{50}B_2N_{12}O_2P_2Yb$: C, 56.12%; H, 4.36%; N, 14.54%. Found: C, 56.52-56.81%; H, 4.61-4.62%; N, 13.86-13.90%. IR (ATR): 3054 (w, $\upsilon_{sp^2\text{-}CH}$), 2454 (w, υ_{BH}), 2403 (w, υ_{BH}), 2372 (w, υ_{BH}), 1589 (w), 1503 (m, $\upsilon_{C=C}$), 1438 (m), 1382

(m), 1300 (m), 1180 (s), 1116 (s, $\upsilon_{P=O}$), 1045 (s), 974 (m), 754 (s), 720 (s), 694 (s), 622 (s), 537 (s), 449 (m) cm^{-1}. λ_{max} MeCN (0.11 mM)/nm ($\varepsilon/M^{-1}cm^{-1}$): 265 (5312), 271 (4331), 299 (1636), 341 (2118), 411 (1071), 517 (1099).

S IV NMR-scale reaction of [Yb(Tp)$_2$] 1-Yb with one equivalent of Ph$_3$PO

The dark-pink powder [Yb(Tp)$_2$] (10.2 mg, 17.0 μmol, 1.0 eq) was weighed into a JY NMR tube and dissolved in d_6-benzene solution (0.10 mL) to give a dark pink solution. To this, a colourless solution of Ph_3PO (5.1 mg, 18.3 μmol, 1.1 eq) in d_6-benzene (0.05 mL) was added by pipette and the resultant purple solution was analysed *via* multinuclear NMR. ^{1}H NMR (d_6-benzene): δ5.10 (very br m, FWHM = 226.5 Hz, Tp-B**H**) 5.86 (6H, t, $^3J_{H-H}$ = 1.9 Hz, Tp-C^4**H**) 6.88 (6H, td, $^3J_{H-H}$ = 7.3 Hz, $^4J_{H-H}$ = 2.3 Hz, *ortho*-Ph-C**H**) 7.01 (3H, t, $^3J_{H-H}$ = 7.2 Hz, *para*-Ph-C**H**) 7.24 (6H, d, $^3J_{H-H}$ = 1.4 Hz, Tp-C^3**H**) 7.36 (6H, dd, $^3J_{H-H}$ = 11.4 Hz, 7.9 Hz, *meta*-Ph-C**H**) 7.74 (6H, d, $^3J_{H-H}$ = 1.7 Hz, Tp-C^5**H**) ppm; ^{13}C{^{1}H} NMR (d_6-benzene): δ 103.81 (s, Tp-**C^4**) 128.66 (d, $^2J_{C-P}$ = 12.2 Hz, *ortho*-Ph-**C**H) 131.89 (d, $^4J_{C-P}$ = 2.6 Hz, *para*-Ph-**C**H) 132.40 (d, $^3J_{C-P}$ = 10.1 Hz, *meta*-Ph-**C**H) 135.52 (d, $^1J_{C-P}$ = 105.2 Hz, *ipso*-Ph-**C**) 134.90 (s, Tp-**C^5**) 140.60 (s, Tp-**C^3**) ppm; ^{31}P NMR (d_6-benzene): δ29.01 (s, FWHM = 42.5 Hz, Ph_3**P**O) ppm; ^{11}B NMR (d_6-benzene): δ-1.69 (s, Tp-**B**) ppm; ^{11}B{^{1}H} NMR (d_6-benzene): δ-1.85 (s, Tp-**B**) ppm.

S V Isolation of [Y(Tp)$_2$(μ-OTf)$_2$K(18-crown-6)] 2-Y from the reaction of [Y(Tp)$_2$(OTf)] with [{K[Al(NON^{Dipp})]}$_2$]

In the glovebox, a 20 mL scintillation vial was charged with a stirrer bar, and then the white powder [Y(Tp)$_2$(OTf)•(toluene)$_{0.04}$] (105.4 mg, 0.16 mmol, 1.0 eq) was added and suspended in toluene (1.5 mL) with stirring. A colourless toluene solution (2.0 mL) of 18-crown-6 (41.6 mg, 0.16 mmol, 1.0 eq) was added by pipette to the yellow powder [{K[Al(NON^{Dipp})]}$_2$] (173.5 mg, 0.16 mmol, 1.0 eq) in a separate 20 mL scintillation vial. This resultant yellow solution was added to the toluene suspension of [Y(Tp)$_2$(OTf)], by pipette dropwise over two minutes, with stirring at ambient temperature. This resulted in a yellow suspension, which was stirred at ambient temperature for two hours after which the suspension became paler yellow and was filtered across a frit into a Büchner funnel to exclude white solids. The white residue on the frit was further extracted using toluene (0.5 mL) and filtered. Toluene (4 mL) was removed *in vacuo* from the combined yellow filtrate, to yield a yellow oily/glassy solid. Hexane (1.5 mL) was added to precipitate pale yellow solids, which were then washed with hexane (3 x 10 mL), until the deep yellow washings were very pale, in order to remove by-products. Then volatiles were removed *in vacuo*, and the beige solids yield were dried *in vacuo* (10^{-2} mbar, 7.5 h, crude yield 51.4 mg). Yellow block-like single-crystals of [Y(Tp)$_2$(μ-OTf)$_2$K(18-crown-6)] **2-Y** suitable for X-ray diffraction were grown from a saturated toluene solution with a hexane antisolvent at -35 °C overnight. The crystals were isolated by washing with cold (-35 °C) hexane (1 mL) and drying *in vacuo* (10^{-2} mbar, 4 h) yielding white crystals of [Y(Tp)$_2$(μ-OTf)$_2$K(18-crown-6)] **2-Y** (8.0 mg, 3.19 μmol, 2%). ^{1}H NMR (d_6-benzene): δ 3.12 (24H, s, 18-crown-6-C**H**$_2$) 4.59 (very br m, FWHM = 305.6 Hz, Tp-B**H**) 5.86 (6H, t, $^3J_{H-H}$ = 1.9 Hz, Tp-C^4**H**) 7.53 (6H, d, $^3J_{H-H}$ = 2.0 Hz, Tp-C^5**H**) 7.61 (6H,

br s, FWHM = 5.4 Hz, Tp-C^{3}**H**) ppm; ^{13}C{^{1}H} NMR (d_6-benzene): δ 69.95 (18-crown-6-**C**H$_2$) 104.02 (Tp-**C^{4}**) 134.81 (Tp-**C^{5}**) 143.49 (Tp-**C^{3}**) ppm; ^{19}F NMR (d_6-benzene): δ -78.08 (s, OTf-C**F**$_3$) ppm; ^{11}B NMR (d_6-benzene): δ -2.53 (apparent d, Tp-**B**) ppm; ^{11}B{^{1}H} NMR (d_6-benzene): δ -2.72 (s, Tp-**B**) ppm. Anal. Calcd. for $C_{32}H_{44}B_2F_6KN_{12}O_{12}S_2Y\bullet(C_7H_8)_{1.5}$: C, 40.68%; H, 4.50%; N, 13.40%. Found: C, 36.75-36.93%; H, 4.01-4.09%; N, 12.96-13.06%. IR (ATR): 2958 (w, $\upsilon_{sp^3\text{-}CH}$), 2891 (w, $\upsilon_{sp^3\text{-}CH}$), 2464 (w, υ_{BH}), 2361 (w, υ_{BH}), 2338 (w, υ_{BH}), 1503 (w, $\upsilon_{C=C}$), 1407 (w), 1353 (w), 1299 (s), 1251 (s), 1219 (s), 1177 (m), 1162 (m), 1107 (s), 1034 (s), 979 (m), 964 (m), 839 (w), 765 (s), 720 (s), 665 (m) cm^{-1}.

S VI Isolation of single-crystals of 1-Yb(DME)

On one occasion a reaction between [Yb(Tp)$_2$(OTf)] and a chunk of high purity K metal under conditions analogous to **SII b**, yielded tablet-shaped red single-crystals of **1-Yb(DME)** co-crystallised with K(OTf), suitable for X-ray diffraction, which were grown from a saturated DME solution with a hexane antisolvent at -35 °C over several weeks.

S VII Isolation of single-crystals of the separated ion pair of [{K[Al(NON^{Dipp})]}$_2$], [K(2.2.2-cryptand)][Al(NON^{Dipp})]

Yellow block-like single-crystals of [K(2.2.2-cryptand)][Al(NON^{Dipp})] suitable for X-ray diffraction were grown from a saturated yellow d_6-benzene solution (0.15 mL) containing [{K[Al(NON^{Dipp})]}$_2$] (2.8 mg, 2.56 μmol, 1.0 eq) and 2.2.2-cryptand (1.8 mg, 4.78 μmol, 1.9 eq) under a N_2 atmosphere at ambient temperature in a JY NMR tube.

B. Spectroscopic Data for Complexes 1-Ln, 1-Ln(OPPh$_3$)$_n$, and 2-Y

S1 Nuclear magnetic resonance (NMR) data

S1.1 [Yb(Tp)$_2$] 1-Yb

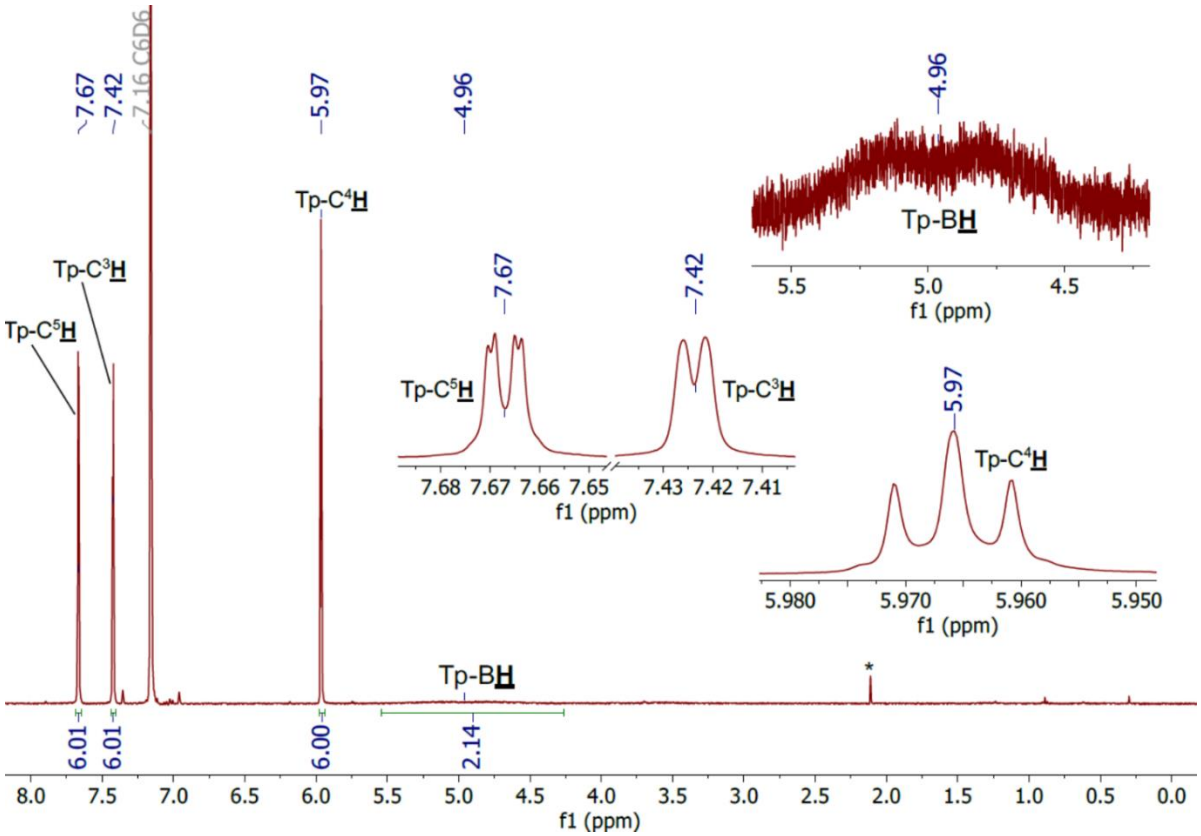

Figure S 1. ^{1}H NMR spectrum of [Yb(Tp)$_2$] **1-Yb**, recorded in d_6-benzene. Toluene is denoted by *.

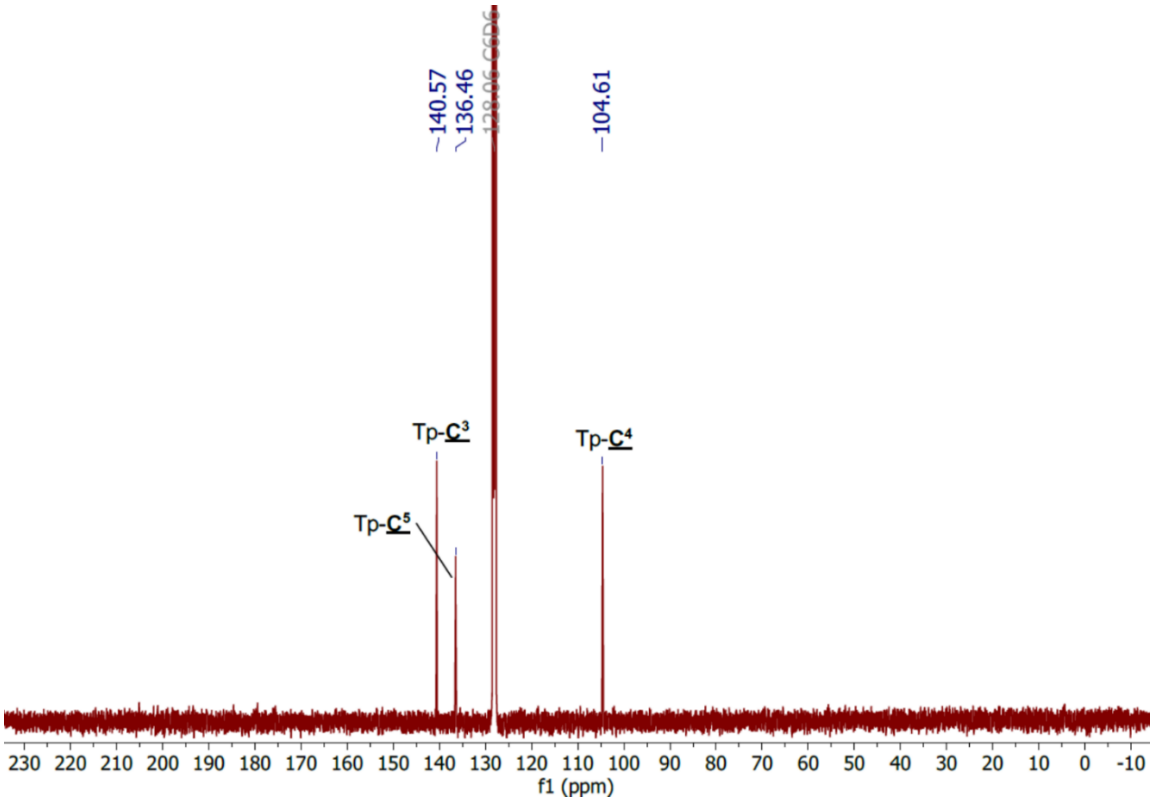

Figure S 2. ^{13}C{^{1}H} NMR spectrum of [Yb(Tp)$_2$] **1-Yb**, recorded in d_6-benzene.

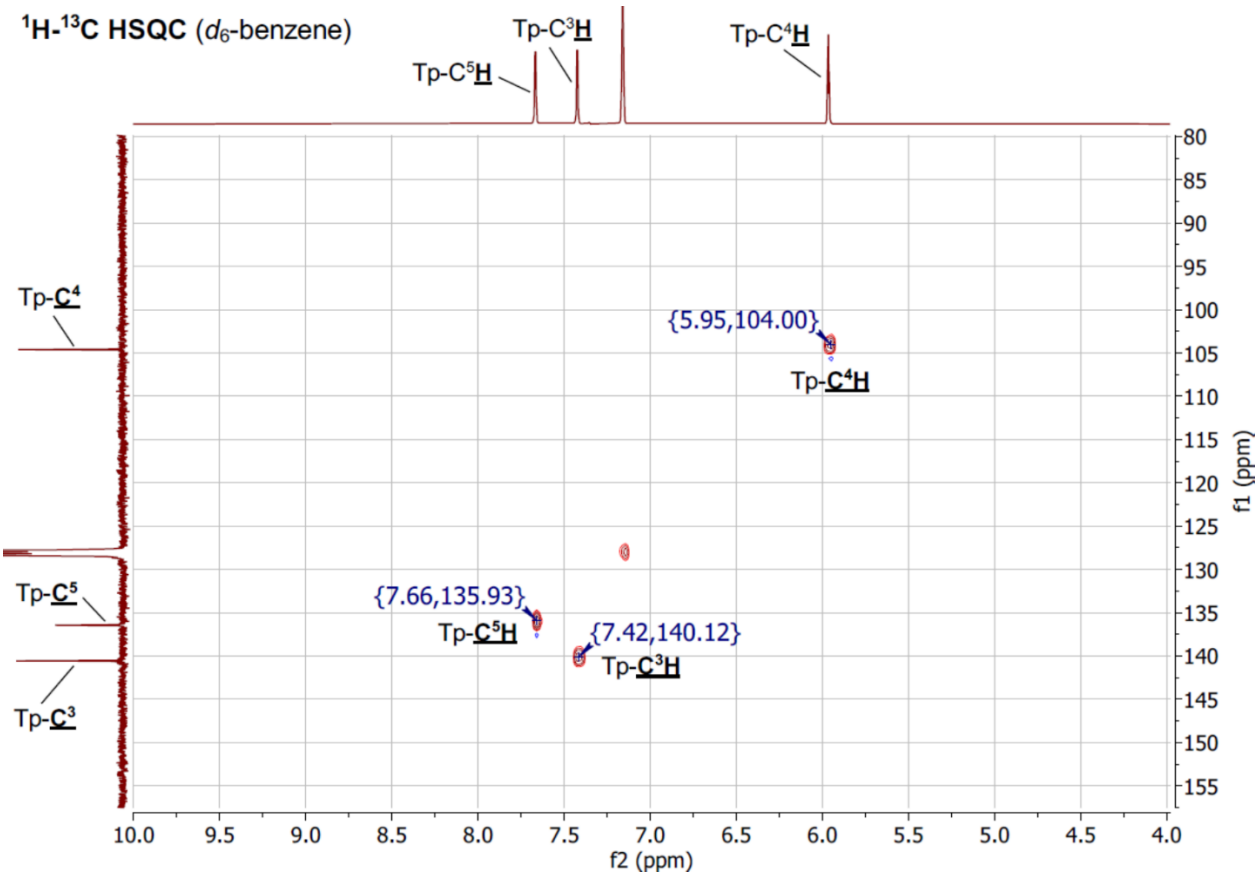

Figure S 3. ^{1}H-^{13}C HSQC NMR spectrum of [Yb(Tp)$_2$] **1-Yb**, recorded in d_6-benzene.

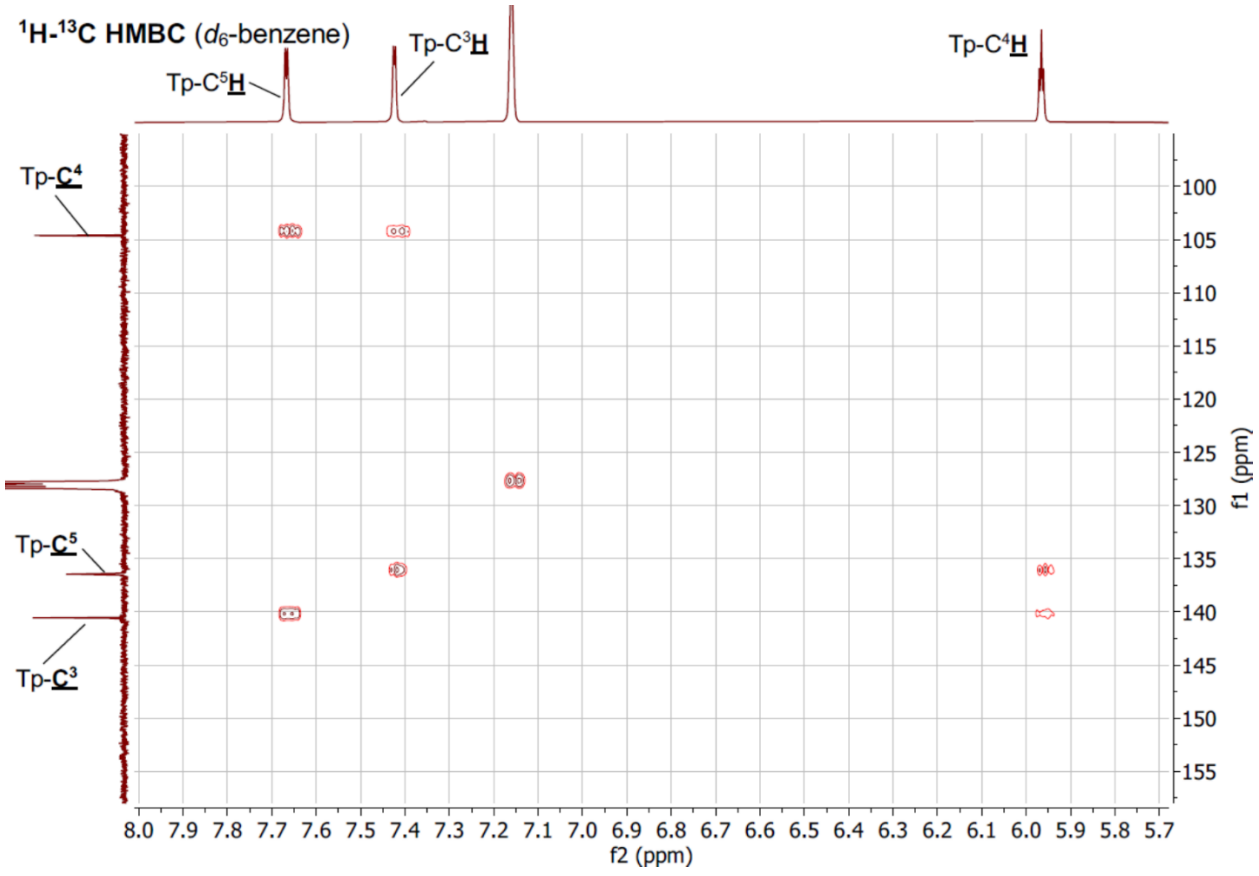

Figure S 4. ^{1}H-^{13}C HMBC NMR spectrum of [Yb(Tp)$_2$] **1-Yb**, recorded in d_6-benzene.

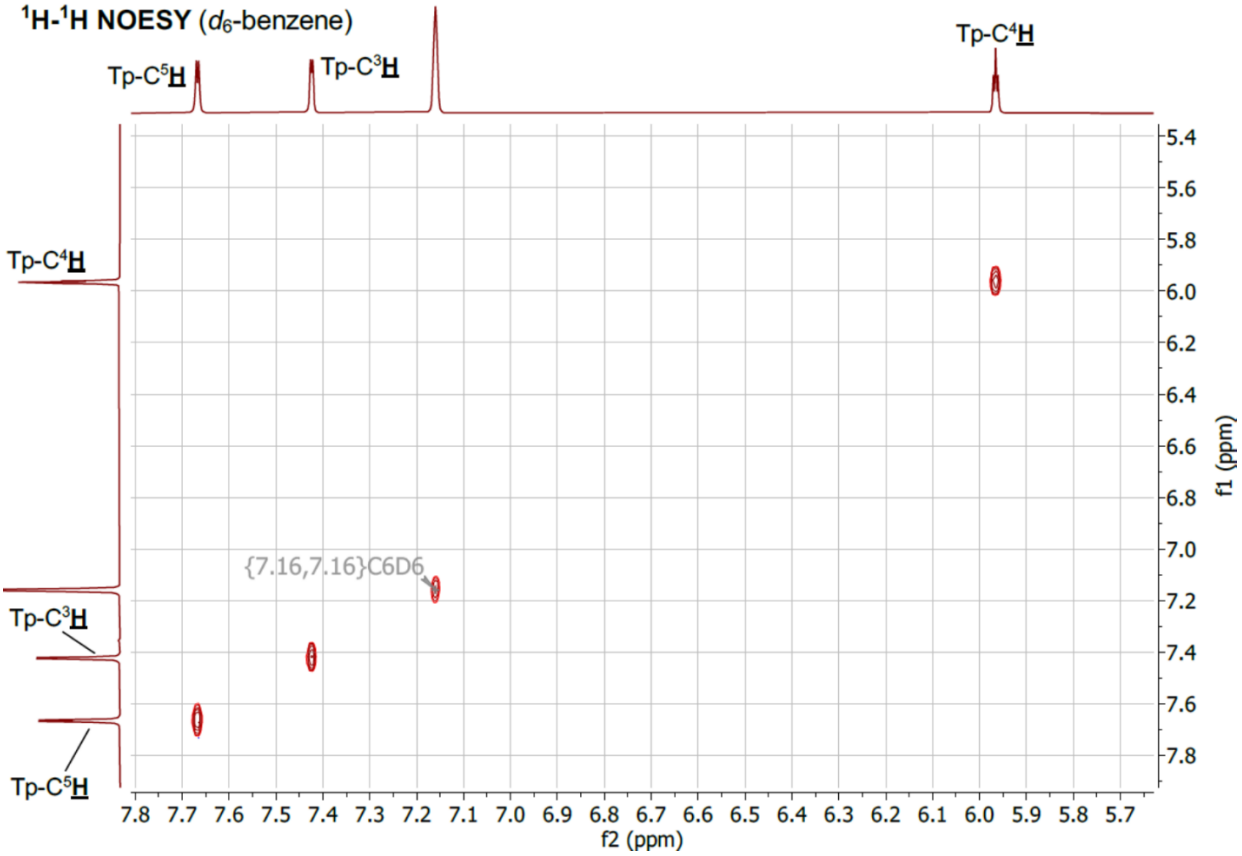

Figure S 5. ^{1}H-^{1}H NOESY NMR spectrum of [Yb(Tp)$_2$] **1-Yb**, recorded in d_6-benzene.

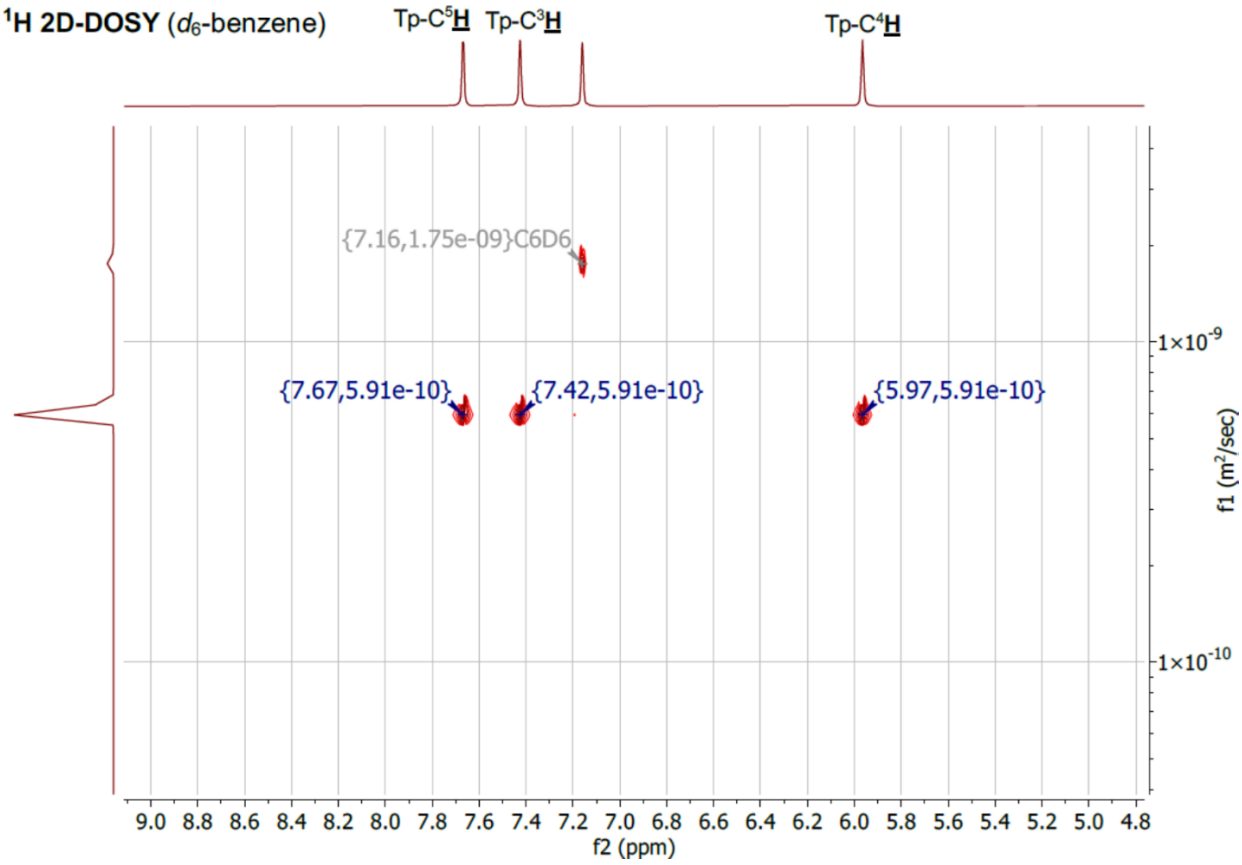

Figure S 6. ^{1}H 2D-DOSY NMR spectrum of [Yb(Tp)$_2$] **1-Yb**, recorded in d_6-benzene. The horizontal scale shows ^{1}H chemical shifts (ppm) and the vertical dimension the diffusion scale (m^2s^{-1}) with diffusion cross-peaks for **1-Yb** centred at 5.91 x 10^{-10} m^2s^{-1}.

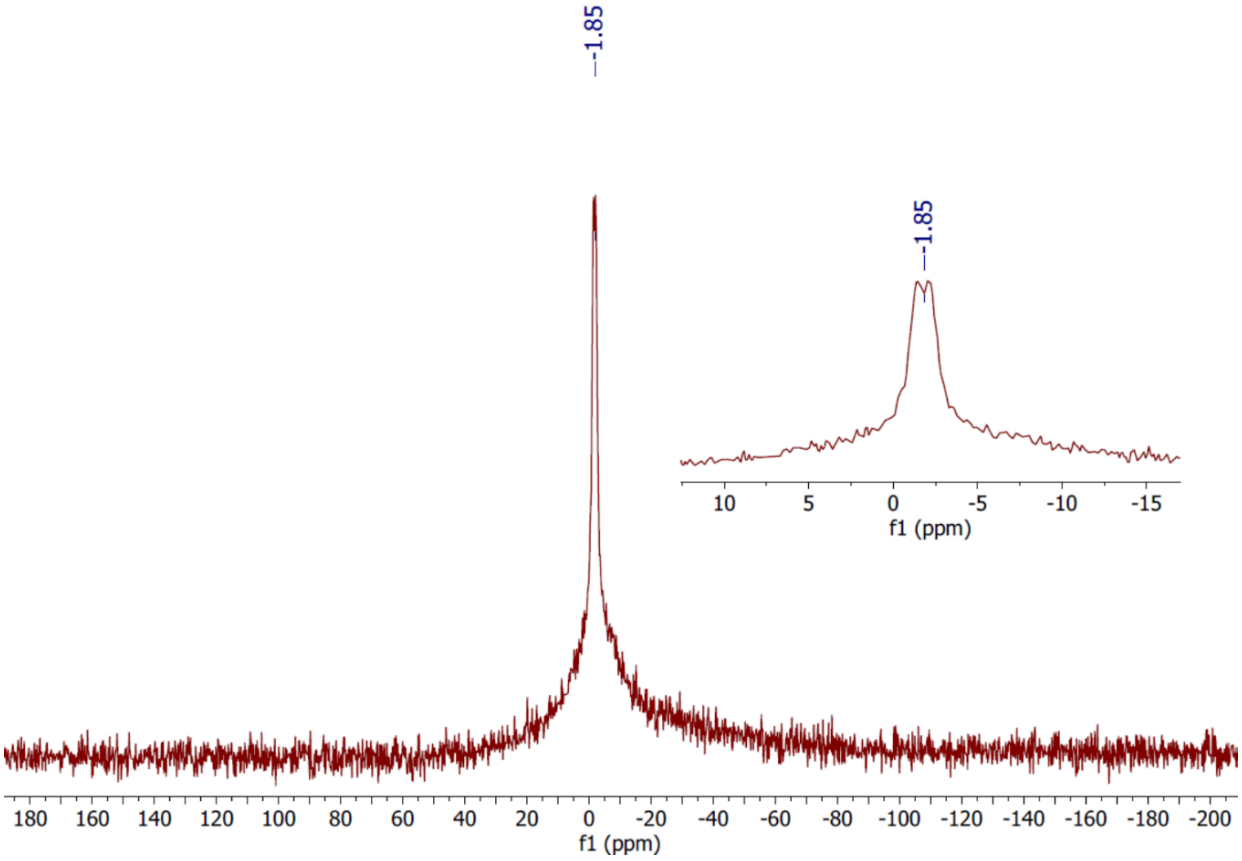

Figure S 7. ^{11}B NMR spectrum of [Yb(Tp)$_2$] **1-Yb**, recorded in d_6-benzene.

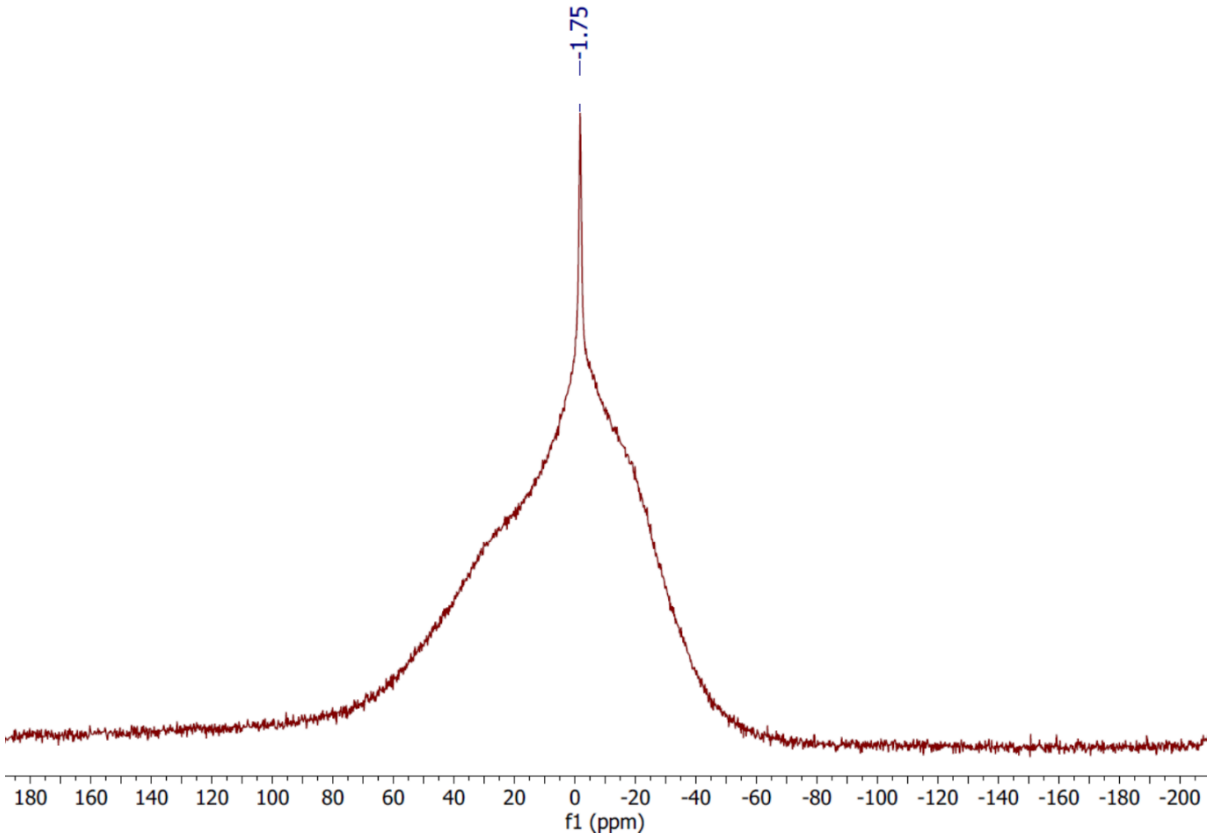

Figure S 8. ^{11}B{^{1}H} NMR spectrum of [Yb(Tp)$_2$] **1-Yb**, recorded in d_6-benzene.

S1.2 [Yb(Tp)$_2$(OPPh$_3$)$_2$] 1-Yb(OPPh$_3$)$_2$

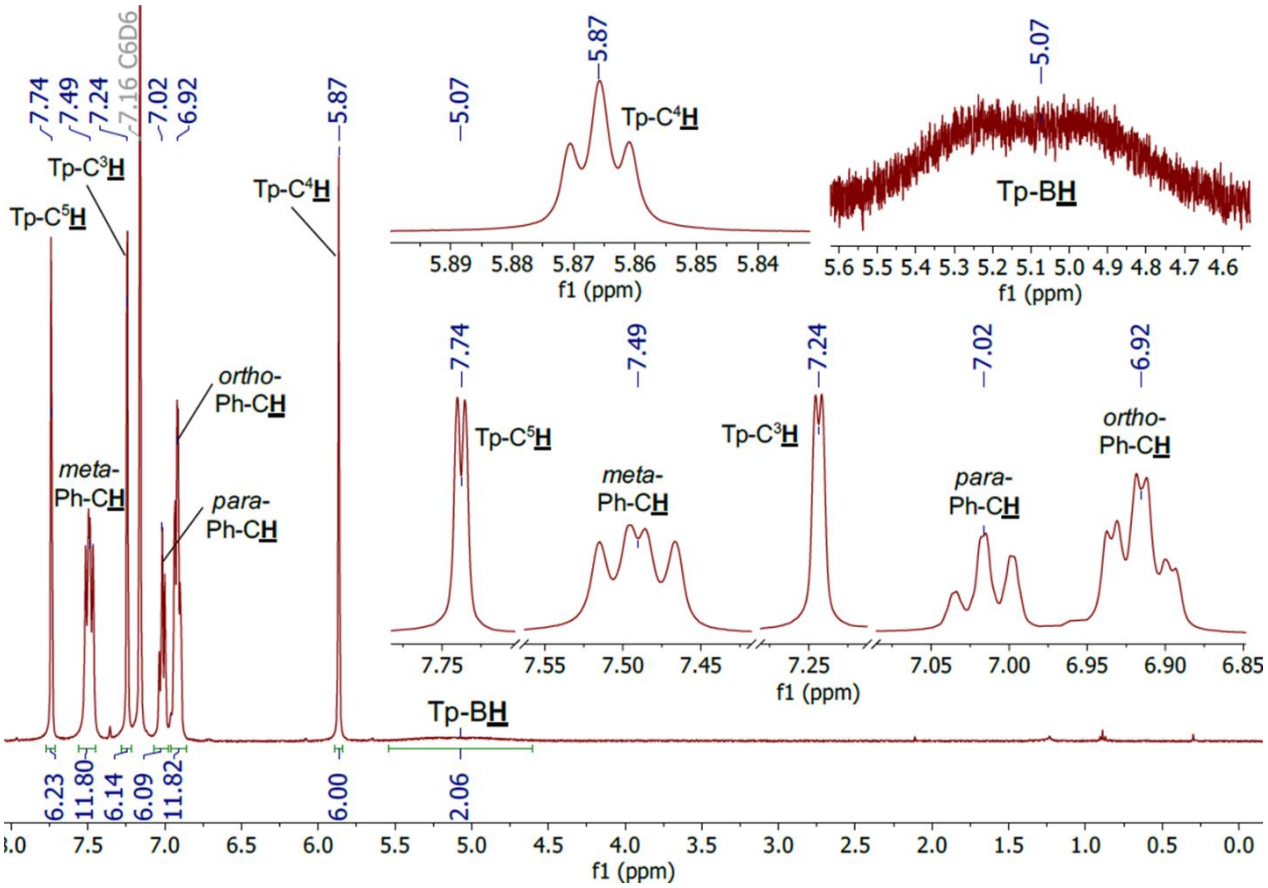

Figure S 9. ^{1}H NMR spectrum of [Yb(Tp)$_2$(OPPh$_3$)$_2$] **1-Yb(OPPh$_3$)$_2$**, recorded in d_6-benzene.

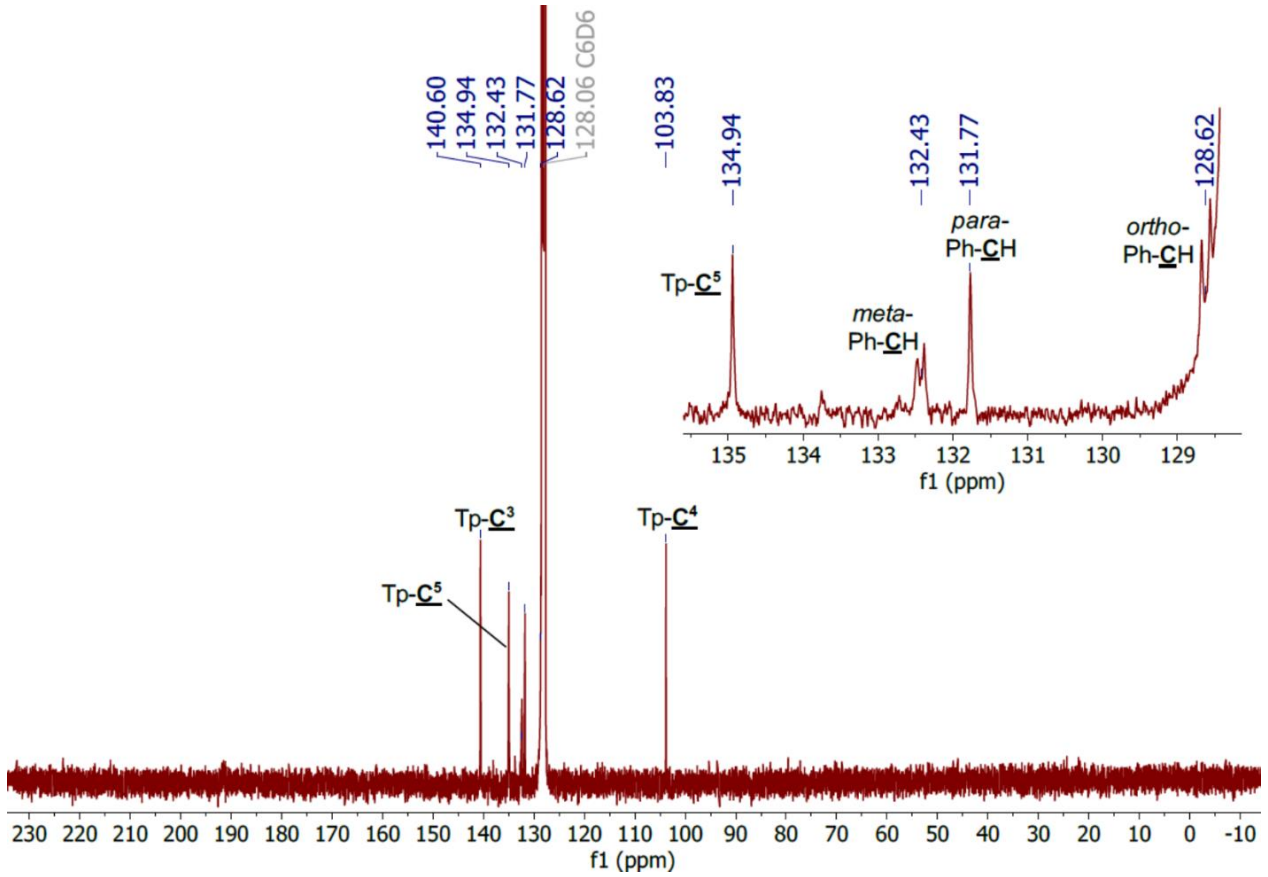

Figure S 10. ^{13}C{^{1}H} NMR spectrum of [Yb(Tp)$_2$(OPPh$_3$)$_2$] **1-Yb(OPPh$_3$)$_2$**, recorded in d_6-benzene.

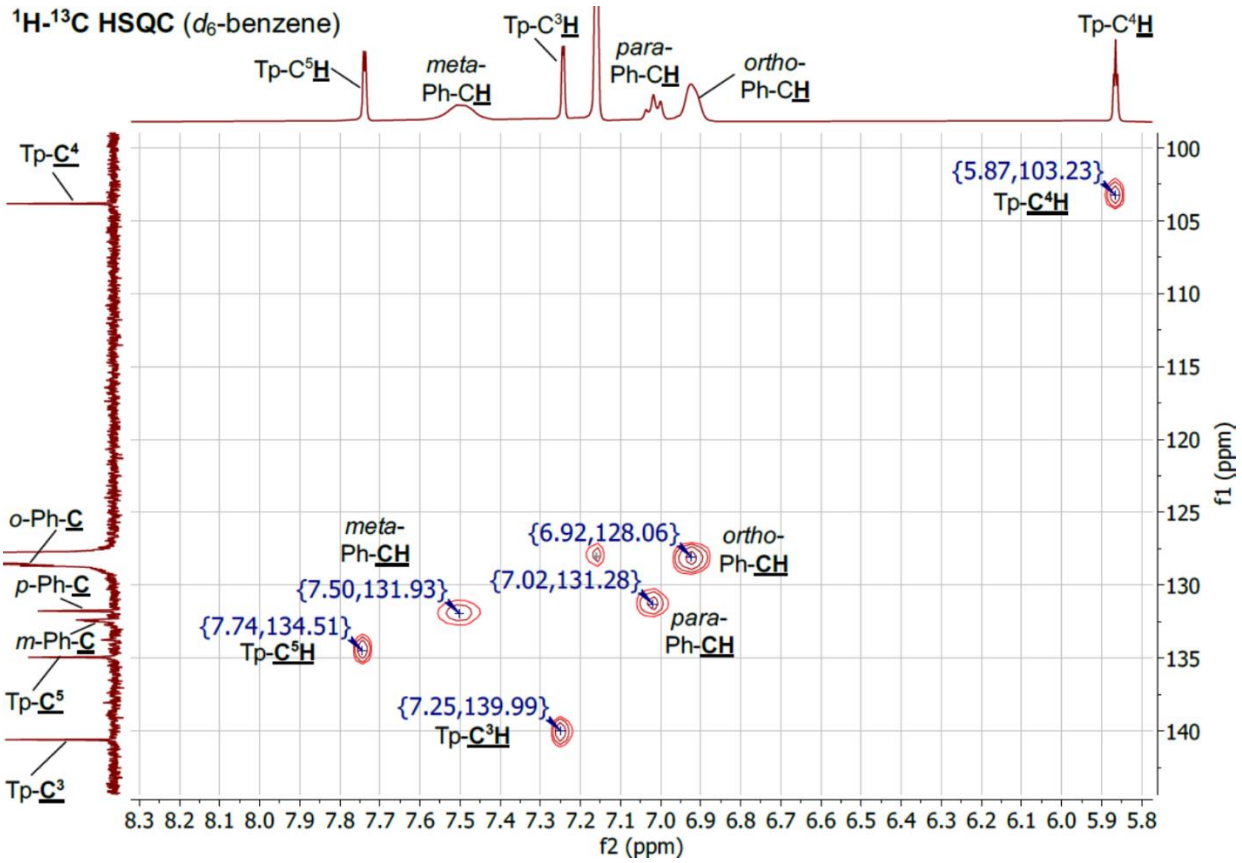

Figure S 11. ^{1}H-^{13}C HSQC NMR spectrum of [Yb(Tp)$_2$(OPPh$_3$)$_2$] **1-Yb(OPPh$_3$)$_2$**, recorded in d_6-benzene.

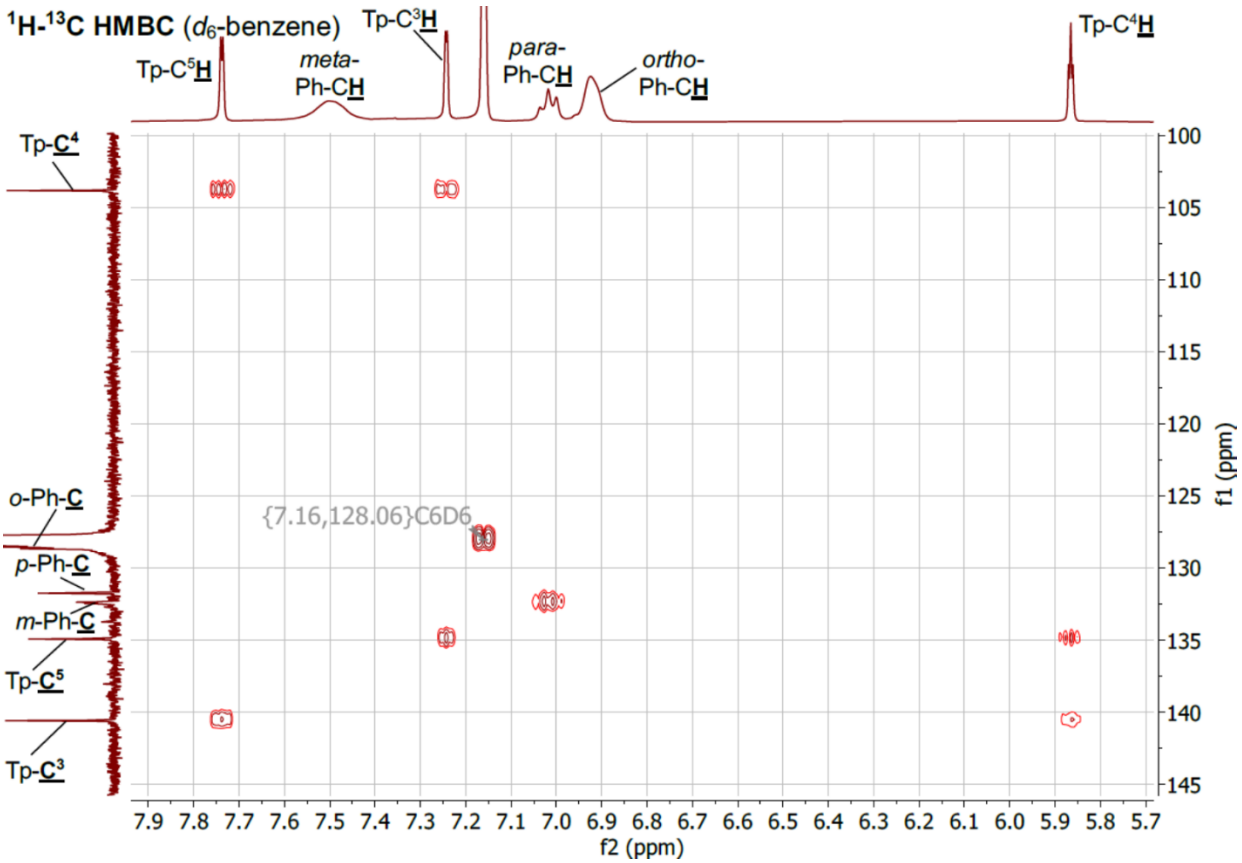

Figure S 12. ^{1}H-^{13}C HMBC NMR spectrum of [Yb(Tp)$_2$(OPPh$_3$)$_2$] **1-Yb(OPPh$_3$)$_2$**, recorded in d_6-benzene.

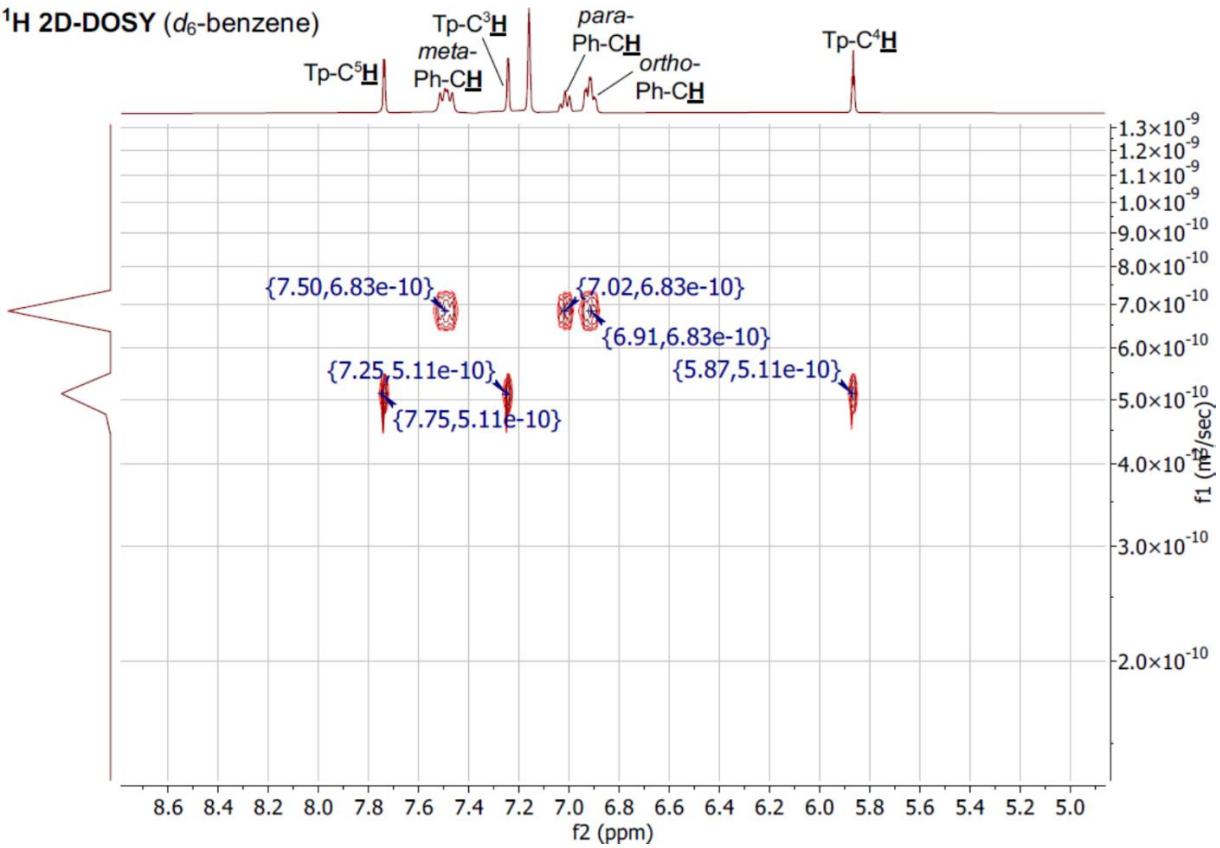

Figure S 13. ^{1}H 2D-DOSY NMR spectrum of [Yb(Tp)$_2$(OPPh$_3$)$_2$] **1-Yb(OPPh$_3$)$_2$**, recorded in d_6-benzene. The horizontal scale shows ^{1}H chemical shifts (ppm) and the vertical dimension the diffusion scale (m^2s^{-1}) with diffusion cross-peaks for **1-Yb(OPPh$_3$)$_x$** centred at 5.11 x 10^{-10} m^2s^{-1}, and for the equilibrium position of the Ph$_3$PO ligand centred at 6.83 x 10^{-10} m^2s^{-1}. In solution 2-x equivalents of the Ph$_3$PO ligand are in equilibrium with **1-Yb(OPPh$_3$)$_x$**.

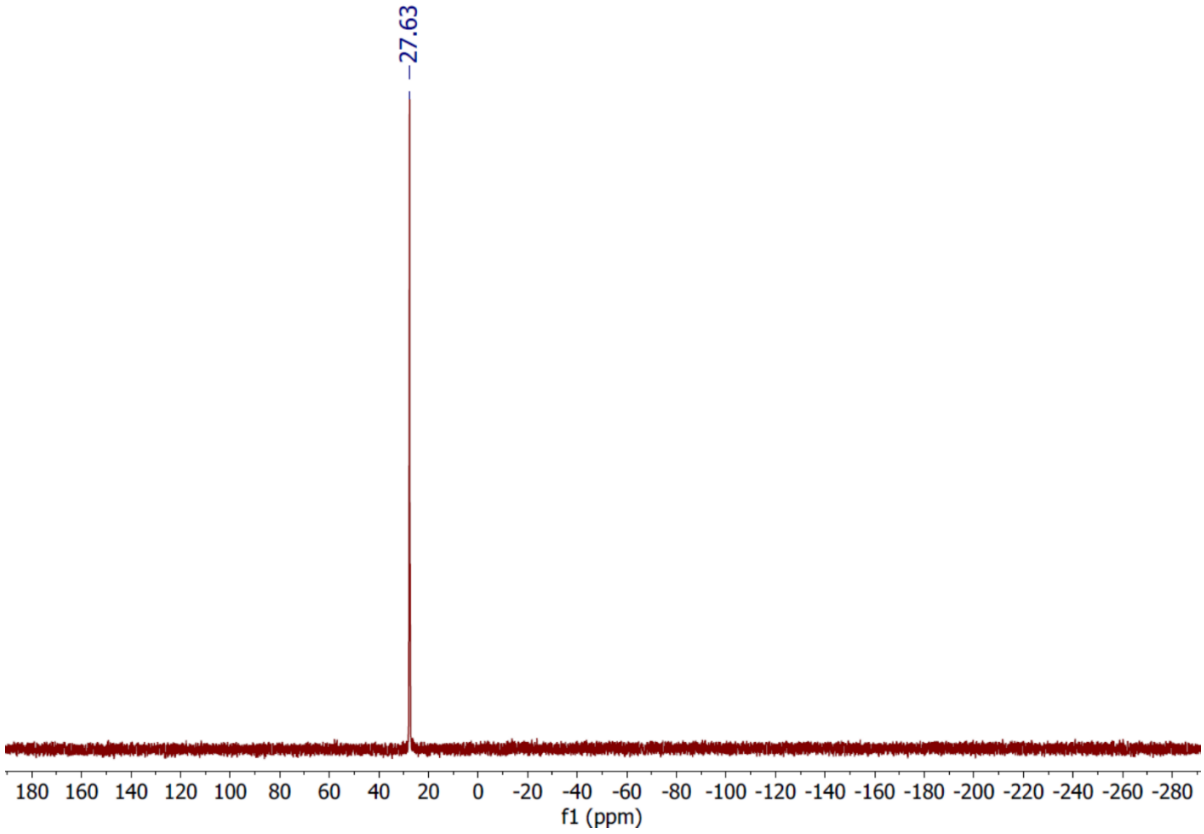

Figure S 14. ^{31}P NMR spectrum of [Yb(Tp)$_2$(OPPh$_3$)$_2$] **1-Yb(OPPh$_3$)$_2$**, recorded in d_6-benzene.

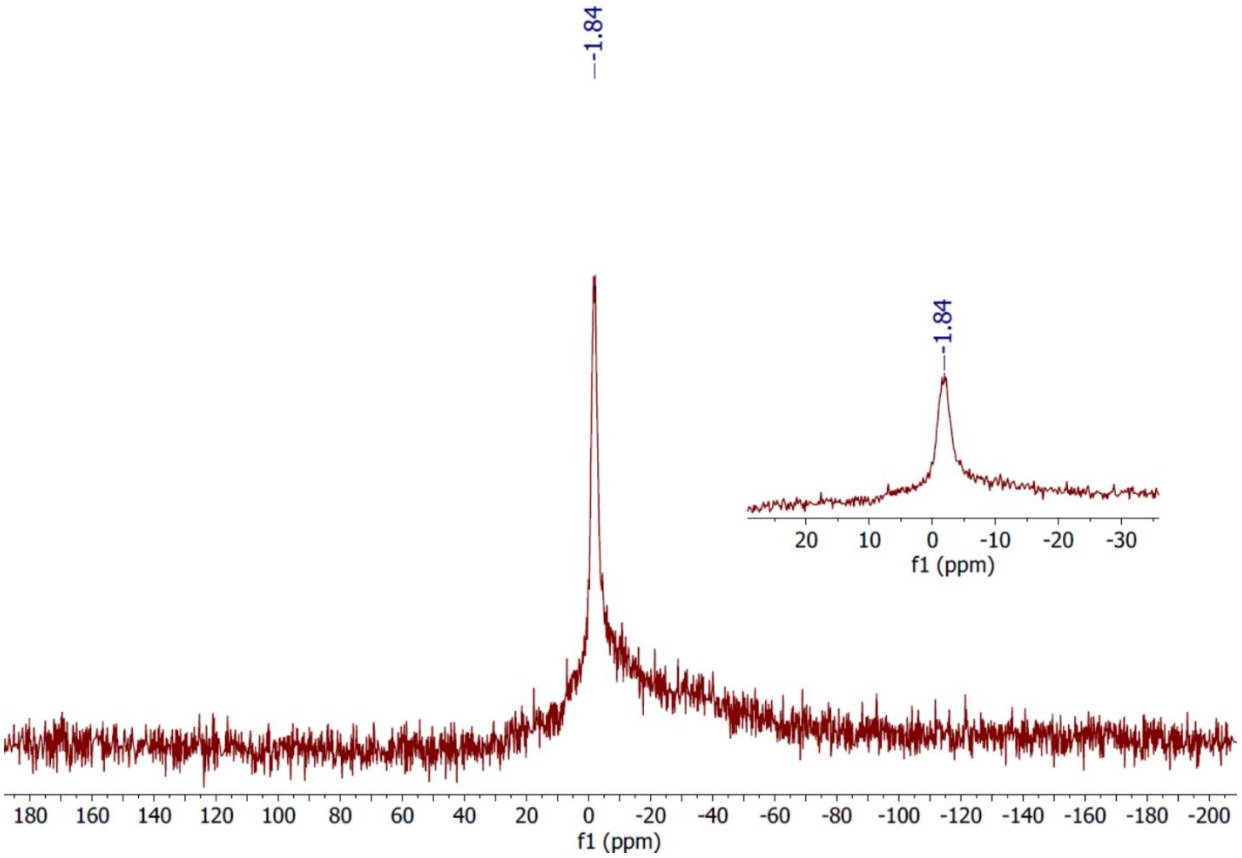

Figure S 15. ^{11}B NMR spectrum of [Yb(Tp)$_2$(OPPh$_3$)$_2$] **1-Yb(OPPh$_3$)$_2$**, recorded in d_6-benzene.

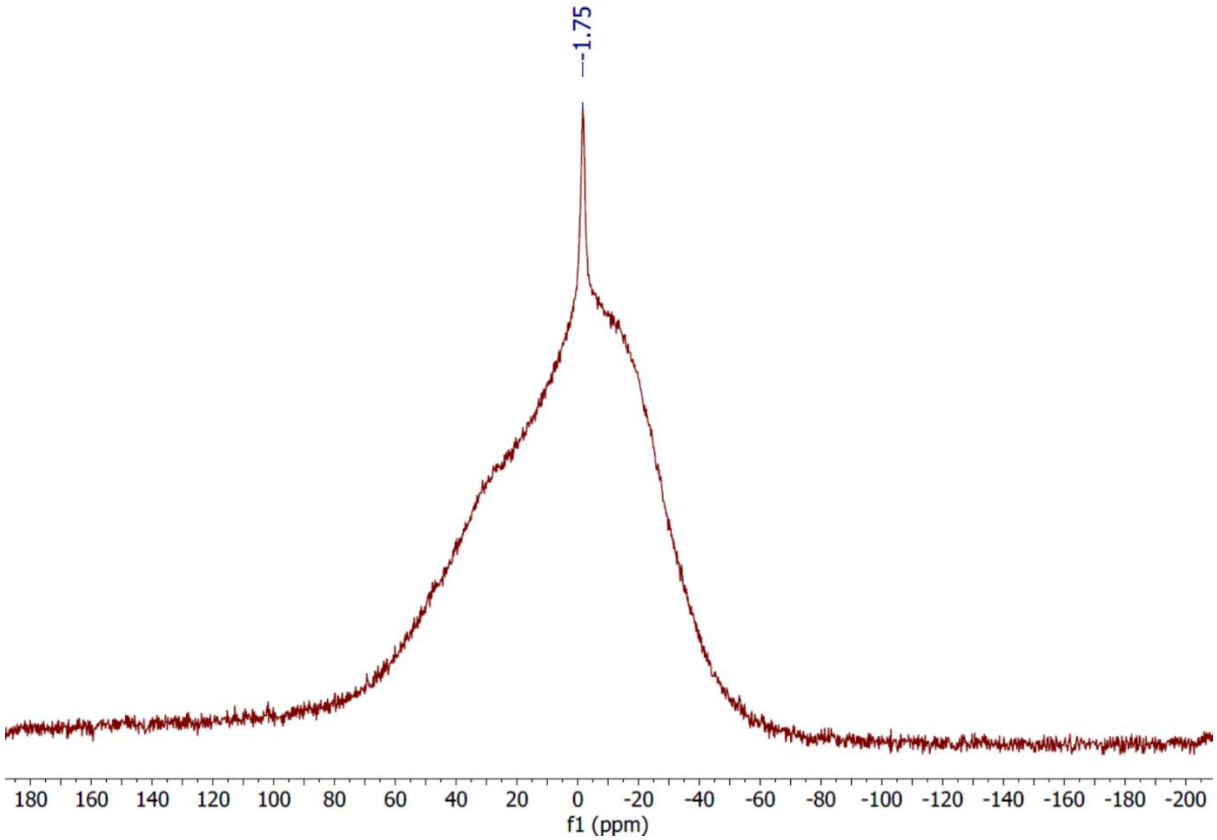

Figure S 16. ^{11}B{^{1}H} NMR spectrum of [Yb(Tp)$_2$(OPPh$_3$)$_2$] **1-Yb(OPPh$_3$)$_2$**, recorded in d_6-benzene.

S1.3 [Yb(Tp)$_2$(OPPh$_3$)] 1-Yb(OPPh$_3$)

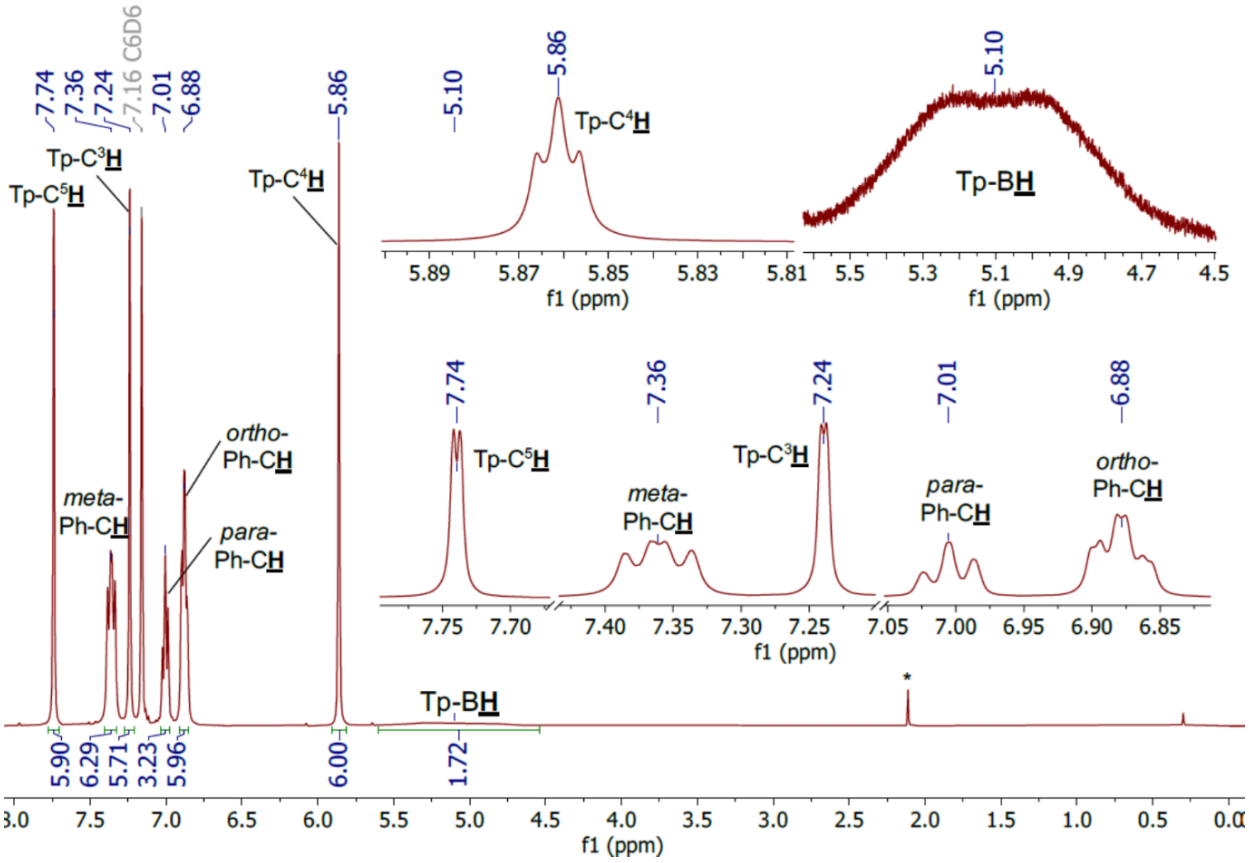

Figure S 17. ^{1}H NMR spectrum of [Yb(Tp)$_2$(OPPh$_3$)] **1-Yb(OPPh$_3$)**, recorded in d_6-benzene. Toluene is denoted by *.

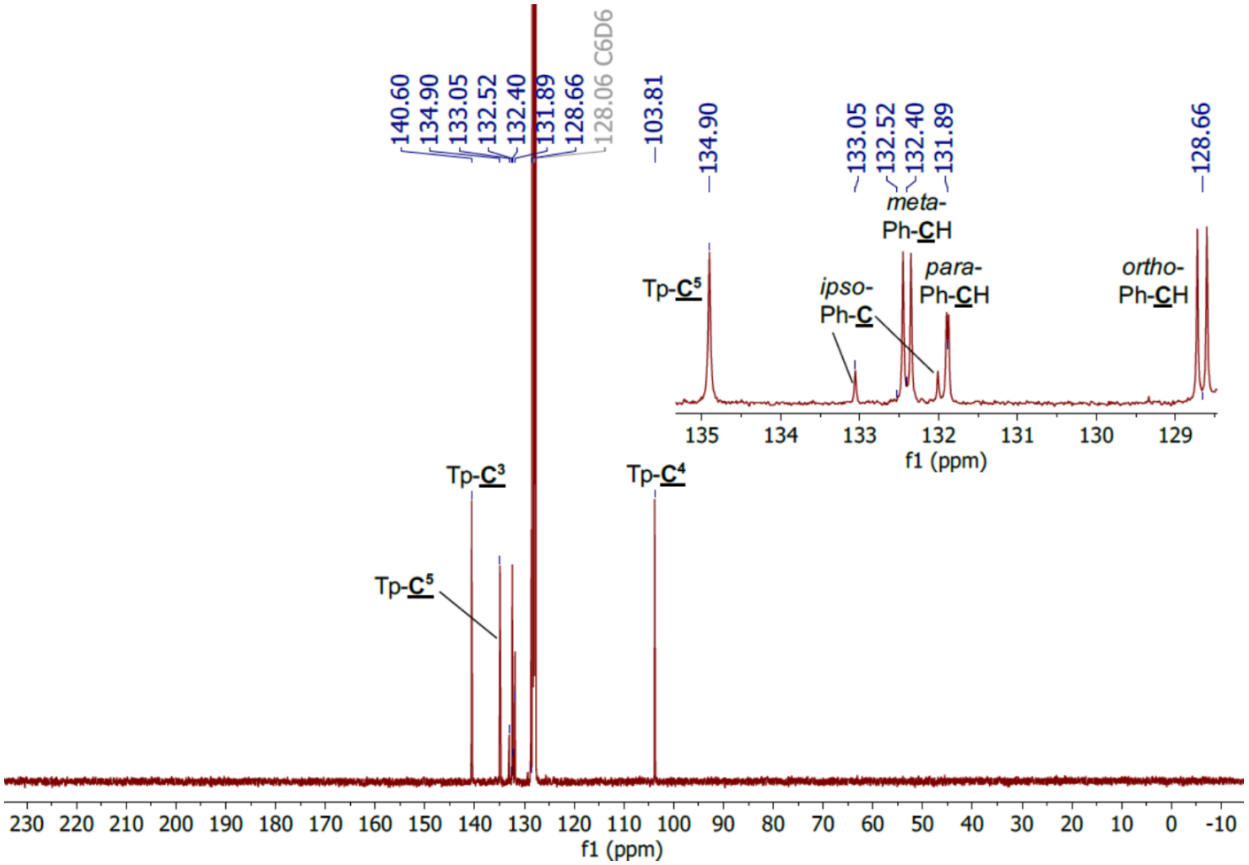

Figure S 18. ^{13}C{^{1}H} NMR spectrum of [Yb(Tp)$_2$(OPPh$_3$)] **1-Yb(OPPh$_3$)**, recorded in d_6-benzene.

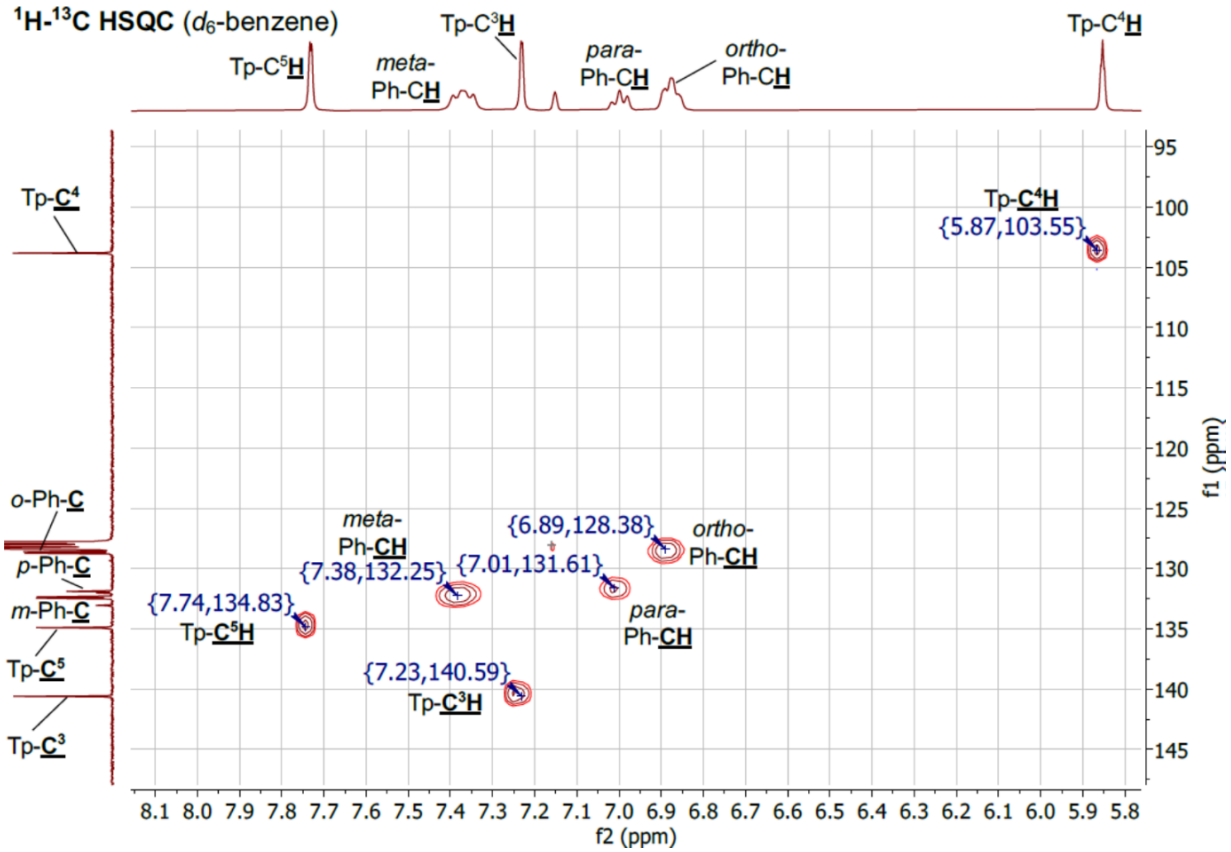

Figure S 19. ^{1}H-^{13}C HSQC NMR spectrum of $[Yb(Tp)_2(OPPh_3)]$ **1-Yb(OPPh$_3$)**, recorded in d_6-benzene.

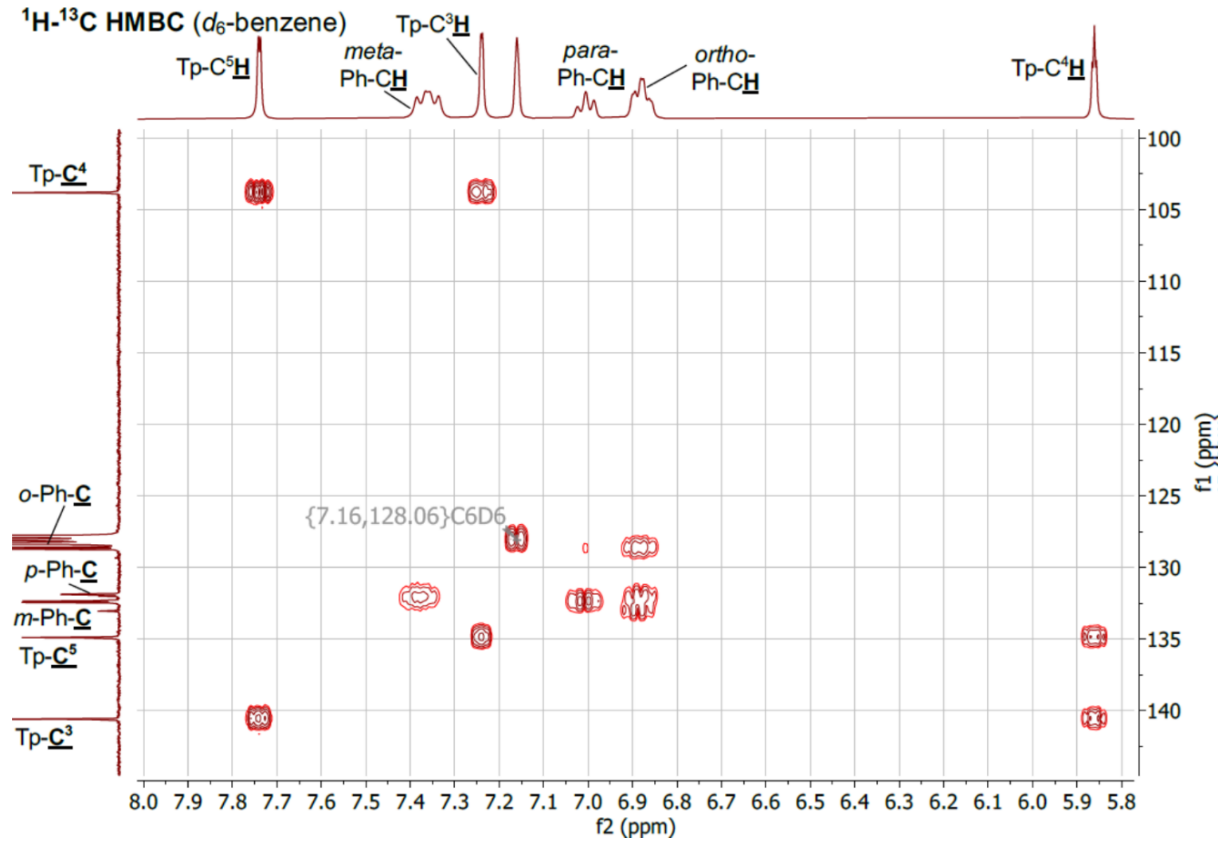

Figure S 20. ^{1}H-^{13}C HMBC NMR spectrum of $[Yb(Tp)_2(OPPh_3)]$ **1-Yb(OPPh$_3$)**, recorded in d_6-benzene.

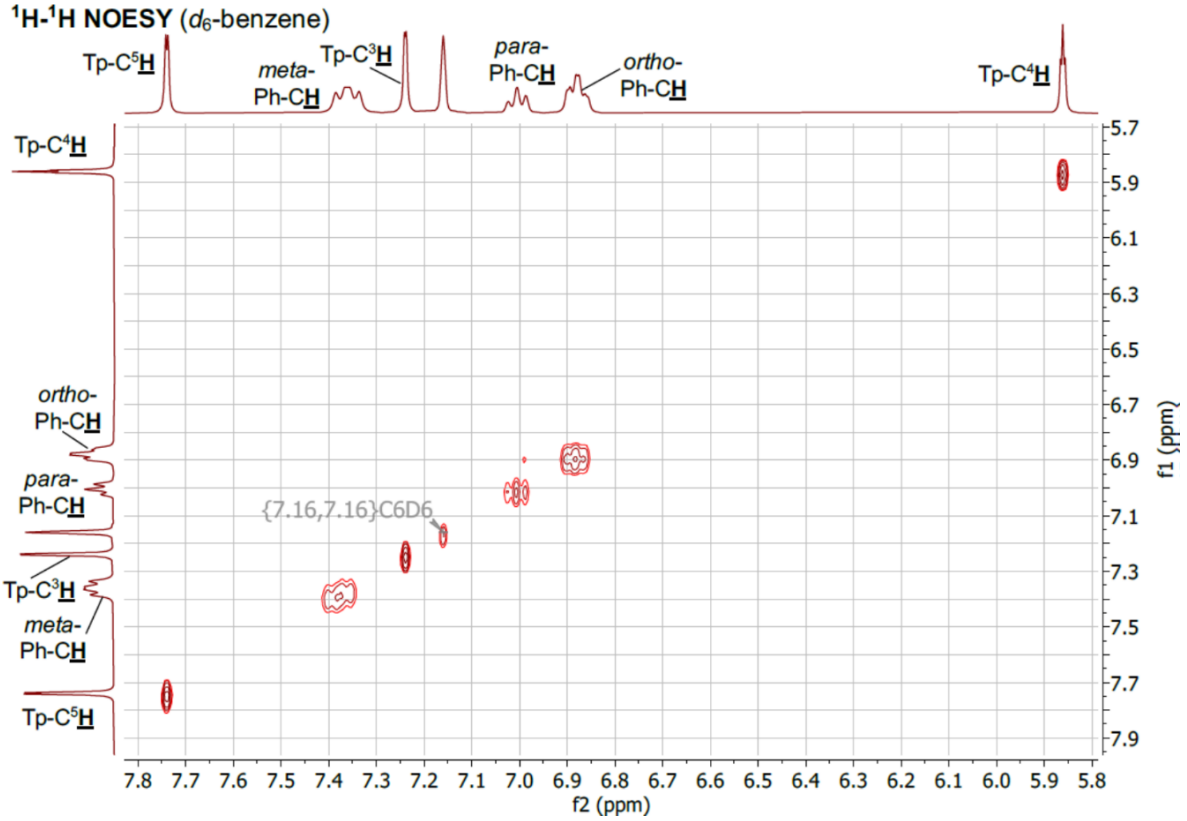

Figure S 21. ^{1}H-^{1}H NOESY NMR spectrum of [Yb(Tp)$_2$(OPPh$_3$)] **1-Yb(OPPh$_3$)**, recorded in d_6-benzene.

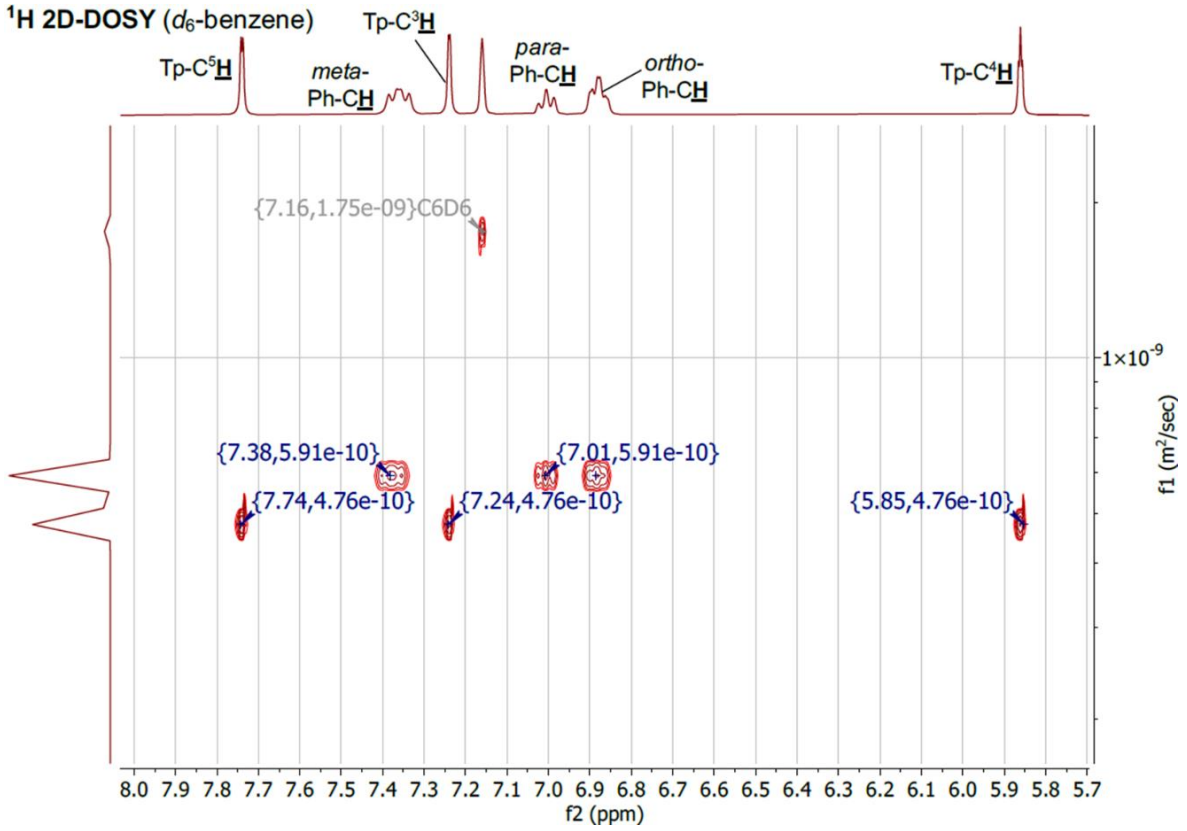

Figure S 22. ^{1}H 2D-DOSY NMR spectrum of [Yb(Tp)$_2$(OPPh$_3$)] **1-Yb(OPPh$_3$)**, recorded in d_6-benzene. The horizontal scale shows ^{1}H chemical shifts (ppm) and the vertical dimension the diffusion scale (m^{2}s^{-1}) with diffusion cross-peaks for **1-Yb(OPPh$_3$)$_x$** centred at 4.76 x 10^{-10} m^{2}s^{-1} and for the equilibrium position of the Ph$_3$PO ligand centred at 5.91 x 10^{-10} m^{2}s^{-1}. In solution 1-x equivalents of the Ph$_3$PO ligand are in equilibrium with **1-Yb(OPPh$_3$)$_x$**.

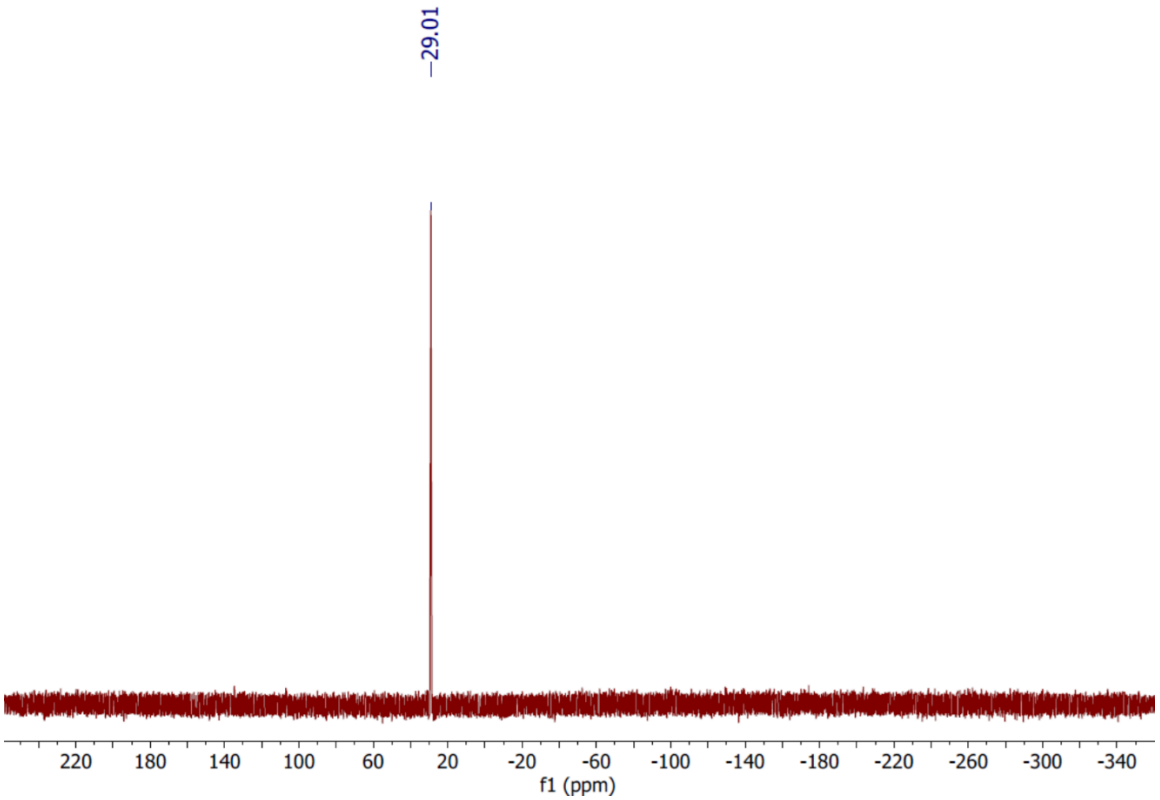

Figure S 23. ^{31}P NMR spectrum of [Yb(Tp)$_2$(OPPh$_3$)] **1-Yb(OPPh$_3$)**, recorded in d_6-benzene.

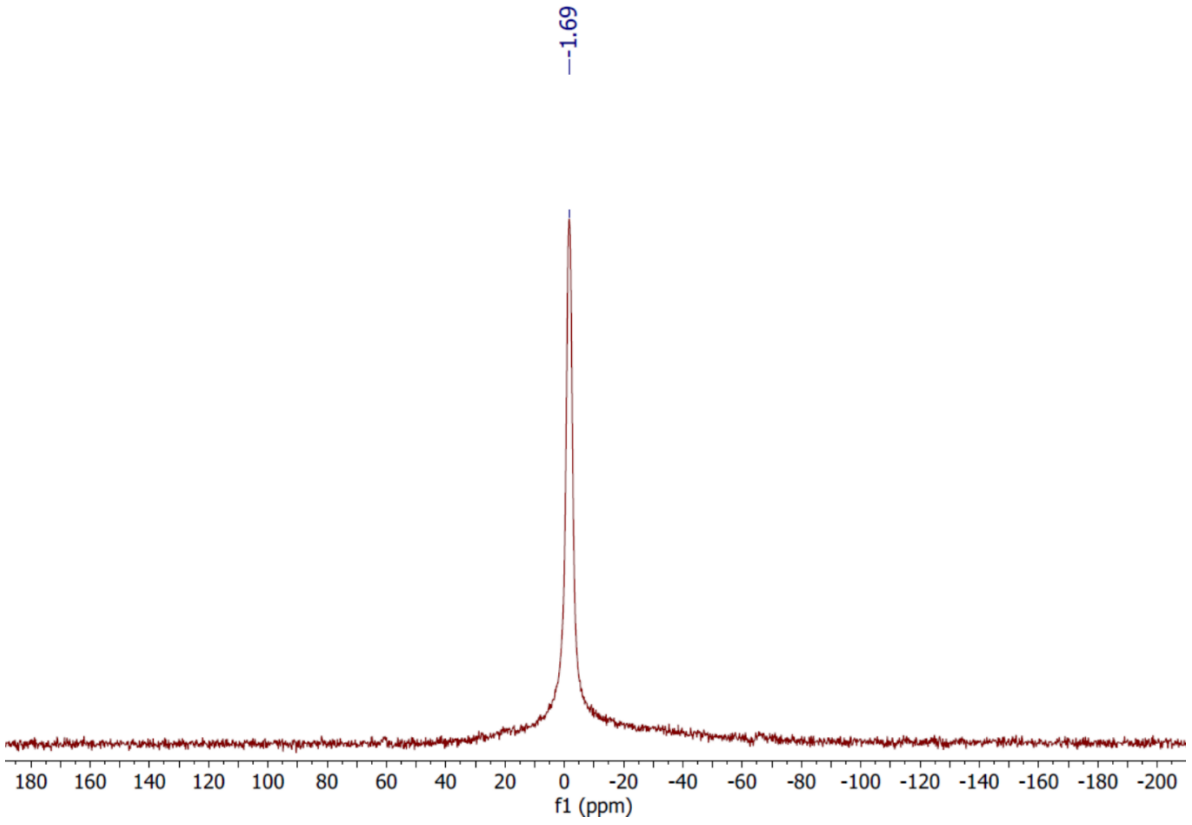

Figure S 24. ^{11}B NMR spectrum of [Yb(Tp)$_2$(OPPh$_3$)] **1-Yb(OPPh$_3$)**, recorded in d_6-benzene.

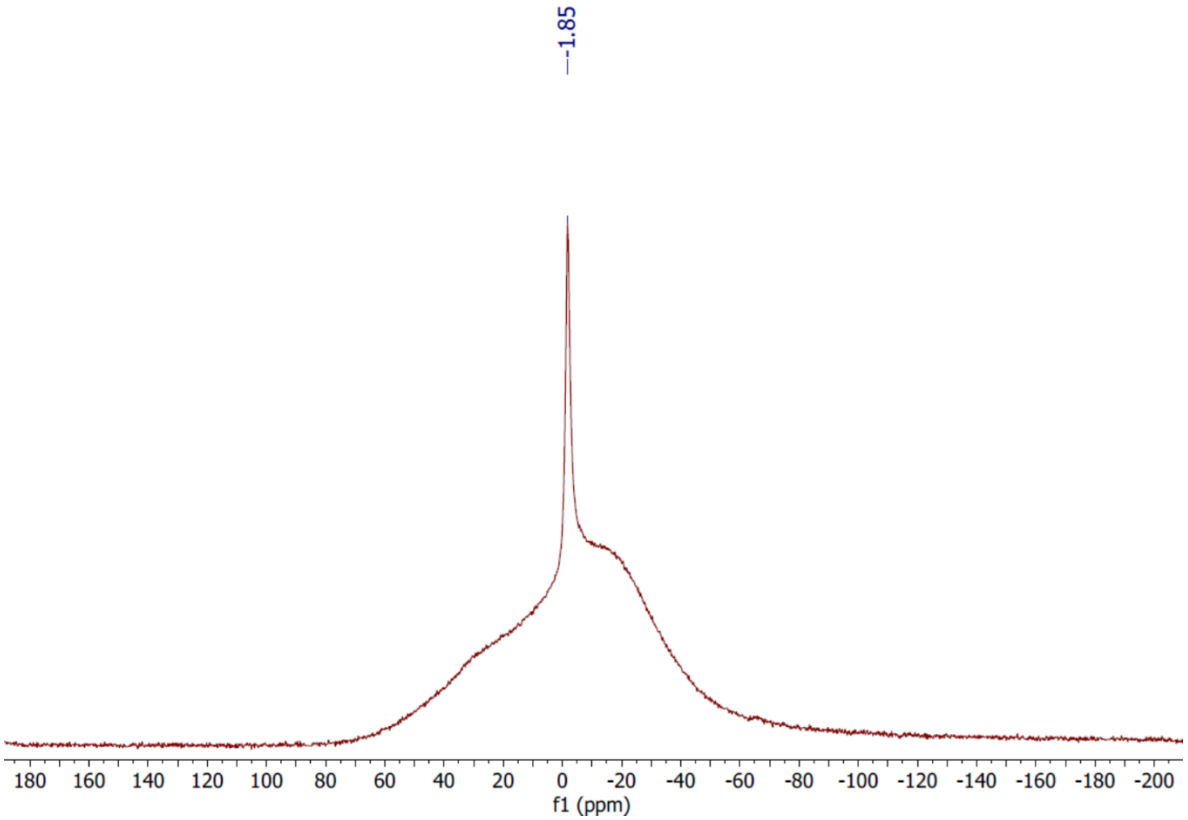

Figure S 25. $^{11}B\{^{1}H\}$ NMR spectrum of [Yb(Tp)$_2$(OPPh$_3$)] 1-Yb(OPPh$_3$), recorded in d_6-benzene.

S1.4 [Y(Tp)$_2$(μ-OTf)$_2$K(18-crown-6)] 2-Y

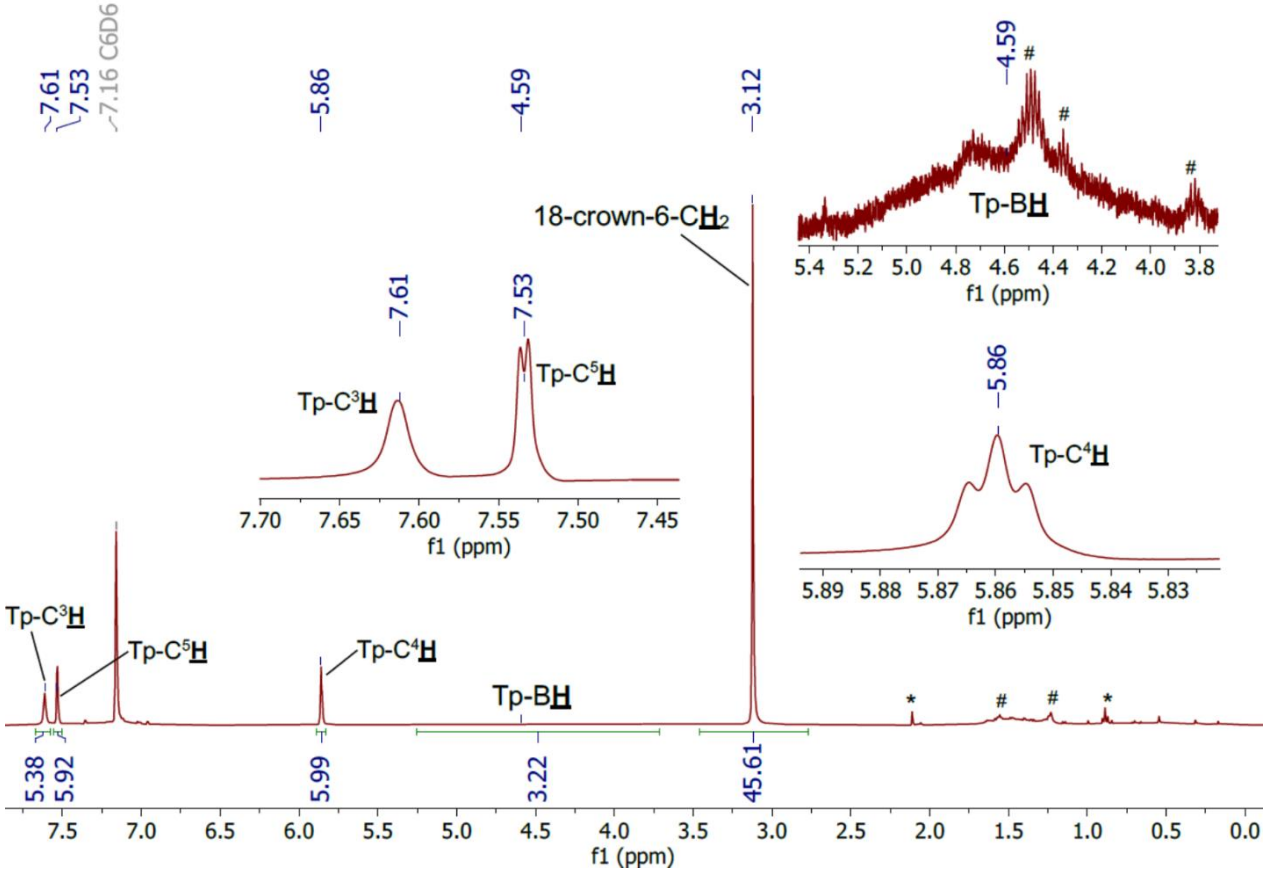

Figure S 26. ^{1}H NMR spectrum of [Y(Tp)$_2$(μ-OTf)$_2$K(18-crown-6)] **2-Y**, recorded in d_6-benzene. Toluene and hexane are denoted by * and very minor by-products are denoted by $^{\#}$.

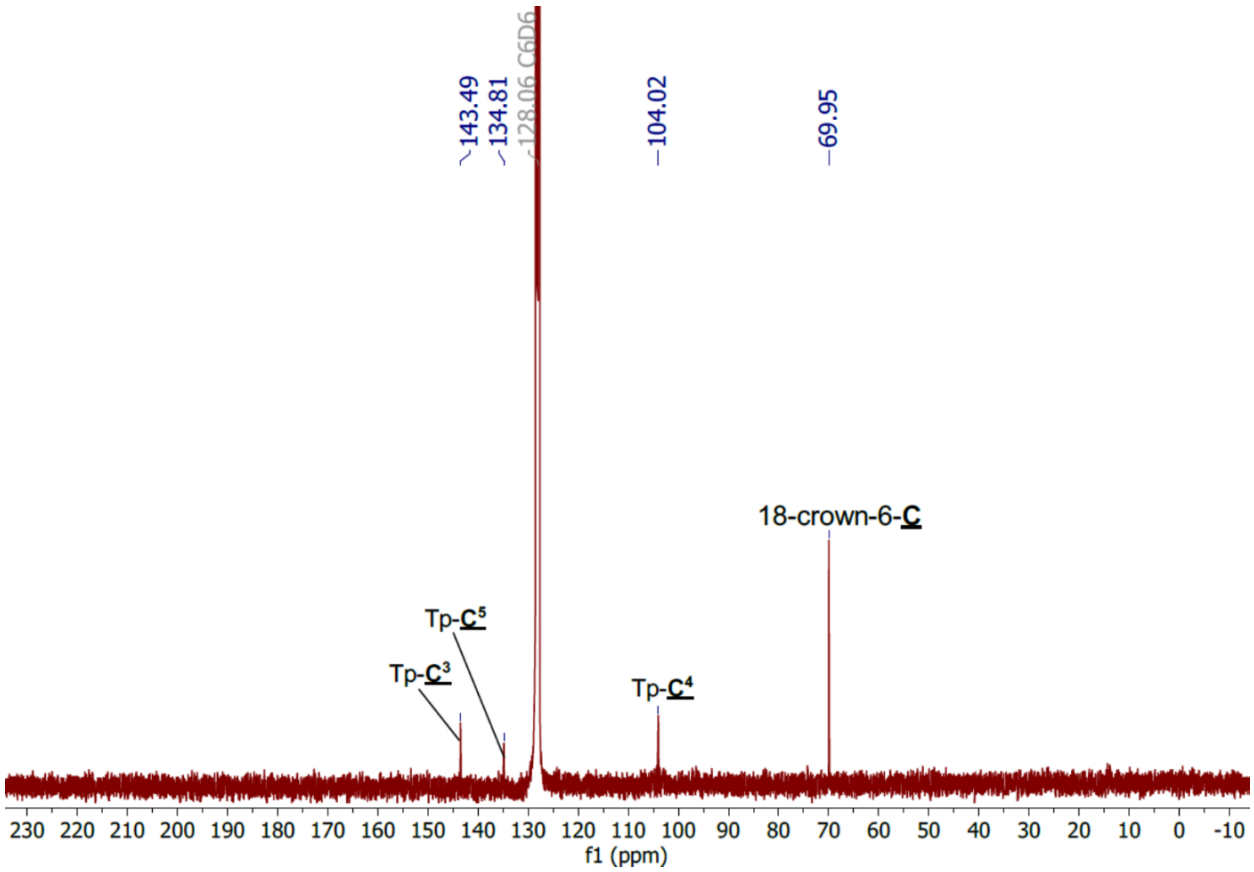

Figure S 27. $^{13}C\{^{1}H\}$ NMR spectrum of $[Y(Tp)_2(\mu\text{-}OTf)_2K(18\text{-crown-6})]$ **2-Y**, recorded in d_6-benzene.

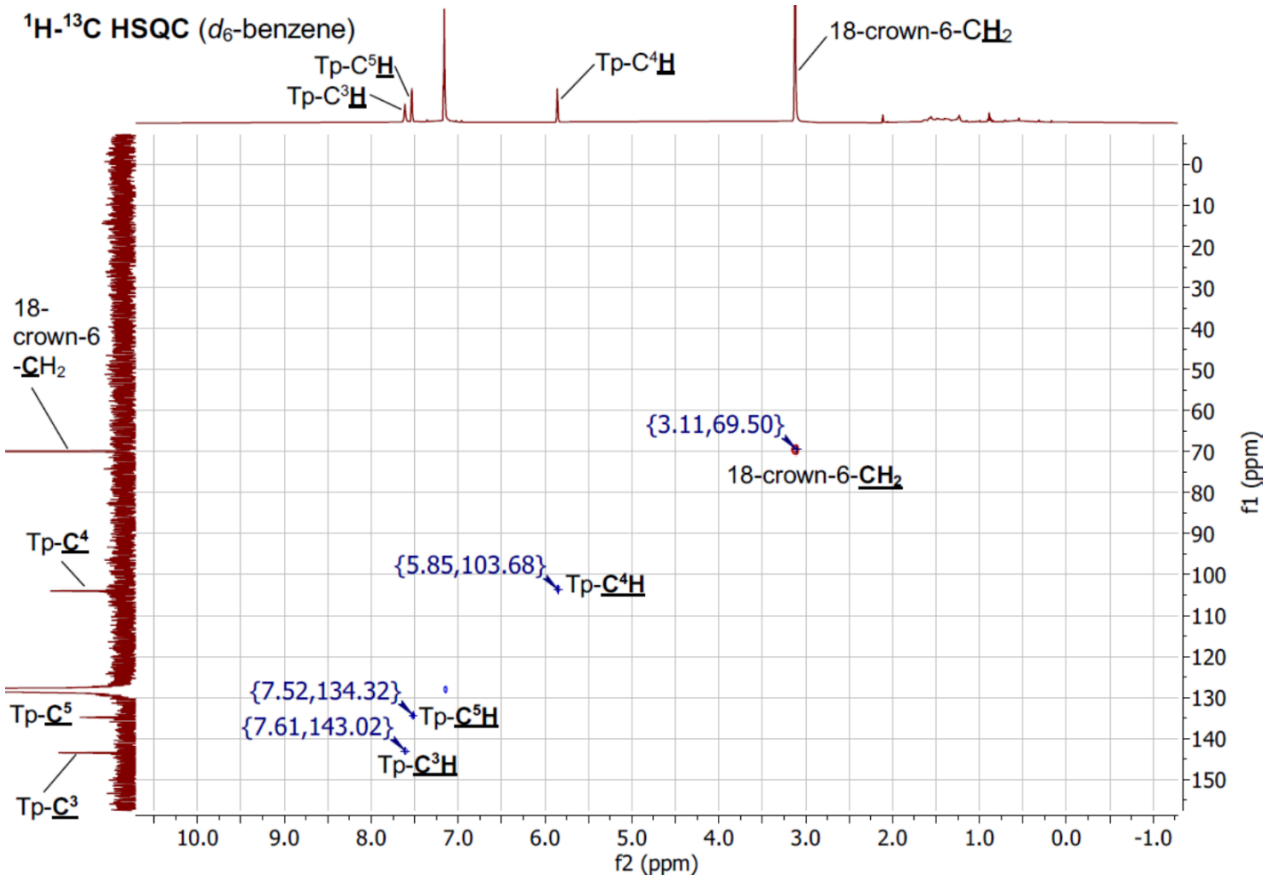

Figure S 28. $^{1}H\text{-}^{13}C$ HSQC NMR spectrum of $[Y(Tp)_2(\mu\text{-}OTf)_2K(18\text{-crown-6})]$ **2-Y**, recorded in d_6-benzene.

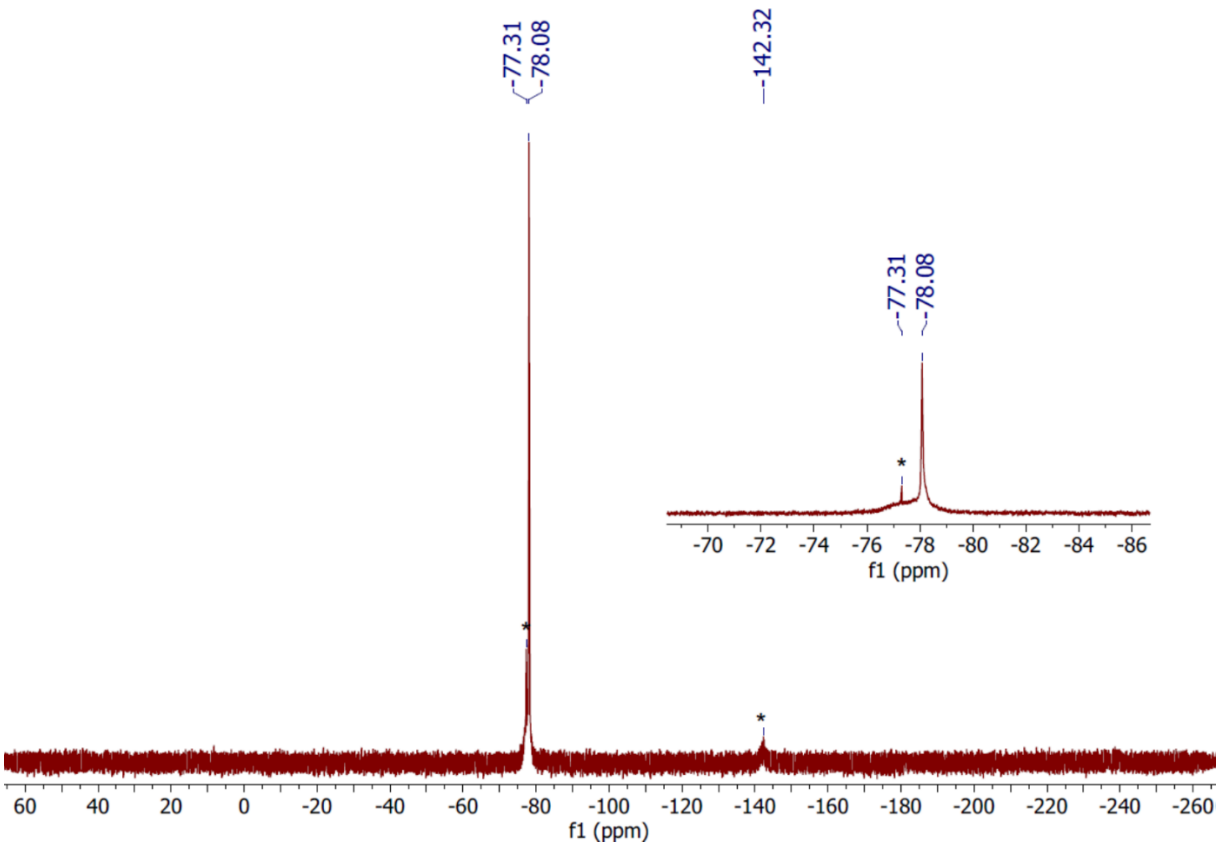

Figure S 29. ^{19}F NMR spectrum of [Y(Tp)$_2$(μ-OTf)$_2$K(18-crown-6)] **2-Y**, recorded in d_6-benzene. Minor triflate-containing impurities are denoted with *.

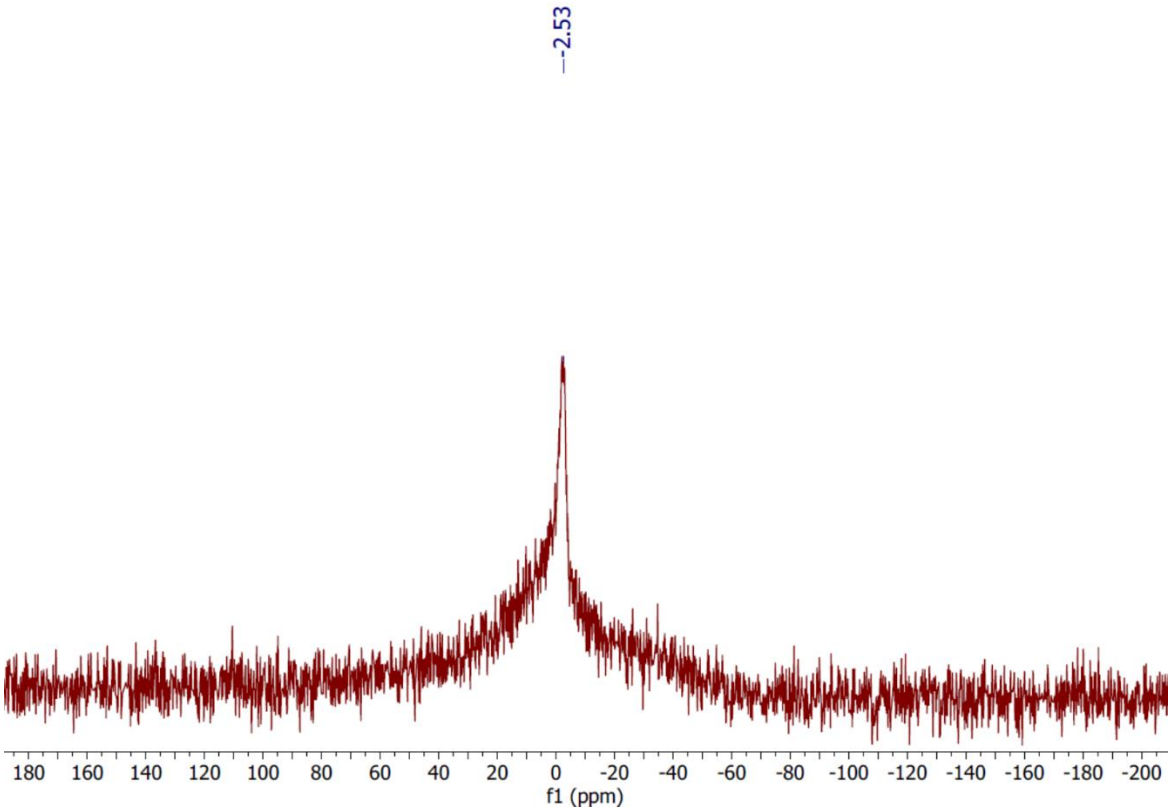

Figure S 30. ^{11}B NMR spectrum of [Y(Tp)$_2$(μ-OTf)$_2$K(18-crown-6)] **2-Y**, recorded in d_6-benzene.

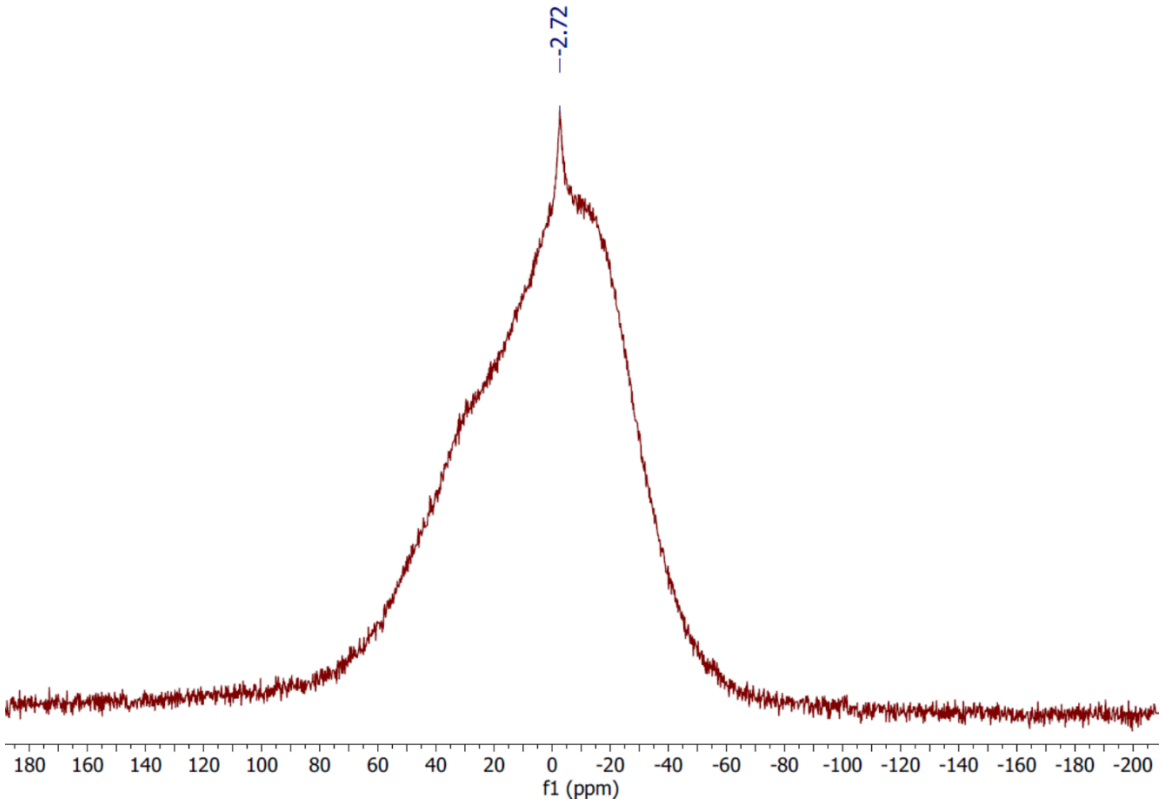

Figure S 31. $^{11}B\{^{1}H\}$ NMR spectrum of $[Y(Tp)_2(\mu\text{-}OTf)_2K(18\text{-crown-6})]$ **2-Y**, recorded in d_6-benzene.

S1.5 Data for NMR-scale reaction between $[Eu(Tp)_2(OTf)]$ with $[\{K[Al(NON^{Dipp})]\}_2]$ (S I a)

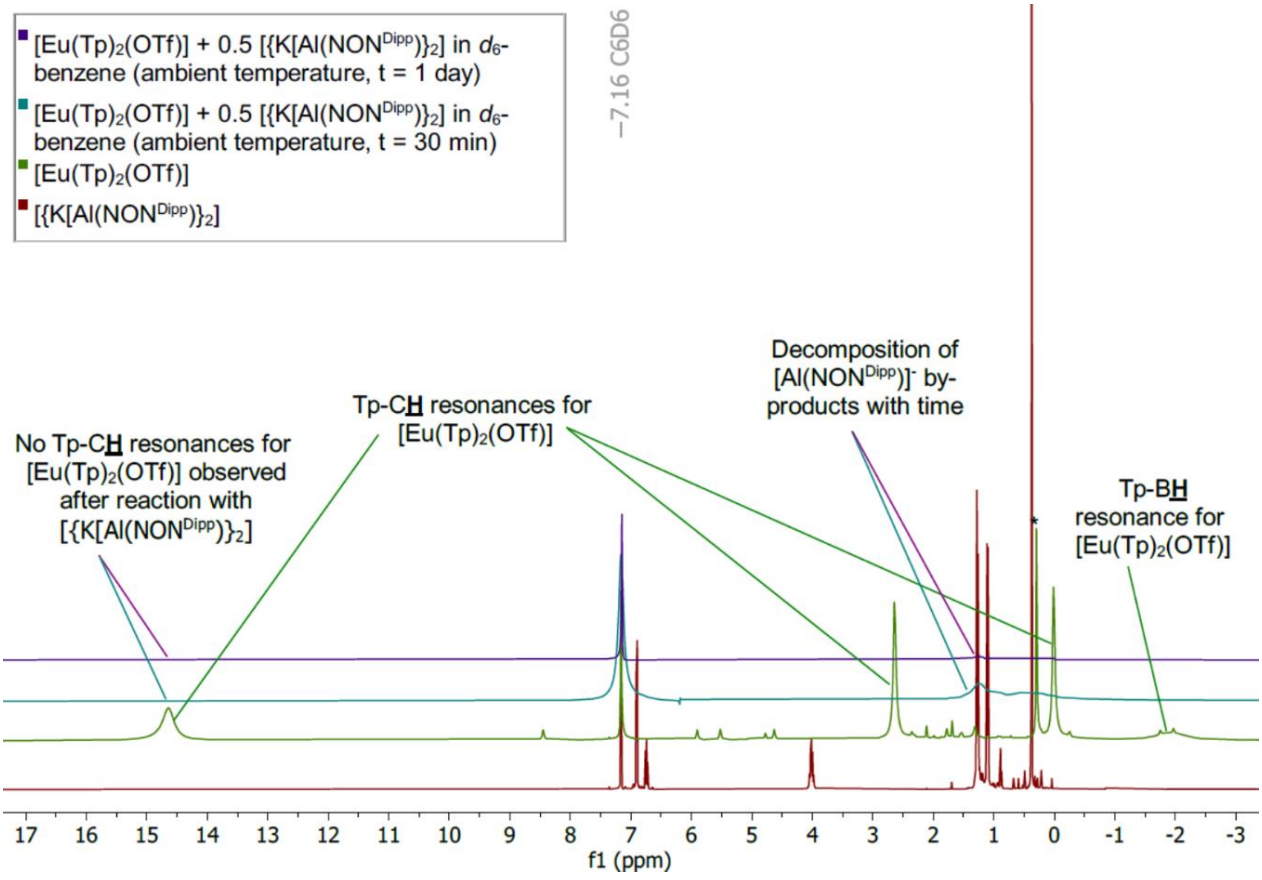

Figure S 32. ^{1}H NMR spectrum of the NMR scale reaction between $[Eu(Tp)_2(OTf)]$ and 0.5 eq $[\{K[Al(NON^{Dipp})]\}_2]$ in d_6-benzene, consistent with consumption of $[Eu(Tp)_2(OTf)]$ and $[\{K[Al(NON^{Dipp})]\}_2]$ under ambient temperatures. Silicon grease is denoted by *.

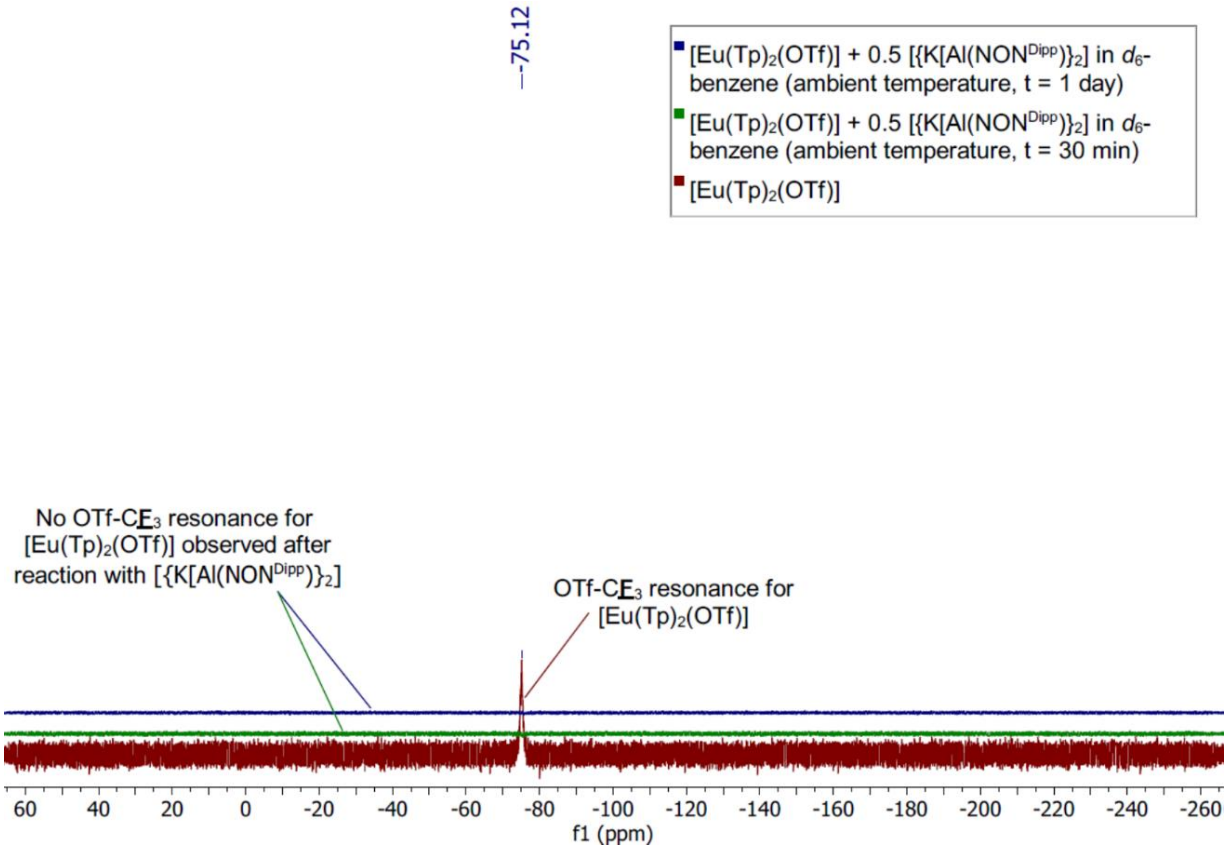

Figure S 33. ^{19}F NMR spectrum of the NMR scale reaction between $[Eu(Tp)_2(OTf)]$ and 0.5 eq $[\{K[Al(NON^{Dipp})]\}_2]$ in d_6-benzene, consistent with consumption of $[Eu(Tp)_2(OTf)]$ at ambient temperature.

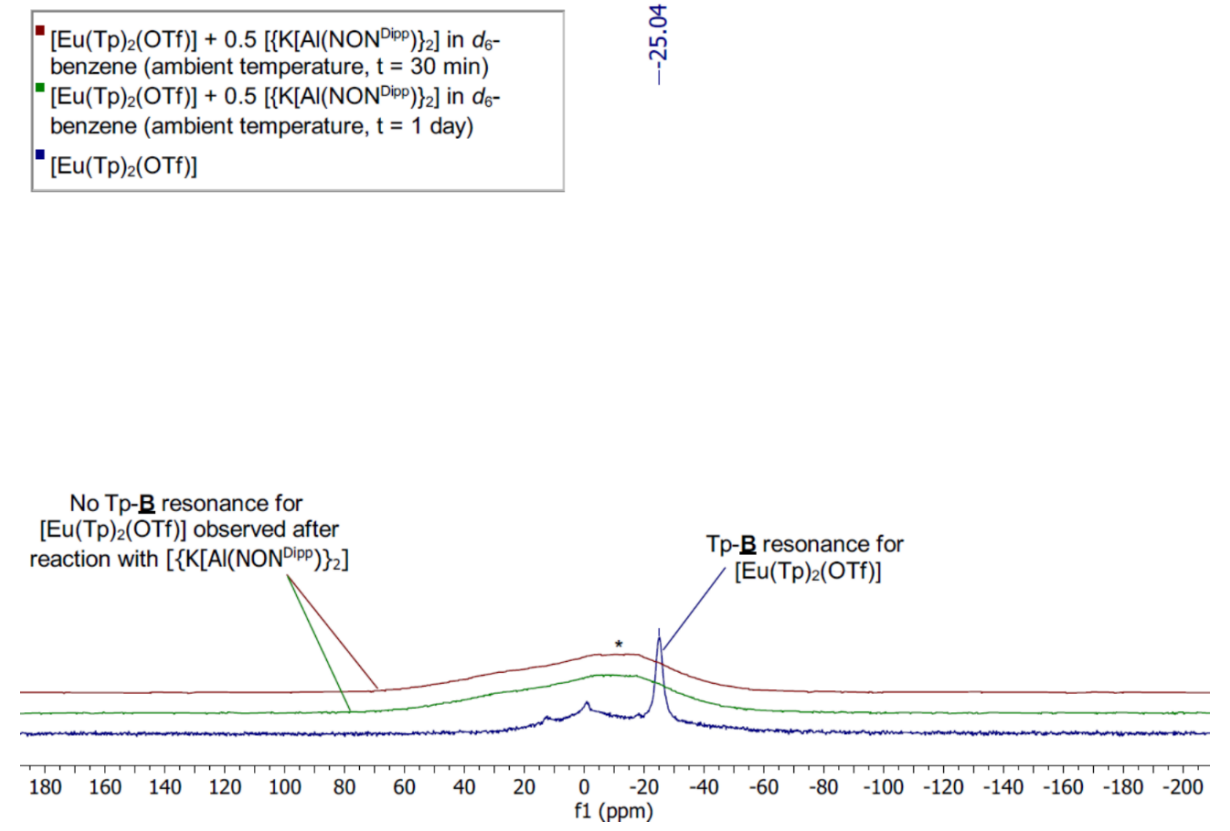

Figure S 34. $^{11}B\{^1H\}$ NMR spectrum of the NMR scale reaction between $[Eu(Tp)_2(OTf)]$ and 0.5 eq $[\{K[Al(NON^{Dipp})]\}_2]$ in d_6-benzene, consistent with consumption of $[Eu(Tp)_2(OTf)]$ at ambient temperature. Borosilicate glass is denoted by *.

S1.6 Comparative ^{1}H 2D-DOSY NMR spectroscopy of the reaction of 1-Yb with different equivalents of Ph_3PO to yield 1-Yb$(OPPh_3)_n$ (n = 1, 2)

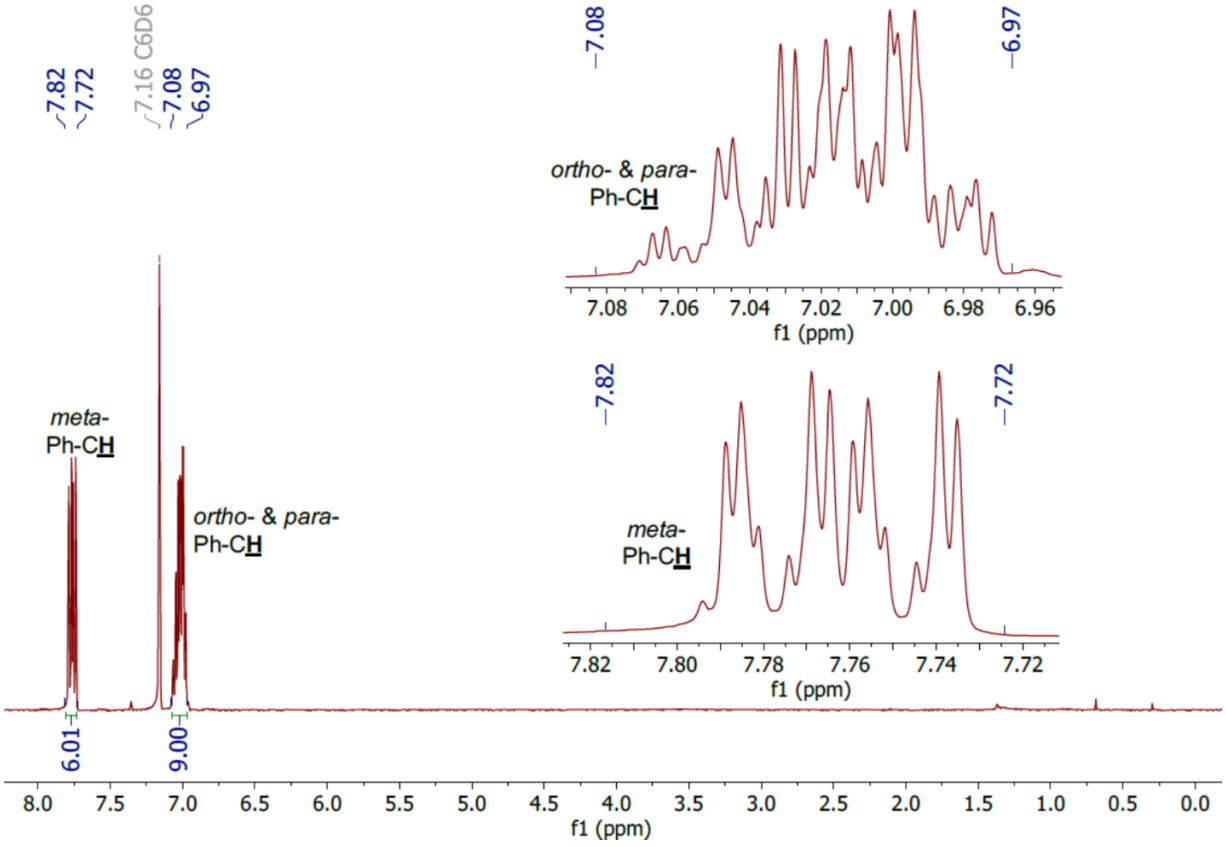

Figure S 35. ^{1}H NMR spectrum of free Ph_3PO, recorded in d_6-benzene.

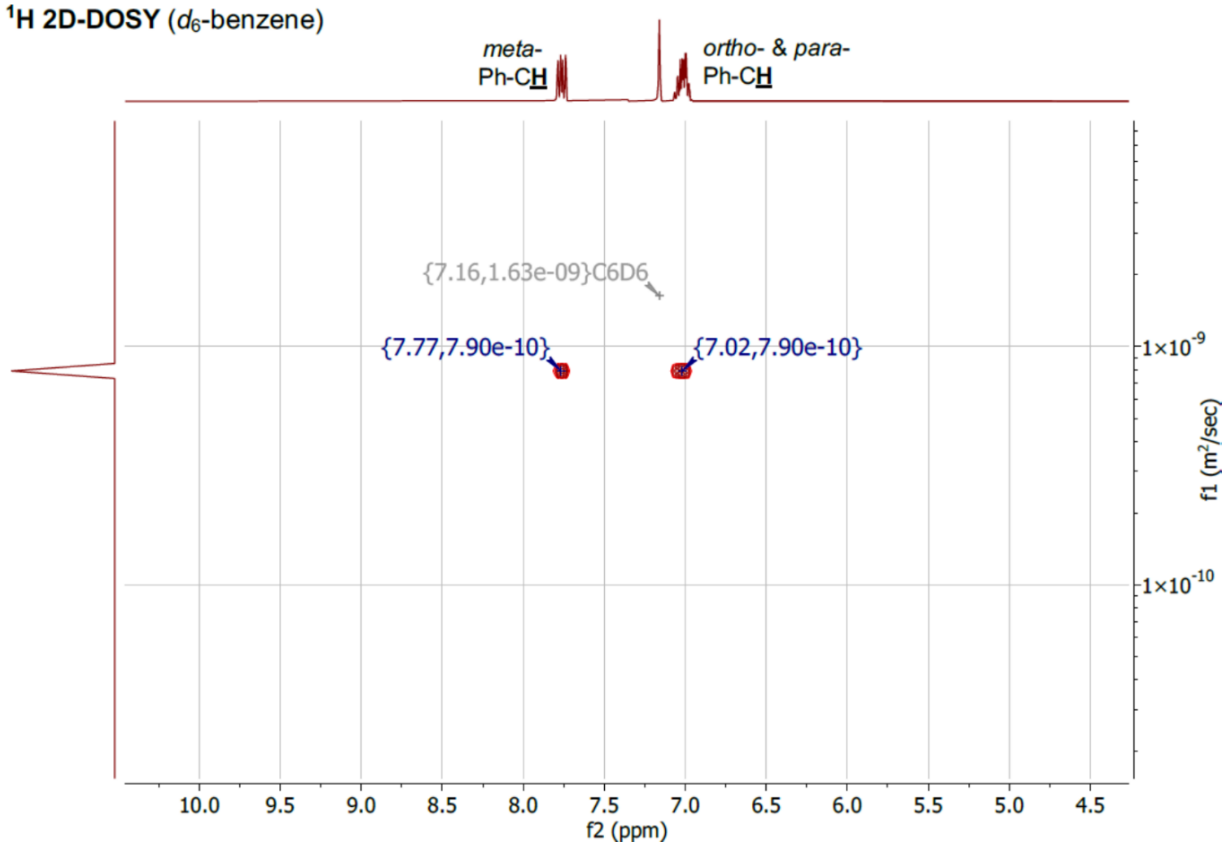

Figure S 36. ^{1}H 2D-DOSY NMR spectrum of Ph_3PO, recorded in d_6-benzene. The horizontal scale shows ^{1}H chemical shifts (ppm) and the vertical dimension the diffusion scale (m^2s^{-1}) with diffusion cross-peaks for free Ph_3PO centred at 7.90 x 10^{-10} m^2s^{-1}.

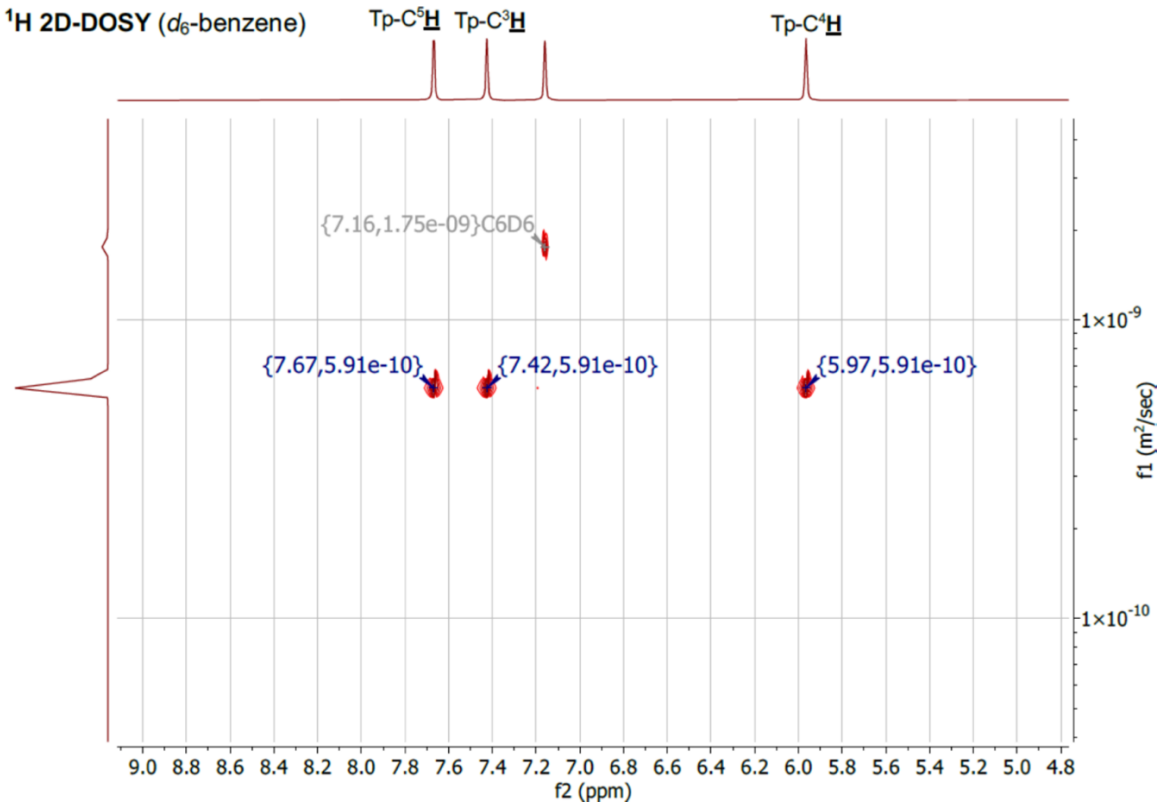

Figure S 37. ^{1}H 2D-DOSY NMR spectrum of [Yb(Tp)$_2$] **1-Yb**, recorded in d_6-benzene. The horizontal scale shows ^{1}H chemical shifts (ppm) and the vertical dimension the diffusion scale (m^2s^{-1}) with diffusion cross-peaks for **1-Yb** centred at 5.91 x 10^{-10} m^2s^{-1}.

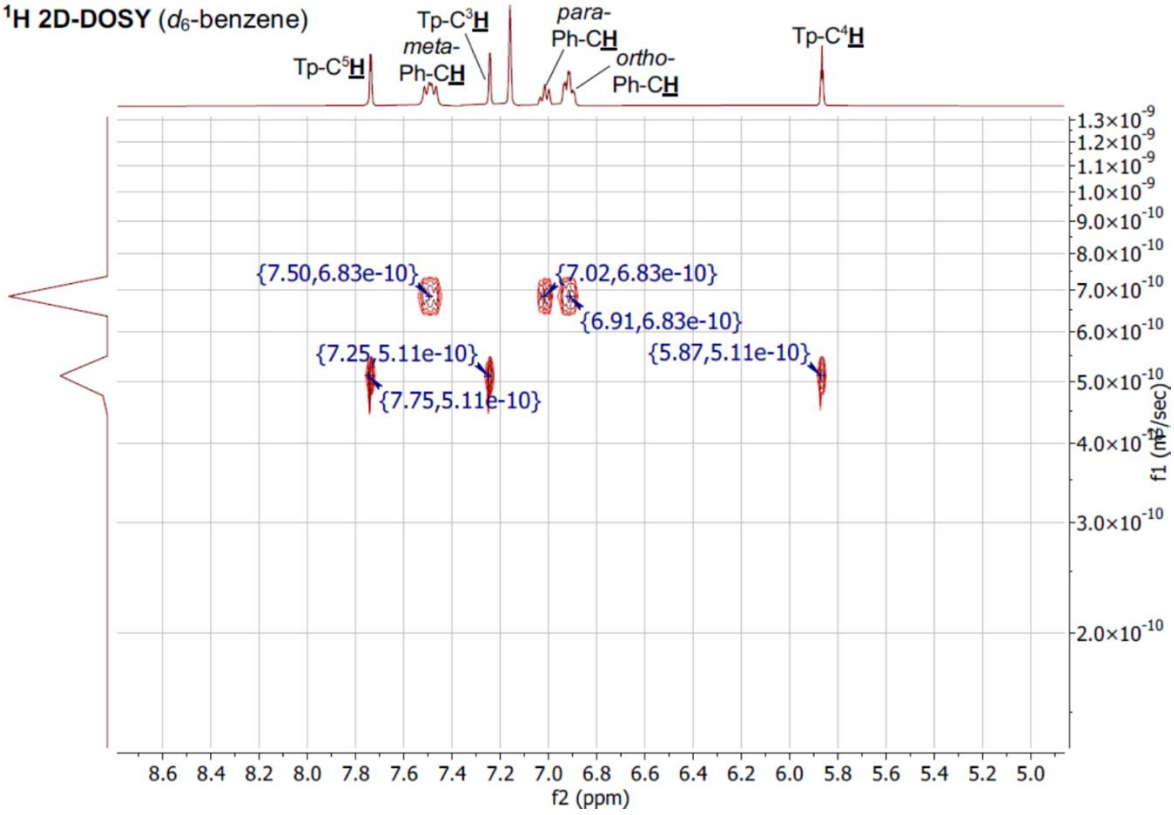

Figure S 38. ^{1}H 2D-DOSY NMR spectrum of [Yb(Tp)$_2$(OPPh$_3$)$_2$] **1-Yb(OPPh$_3$)$_2$**, recorded in d_6-benzene. The horizontal scale shows ^{1}H chemical shifts (ppm) and the vertical dimension the diffusion scale (m^2s^{-1}) with diffusion cross-peaks for **1-Yb(OPPh$_3$)$_x$** centred at 5.11 x 10^{-10} m^2s^{-1}, and for the equilibrium position of the Ph$_3$PO ligand centred at 6.83 x 10^{-10} m^2s^{-1}. In solution 2-x equivalents the Ph$_3$PO ligand are in equilibrium with **1-Yb(OPPh$_3$)$_x$**.

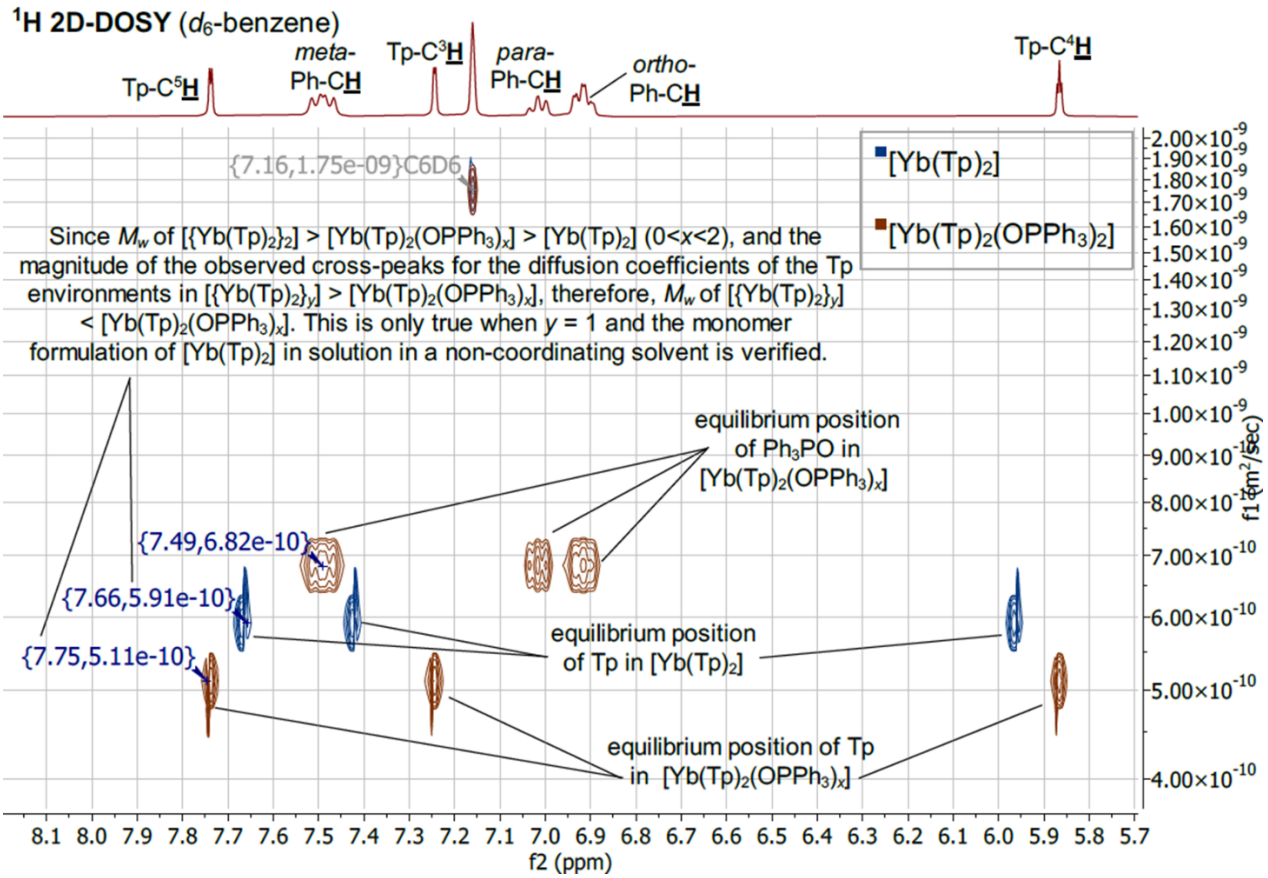

Figure S 39. Overlay of the ^{1}H 2D-DOSY NMR spectra of [Yb(Tp)$_2$] **1-Yb** and [Yb(Tp)$_2$(OPPh$_3$)$_2$] **1-Yb(OPPh$_3$)$_2$**, recorded in d_6-benzene. The horizontal scale shows ^{1}H chemical shifts (ppm) (^{1}H NMR resonances for **1-Yb(OPPh$_3$)$_2$**) and the vertical dimension the diffusion scale (m^{2}s^{-1}). Since the data show that the diffusion coefficient of the horizontally aligned cross-peaks of the three Tp-C**H** environments of [{Yb(Tp)$_2$}$_y$] is observed to be larger in magnitude than that of the equilibrium species [Yb(Tp)$_2$(OPPh$_3$)$_x$], the molecular weight (M_w) of [{Yb(Tp)$_2$}$_y$] must be smaller than [Yb(Tp)$_2$(OPPh$_3$)$_x$]. Since this will be only true only when y = 1 and not y = 2, therefore, it demonstrates that [Yb(Tp)$_2$] **1-Yb** is a monomer in solution in a non-coordinating solvent.

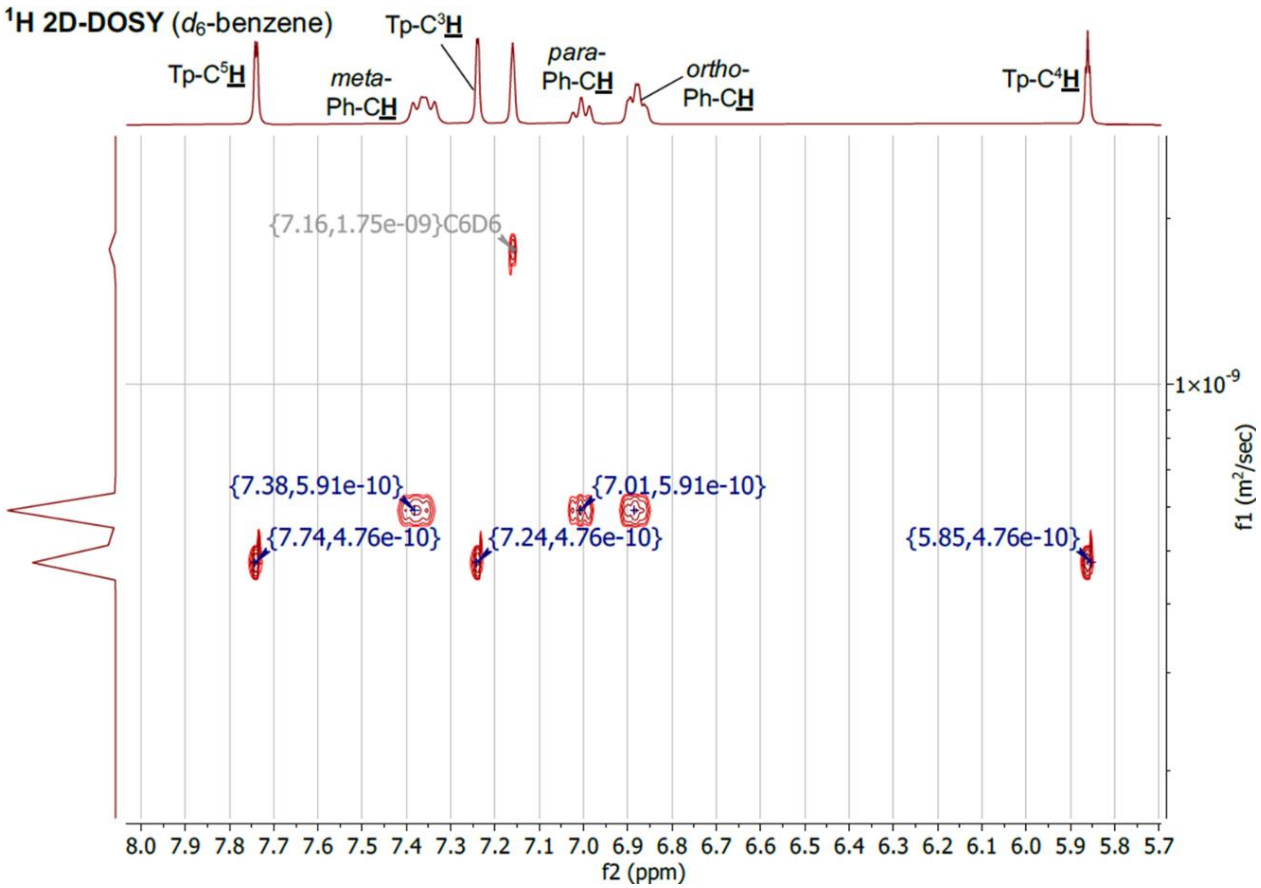

Figure S 40. ^{1}H 2D-DOSY NMR spectrum of [Yb(Tp)$_2$(OPPh$_3$)] **1-Yb(OPPh$_3$)**, recorded in d_6-benzene. The horizontal scale shows ^{1}H chemical shifts (ppm) and the vertical dimension the diffusion scale (m^{2}s^{-1}) with diffusion cross-peaks for **1-Yb(OPPh$_3$)$_x$** centred at 4.76 x 10^{-10} m^{2}s^{-1} and for the equilibrium position of the Ph$_3$PO ligand centred at 5.91 x 10^{-10} m^{2}s^{-1}. In solution 1-*x* equivalents of the Ph$_3$PO ligand are in equilibrium with **1-Yb(OPPh$_3$)$_x$**.

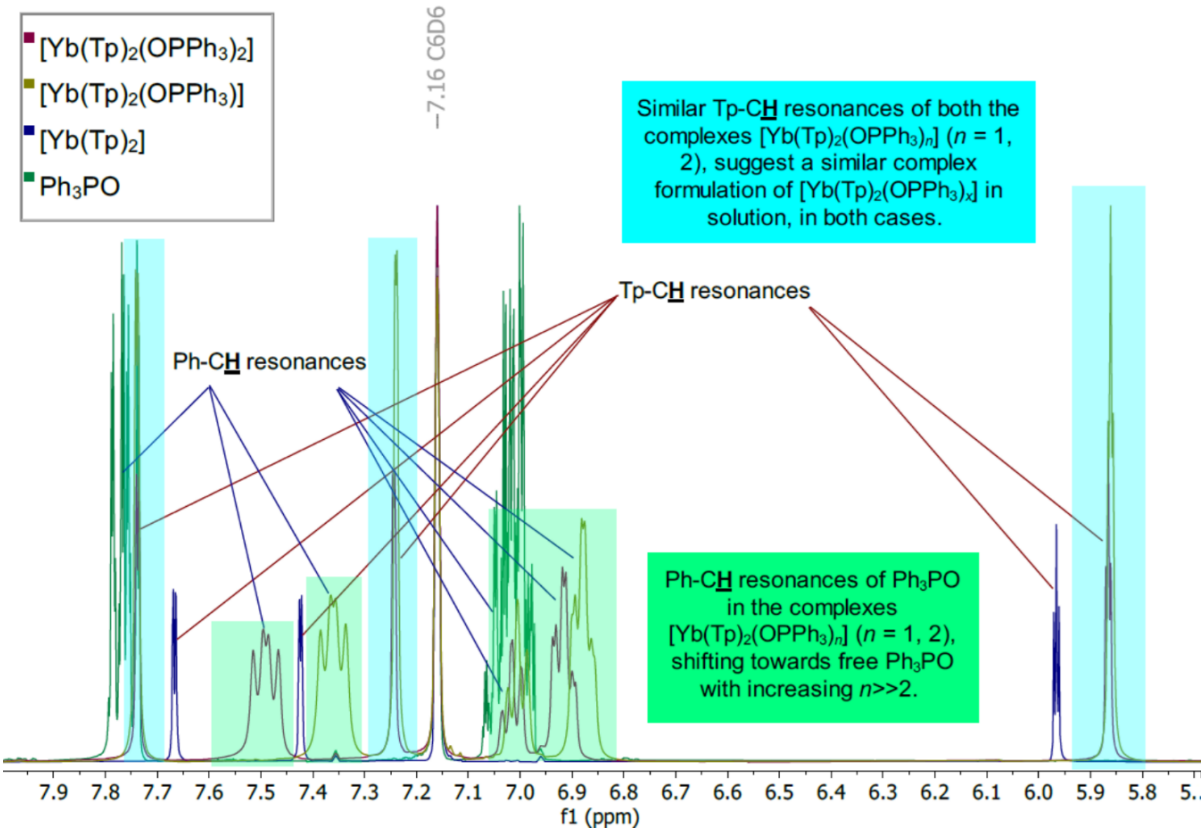

Figure S 41. Overlay of the ^{1}H NMR spectra of [Yb(Tp)$_2$] **1-Yb**, [Yb(Tp)$_2$(OPPh$_3$)$_n$] **1-Yb(OPPh$_3$)$_n$** (n = 1, 2), and Ph$_3$PO, recorded in d_6-benzene. The overlay demonstrates that the complexes **1-Yb(OPPh$_3$)$_n$** (n = 1, 2) are different to both the starting complex **1-Yb** and Ph$_3$PO. The three similar Tp-C**H** resonances of **1-Yb(OPPh$_3$)$_n$** (n = 1, 2) are consistent with the formation of a common complex **1-Yb(OPPh$_3$)$_x$** in solution, which is in equilibrium with n-x equivalents of Ph$_3$PO in solution. The Ph$_3$PO ligand ^{1}H resonances in **1-Yb(OPPh$_3$)$_2$** are intermediate of that of free Ph$_3$PO and **1-Yb(OPPh$_3$)**.

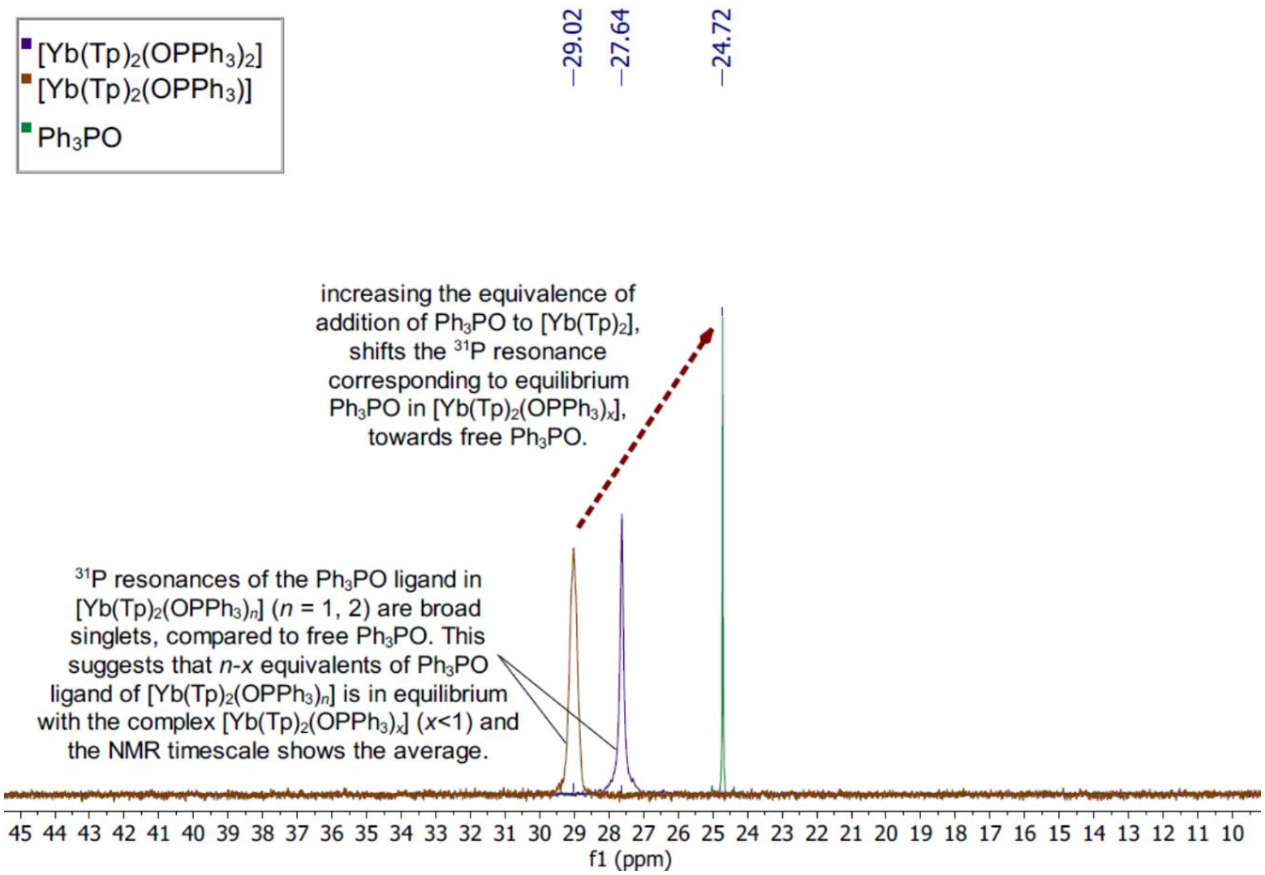

Figure S 42. Overlay of the ^{31}P NMR spectra of [Yb(Tp)$_2$(OPPh$_3$)$_n$] **1-Yb(OPPh$_3$)$_n$** (n = 1, 2), and Ph$_3$PO, recorded in d_6-benzene. The overlay demonstrates that the complexes **1-Yb(OPPh$_3$)$_n$** (n = 1, 2) result in an equilibrium between the complex **1-Yb(OPPh$_3$)$_x$** with n-x equivalents of Ph$_3$PO in solution, resulting in the broad line shapes of the ^{31}P singlet resonances corresponding to the Ph$_3$PO ligands. The Ph$_3$PO ligand ^{31}P resonance in **1-Yb(OPPh$_3$)$_2$** is intermediate of that of free Ph$_3$PO and **1-Yb(OPPh$_3$)**.

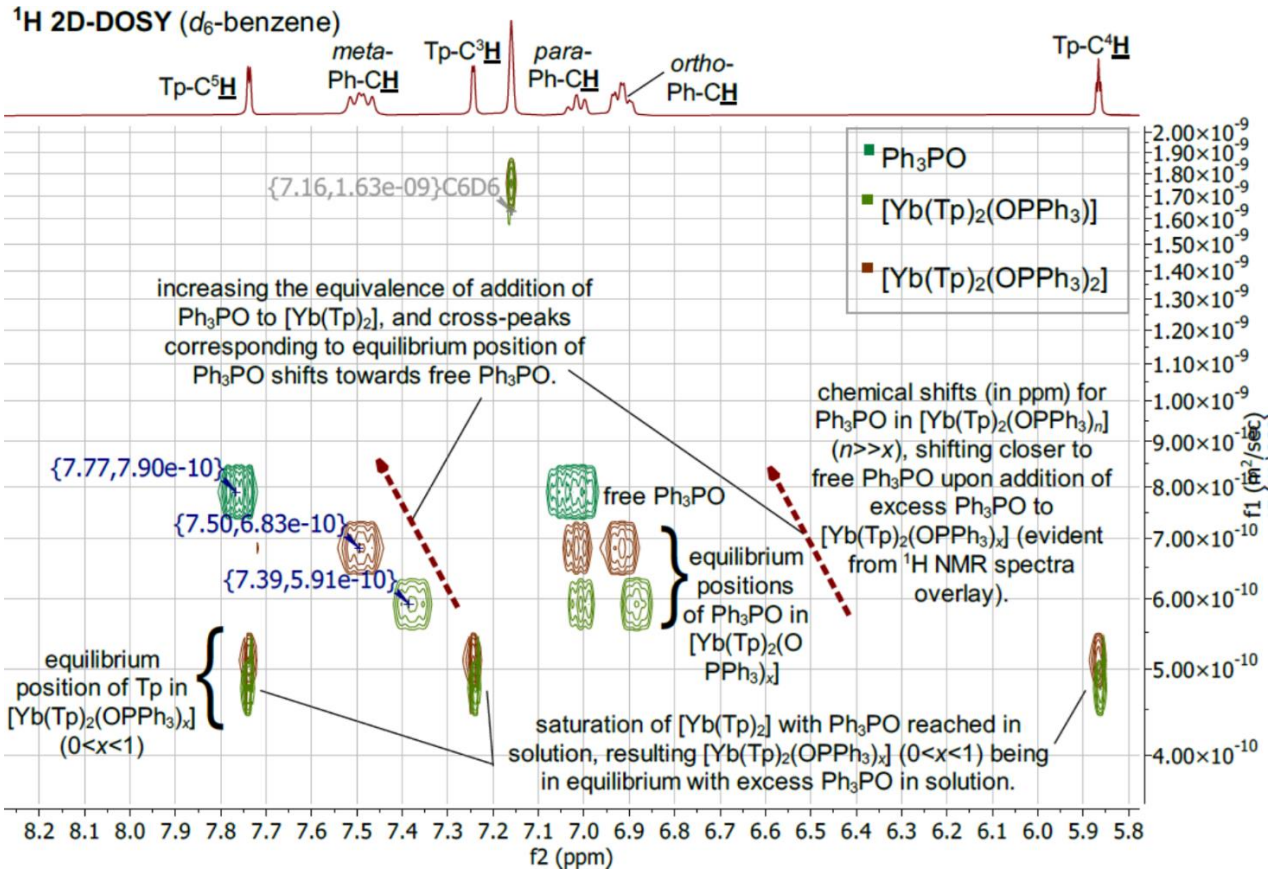

Figure S 43. Overlay of the ^{1}H 2D-DOSY NMR spectra of Ph_3PO and $[Yb(Tp)_2(OPPh_3)_n]$ **1-Yb(OPPh$_3$)$_n$** (n = 1, 2), recorded in d_6-benzene. The horizontal scale shows ^{1}H chemical shifts (ppm) (^{1}H NMR resonances for **1-Yb(OPPh$_3$)$_2$**) and the vertical dimension the diffusion scale (m^2s^{-1}). The three similar Tp-C<u>H</u> resonances of **1-Yb(OPPh$_3$)$_n$** (n = 1, 2) are consistent with the formation of a common complex **1-Yb(OPPh$_3$)$_x$** in solution, which is in equilibrium with n-x equivalents of Ph_3PO in solution. The Ph_3PO ligand cross-peaks in **1-Yb(OPPh$_3$)$_2$** are intermediate of that of free Ph_3PO and **1-Yb(OPPh$_3$)**. Therefore, in the complex **1-Yb(OPPh$_3$)$_x$** and $0<x<1$ Ph_3PO ligands and $0<x<1$ in solution.

S2 Infrared (IR) data

S2.1 [{Eu(Tp)$_2$}$_2$] 1-Eu and [Yb(Tp)$_2$] 1-Yb

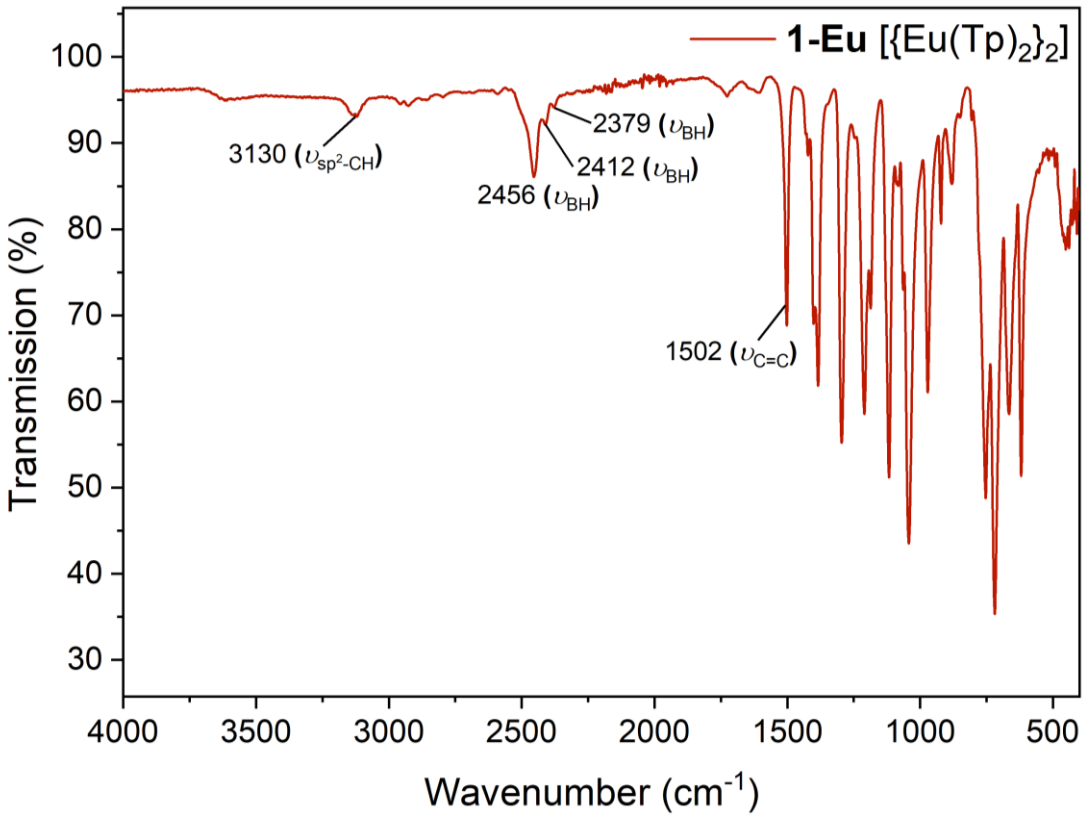

Figure S 44. ATR-IR spectrum of [{Eu(Tp)$_2$}$_2$] **1-Eu**.

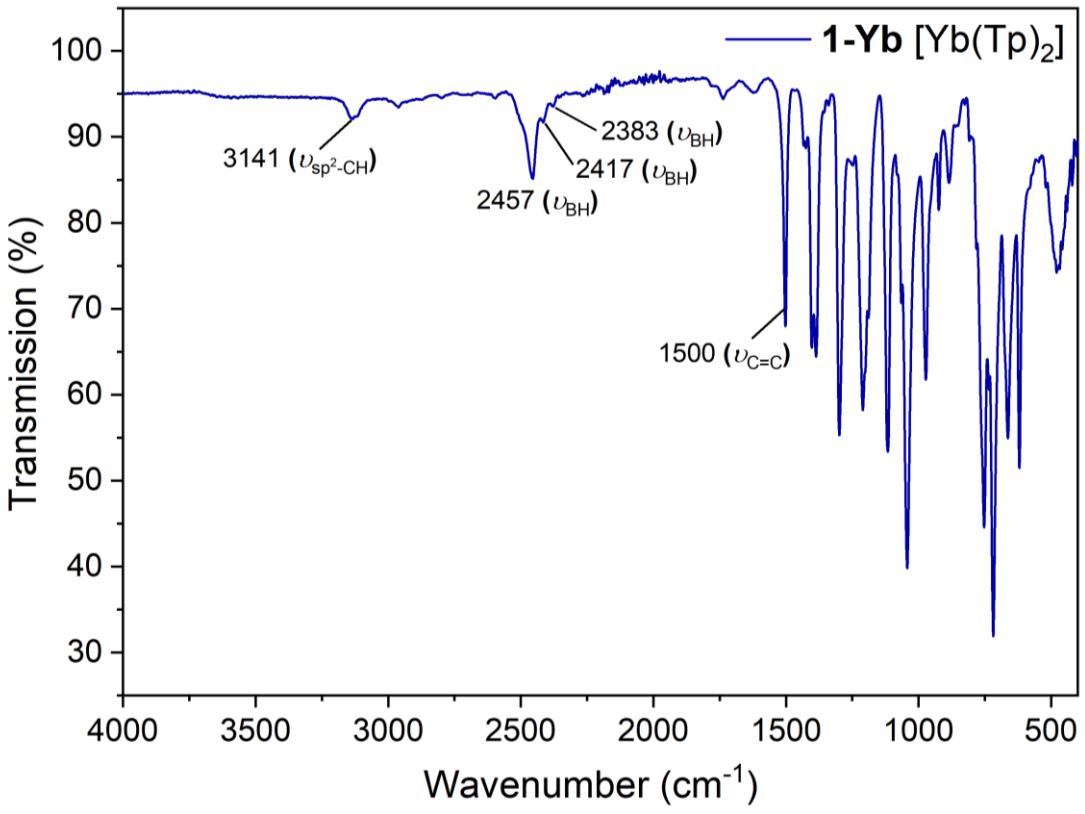

Figure S 45. ATR-IR spectrum of [Yb(Tp)$_2$] **1-Yb**.

S2.2 $[Ln(Tp)_2(OPPh_3)_2]$ 1-$Ln(OPPh_3)_2$ (Ln = Eu, Yb)

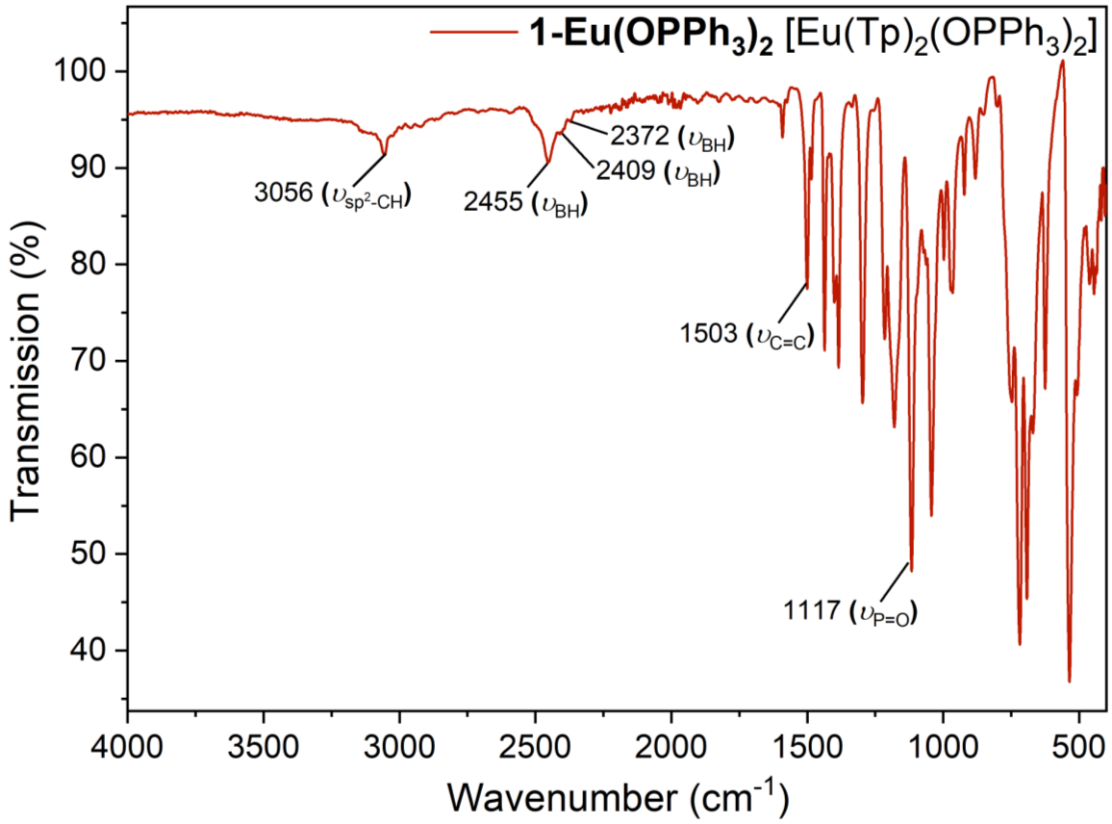

Figure S 46. ATR-IR spectrum of $[Eu(Tp)_2(OPPh_3)_2]$ **1-Eu(OPPh$_3$)$_2$**.

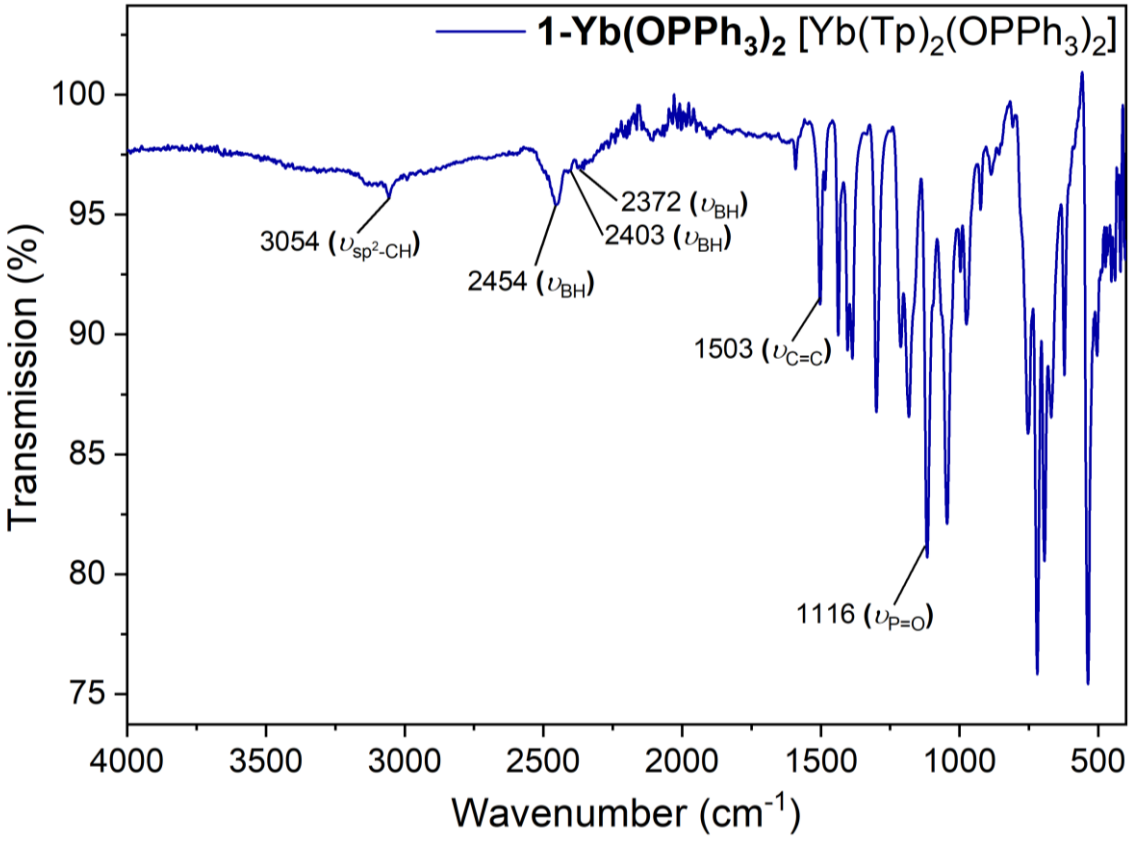

Figure S 47. ATR-IR spectrum of $[Yb(Tp)_2(OPPh_3)_2]$ **1-Yb(OPPh$_3$)$_2$**.

S2.3 [Y(Tp)$_2$(μ-OTf)$_2$K(18-crown-6)] 2-Y

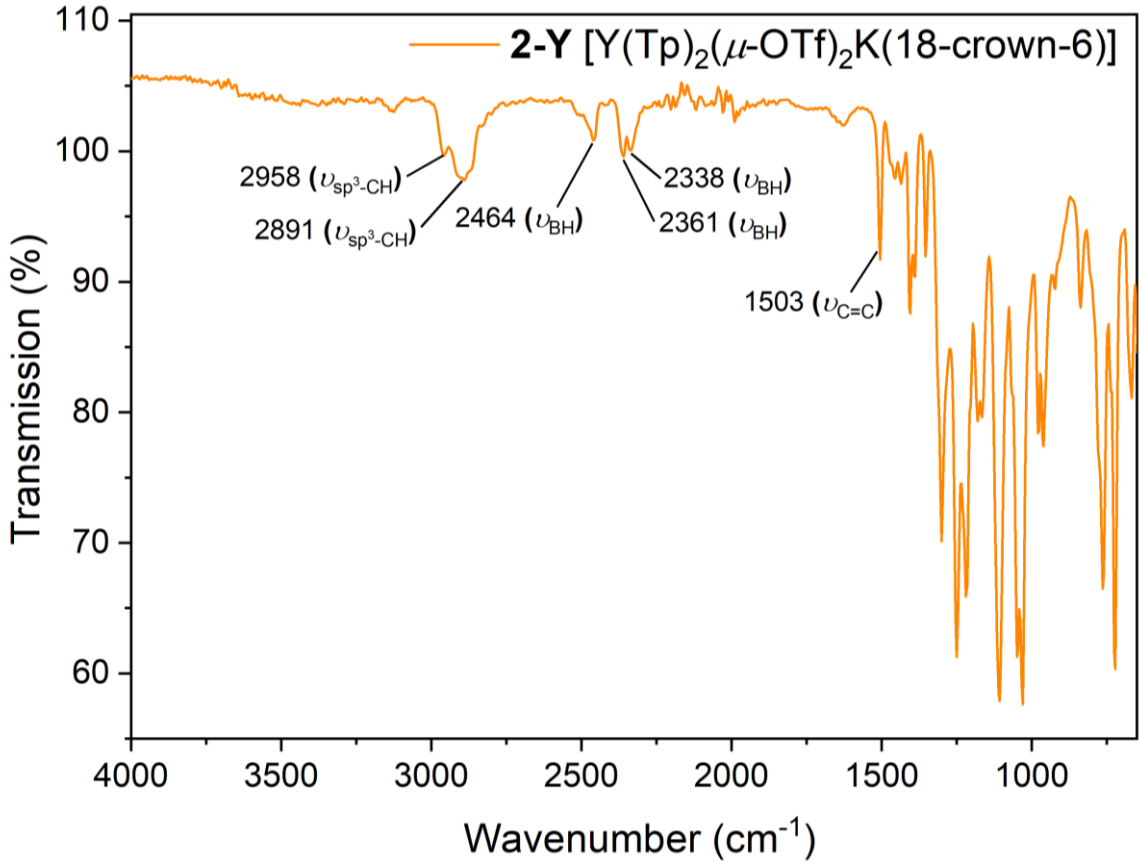

Figure S 48. ATR-IR spectrum of [Y(Tp)$_2$(μ-OTf)$_2$K(18-crown-6)] **2-Y**.

S3 Electronic spectroscopy

Experimental protocol for electronic spectroscopic measurements

1. Instrumentation and software details: Electronic absorption (UV/vis/NIR) and excitation-emission matrix (EEM) spectra were collected using a Horiba Duetta Bio fluorimeter. Data was obtained in and exported from the EZSpec™ software package and treated in the Origin 2020 software package to create the graphical representations of the data collected.

2. Sample preparation: Fine white Celite® powder was stored in a Binder ED53 Drying Oven/Hot Air Steriliser (130-135 °C) and dried *in vacuo* (150-200 °C, 10^{-2} mbar, 5-6 h), before taking it into the glovebox. In the glovebox, anhydrous solvents (acetonitrile, toluene, hexane) were filtered across a Celite®-coated frit into a Büchner flask, prior to using them for preparation of sample solutions. The sample solutions were prepared according to the following method. A known mass of compound (*ca* >10 mg) was weighed into a 20 mL scintillation vial and a known amount of the filtered anhydrous solvent added by a 1 mL micropipette. The compound was dissolved in the solvent by closing the lid and shaking the vial. This stock solution was subsequently diluted into other 20 mL scintillation vials with anhydrous solvent to afford the desired concentrations for the measurements. The same 1 mL micropipette was used throughout, to minimise the systematic error in pipetting. The same batch of filtered anhydrous solvent, used for preparing the various concentrations of the sample under investigation, was used as a blank background for the measurements.

3. Cleaning the cuvettes and respective caps: The UV/vis/NIR and EEM data were collected at ambient temperature in 1 cm path-length cuvettes, fitted with either a screw-cap or J. Young's (JY) Teflon seal. Cuvettes (screw-cap and JY) were cleaned by disposing off any sample solutions in them (after measurements) and rinsing with acetone, then water and then finally with concentrated HCl (6 M) *e.g.*, in the acid bath. After soaking the immersed cuvettes in the acid bath for 5-10 minutes, the cuvettes were cleaned with water again, followed by an acetone rinse and subsequently air-dried. When HCl was unable to clean the cuvettes concentrated HNO_3 acid was used instead. Caution must be observed when handling concentrated HNO_3 acid. The concentrated HNO_3 acid was pipetted into the cuvettes and soaked for 10-15 minutes, before the acid was disposed of by diluting it into the sink with copious amounts of cold water. The screw caps were cleaned by cycles of rinsing with acetone first, then water, then acetone again, followed by air-drying. The JY Teflon-seals were cleaned by soaking a kimwipe™ with acetone and gently wiping the seal, followed by air-drying.

4. Checking for cross-contamination prior to measurements: The empty air-dried screw-cap or J. Young's (JY) cuvettes were sealed and placed within the sample holder of the fluorimeter. To ensure the exclusion of light from the measurement, black cloth was placed over the instrument and taped in place (the instrument hatch cannot be closed on the JY cuvettes due to their height). Emission spectra were recorded at various chosen wavelengths, with a set of optimised parameters

based on the possible contaminants, to detect residual contamination. For example, to detect trace metal ions such as Eu^{3+} excitation in the UV was used and emission in the region 612-614 nm monitored. The specific parameters used for detecting trace Eu^{3+} were: emission range = 400-1000 nm, excitation wavelengths = 200 nm, 220 nm and 395 nm, band passes for both excitation and emission = 10 nm, integration time = 0.50 s, number of detector accumulations = 1. If there was any emission, then the cuvette underwent the same cleaning protocol described above again. However, if only baseline/noise was seen in the emission spectrum, the cuvette was deemed to be clean and used for measurements.

5. Cuvettes for the solutions: Once the cuvettes were clean, the measurements were undertaken using the same type of cuvettes, either using screw-cap cuvettes for both the sample and the blank or the JY for both, to maintain consistency. For low sample concentrations and air-sensitive samples, the JY cuvettes were preferentially used. The sample solution and the blank were taken up into the desired cuvettes using a pipette (*ca* 3-4 mL), respectively and then the two cuvettes sealed inside the glovebox and cycled out of the glovebox for measurements.

6. Parameters for obtaining absorption data: Absorption (UV/vis/NIR) data were collected and referenced against a solvent blank in a matched cuvette. Absorption data (in **Sections 3.1** and **3.2**) were collected using the parameters: range = 200-1000 nm, step increment = either 1 or 2 nm (1 nm for high resolution and more data points), excitation band pass = 5 nm, integration time = 0.05 s, number of repetitions = 1 (time between repetitions = 0 s), resolution of 0.5 nm, detector binning = 1 pixel. Samples were measured at concentrations of <500 μM for absorption data and respective absorptions were kept below 1.0 to ensure that the Beer-Lambert-Law ($A = \varepsilon cL$; A = absorbance, ε = molar extinction/attenuation coefficient, c = concentration, L = path-length) was operational.

For excitation and emission data, low concentrations resulting in absorptions <0.1 were used to minimise inner filter effects. Further details of experimental parameters are listed along with the data in the respective figure captions in **Section 3.2**.

S3.1 Electronic absorption (UV-Vis-NIR) data

S3.1.1 [{Eu(Tp)$_2$}$_2$] 1-Eu and [Yb(Tp)$_2$] 1-Yb in MeCN

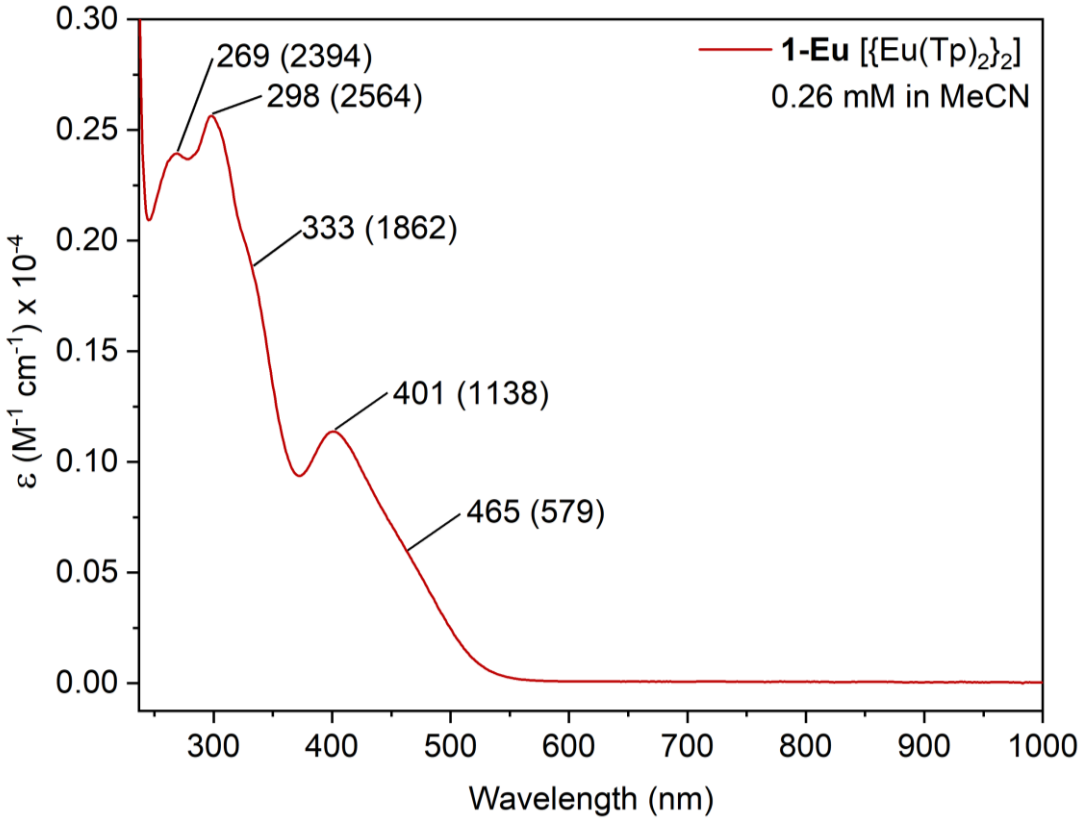

Figure S 49. UV-vis-NIR spectrum of [{Eu(Tp)$_2$}$_2$] **1-Eu**, recorded in MeCN (0.26 mM).

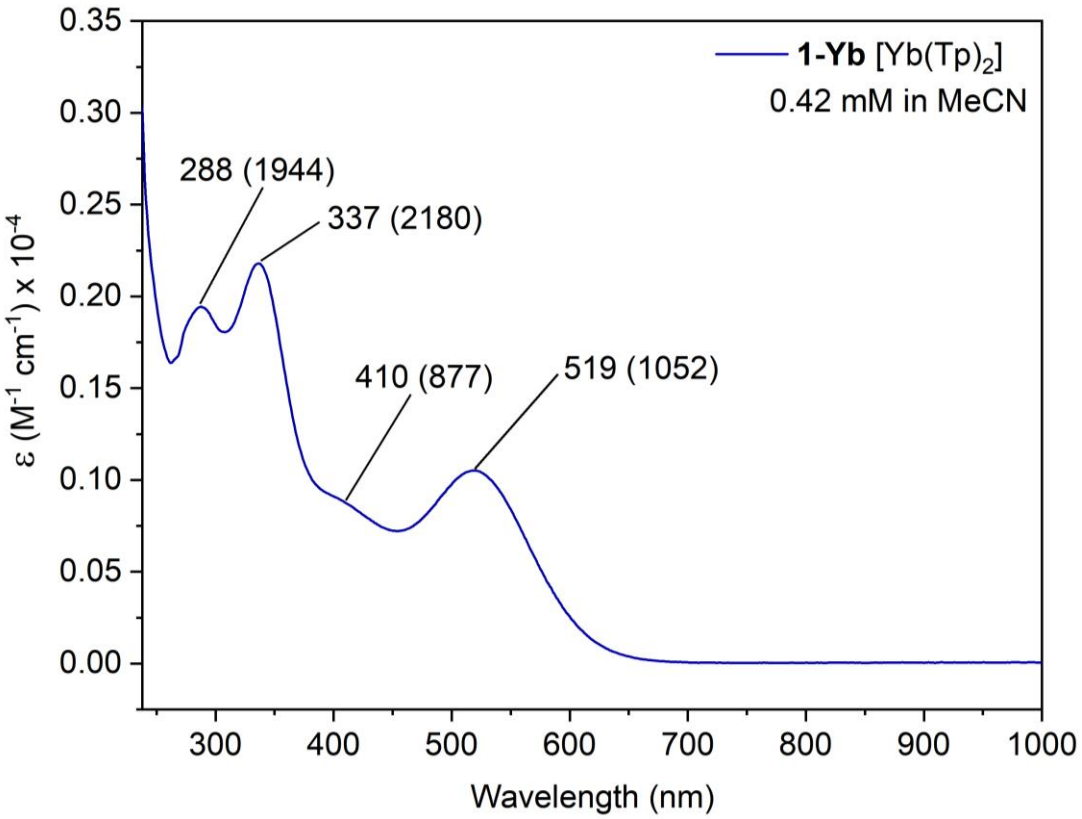

Figure S 50. UV-vis-NIR spectrum of [Yb(Tp)$_2$] **1-Yb**, recorded in MeCN (0.42 mM).

S3.1.2 [{Eu(Tp)$_2$}$_2$] 1-Eu and [Yb(Tp)$_2$] 1-Yb in toluene

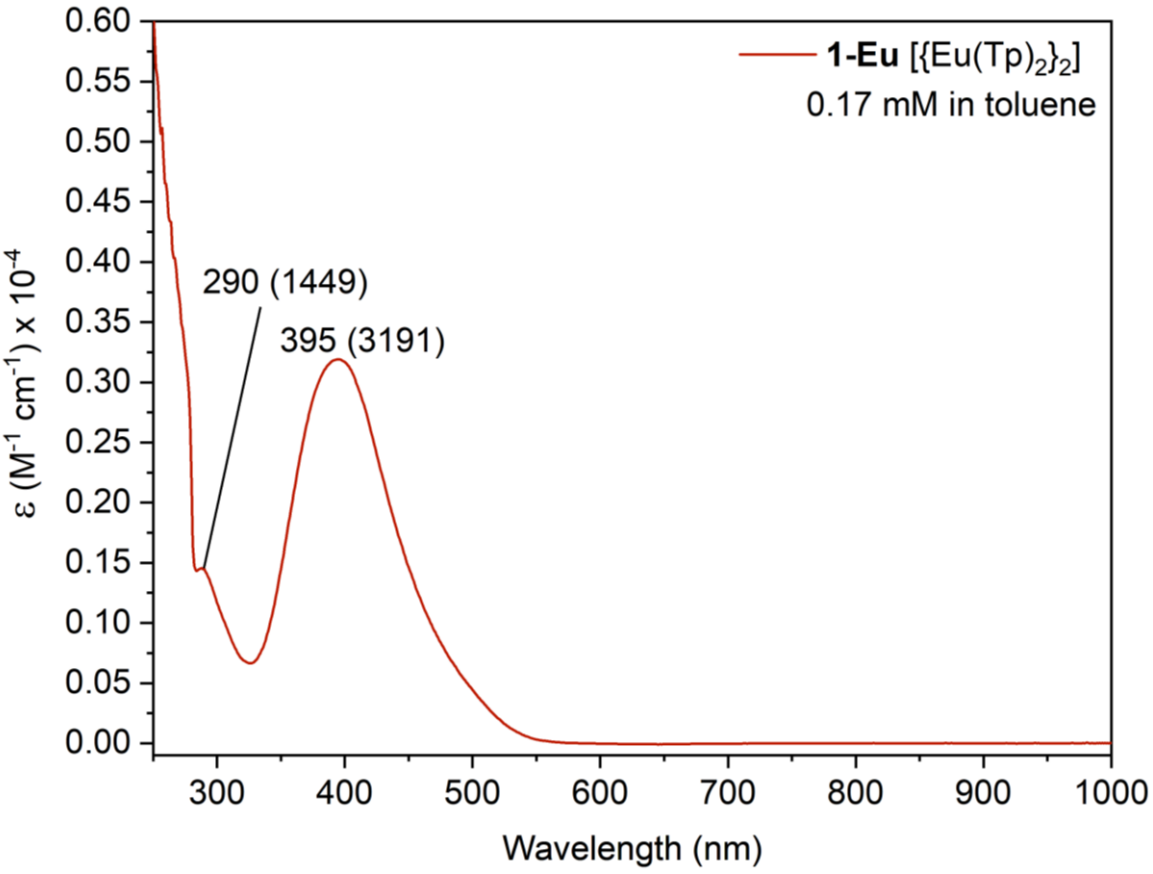

Figure S 51. UV-vis-NIR spectrum of [{Eu(Tp)$_2$}$_2$] **1-Eu**, recorded in toluene (0.17 mM).

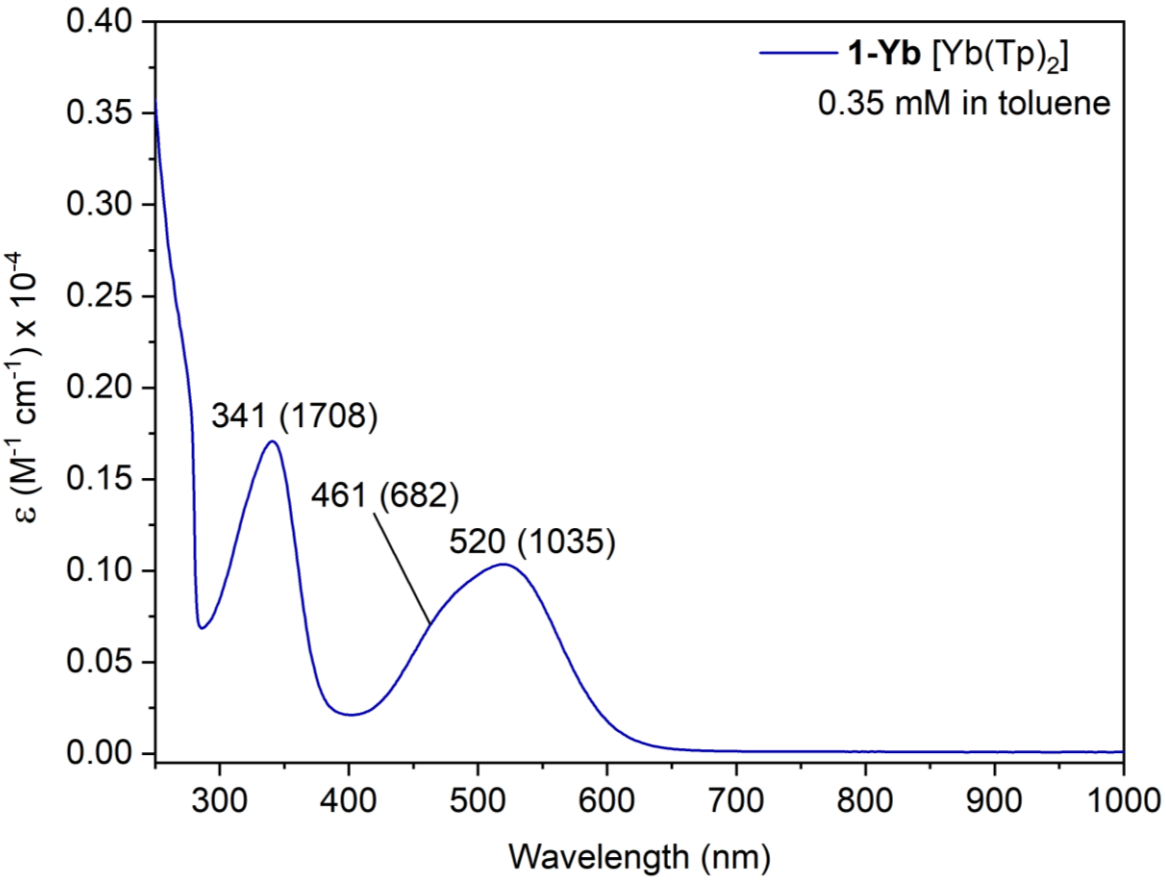

Figure S 52. UV-vis-NIR spectrum of [Yb(Tp)$_2$] **1-Yb**, recorded in toluene (0.35 mM).

S3.1.3 [{Eu(Tp)$_2$}$_2$] 1-Eu and [Yb(Tp)$_2$] 1-Yb in hexane

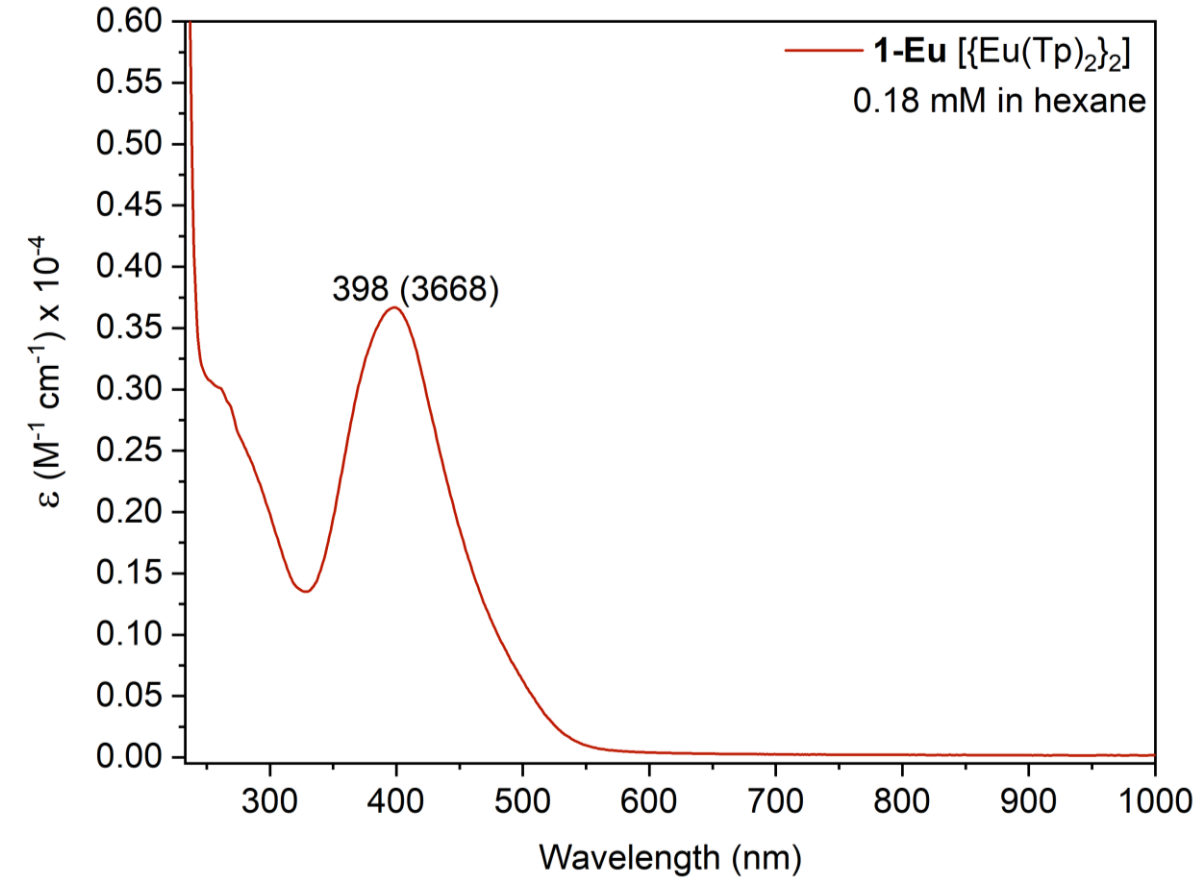

Figure S 53. UV-vis-NIR spectrum of [{Eu(Tp)$_2$}$_2$] **1-Eu**, recorded in hexane (0.18 mM).

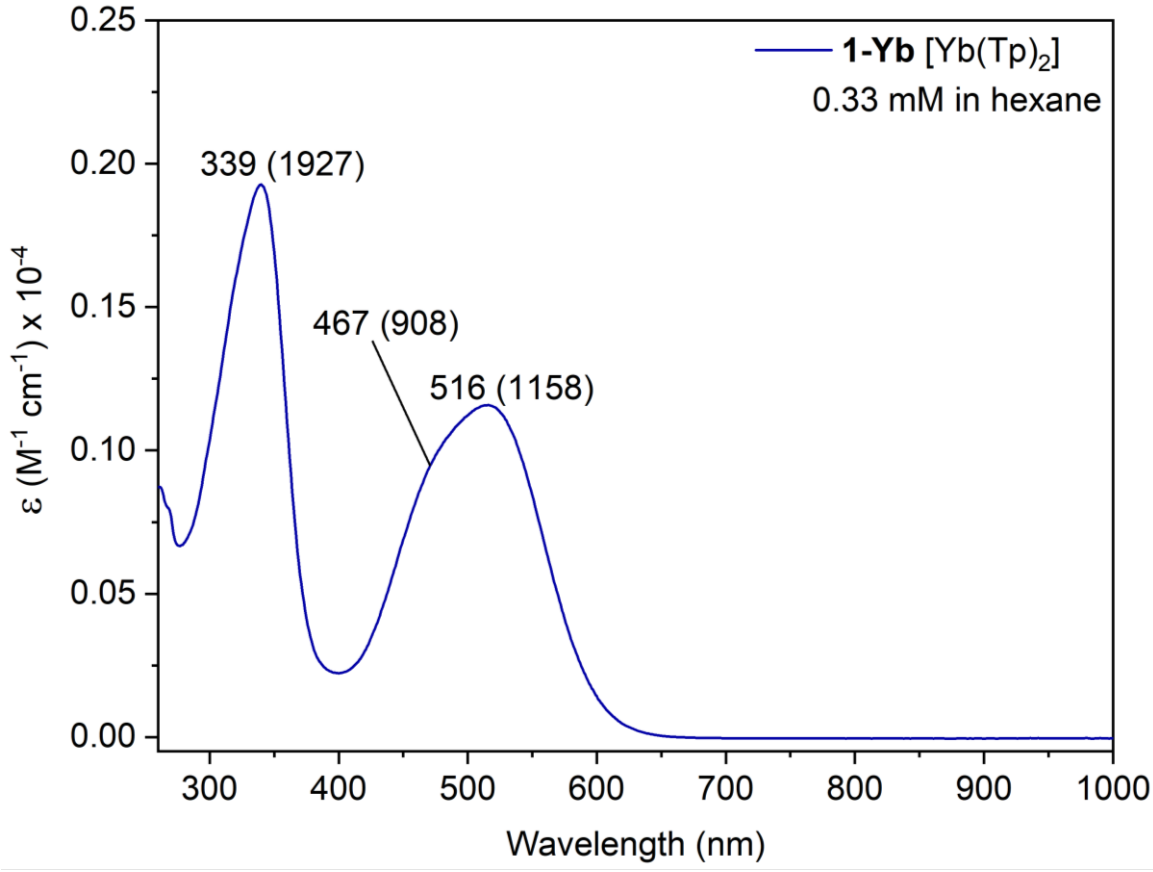

Figure S 54. UV-vis-NIR spectrum of [Yb(Tp)$_2$] **1-Yb**, recorded in hexane (0.33 mM).

S3.1.4 $[Ln(Tp)_2(OPPh_3)_2]$ 1-$Ln(OPPh_3)_2$ (Ln = Eu, Yb) in MeCN

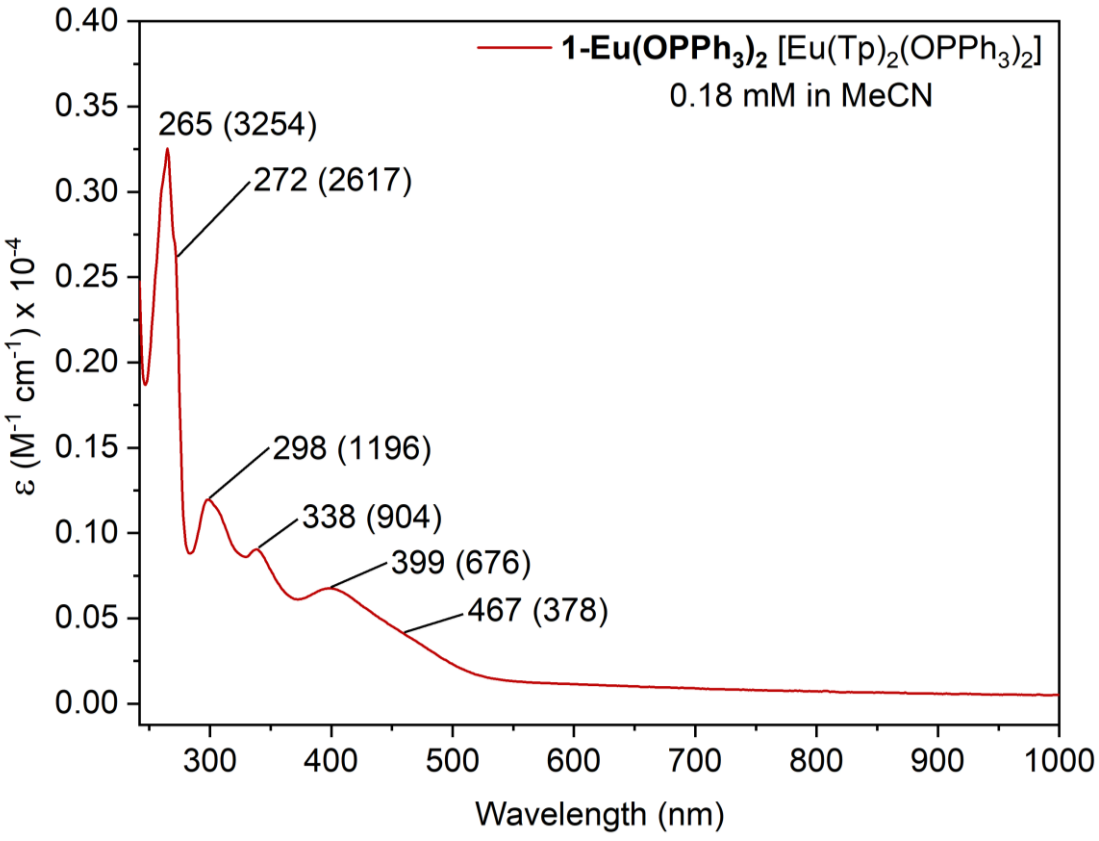

Figure S 55. UV-vis-NIR spectrum of $[Eu(Tp)_2(OPPh_3)_2]$ **1-$Eu(OPPh_3)_2$**, recorded in MeCN (0.18 mM).

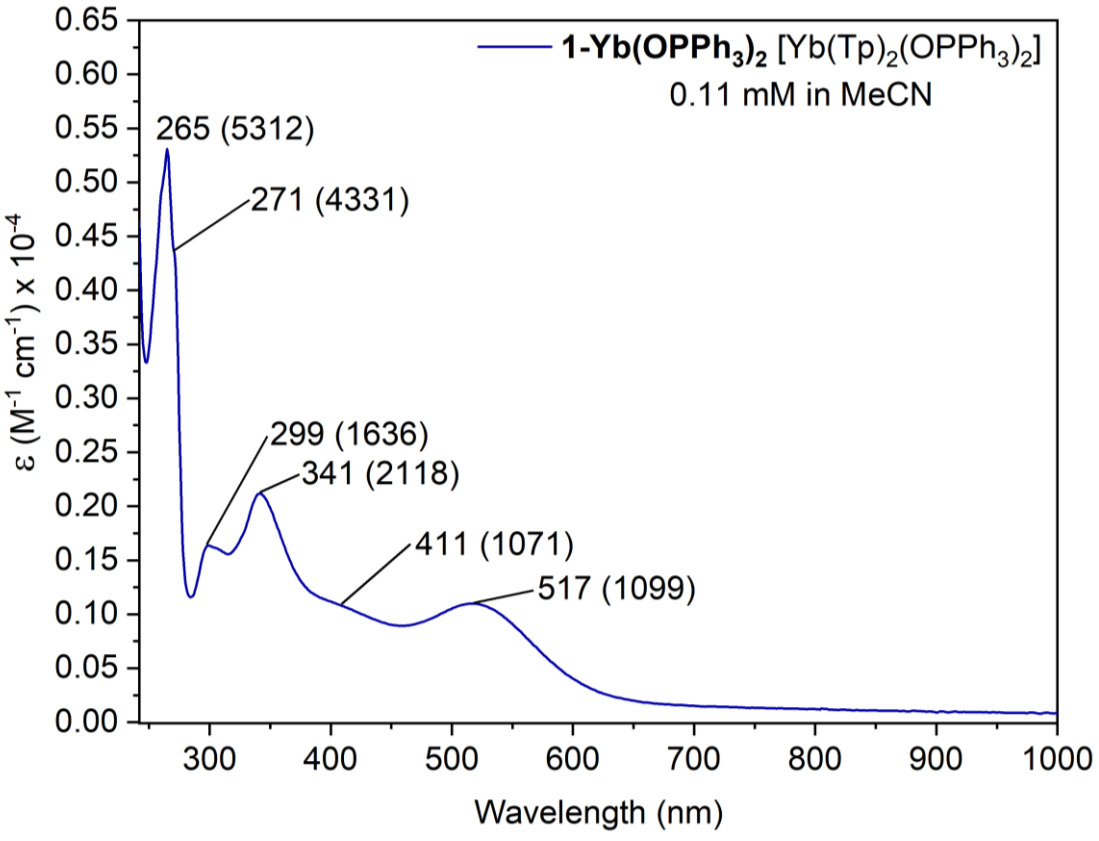

Figure S 56. UV-vis-NIR spectrum of $[Yb(Tp)_2(OPPh_3)_2]$ **1-$Yb(OPPh_3)_2$**, recorded in MeCN (0.11 mM).

Table 3. Complied data and assignments of the absorbance spectra of **1-Ln** (Ln = Eu, Yb) and **1-Ln(OPPh$_3$)$_2$** complexes in a range of solvents.

Complex	Solvent	λ_{max}/nm (ε/M^{-1}cm^{-1})							
		4f-5d transition envelopes of Ln(II)						π-π* transitions of Ph_3PO	
1-Eu	Toluene	-	290 (1449)	-	395 (3191)	-	-	-	-
1-Eu	Hexane	-	-	-	398 (3668)	-	-	-	-
1-Eu	MeCN	269 (2394)	298 (2564)	333 (1862)	401 (1138)	465 (579)	-	-	-
1-Eu(OPPh$_3$)$_2$	MeCN	-	298 (1196)	338 (904)	399 (676)	467 (378)	-	265 (3254)	272 (2617)
1-Yb	Toluene	-	-	341 (1708)	-	461 (682)	520 (1035)	-	-
1-Yb	Hexane	-	-	339 (1927)	-	467 (908)	516 (1158)	-	-
1-Yb	MeCN	-	288 (1944)	337 (2180)	410 (877)	-	519 (1052)	-	-
1-Yb(OPPh$_3$)$_2$	MeCN	-	299 (1636)	341 (2118)	411 (1071)	-	517 (1099)	265 (5312)	271 (4331)

S3.2 Photoluminescence data for [{Eu(Tp)$_2$}$_2$] 1-Eu in toluene

S3.2.1 Excitation-Emission data for 1-Eu 0.17 mM in toluene

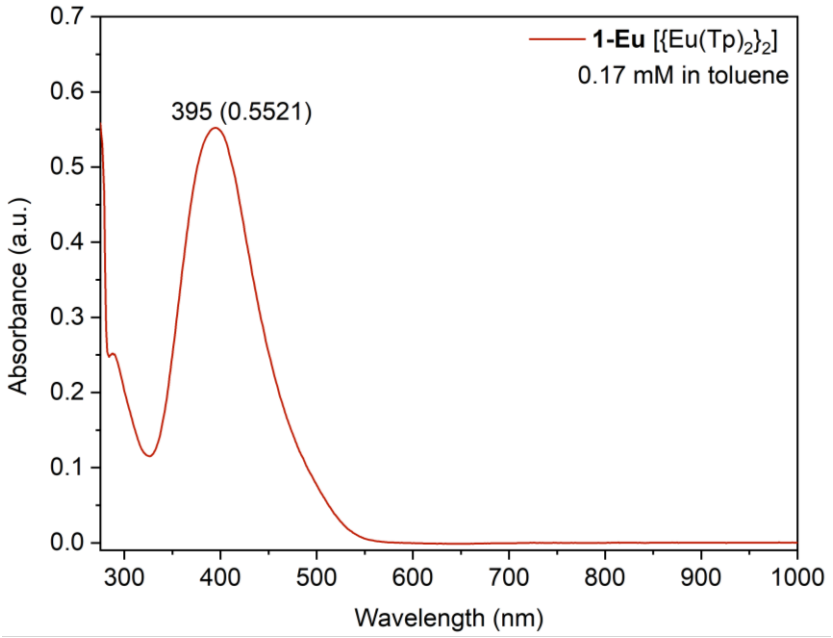

Figure S 57. UV-vis-NIR spectrum of [{Eu(Tp)$_2$}$_2$] **1-Eu**, recorded in toluene (0.17 mM), showing the absorbance (in arbitrary units).

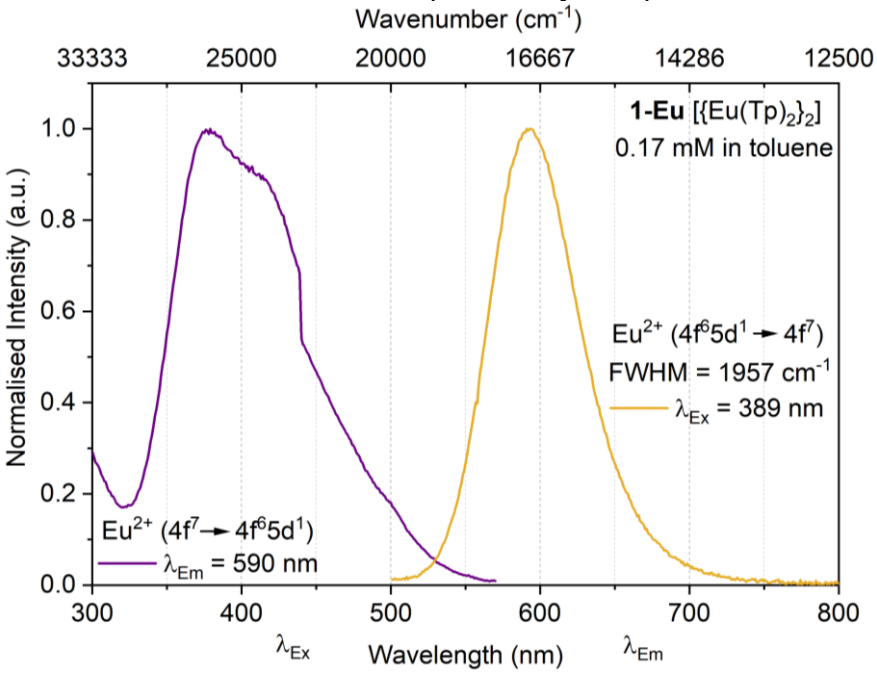

Figure S 58. Excitation (LHS, λ_{Em} = 590 nm) and emission (RHS, λ_{Ex} = 389 nm) spectra of [{Eu(Tp)$_2$}$_2$] **1-Eu**, recorded in toluene (0.17 mM). The steep gradient change around 440 nm in the excitation spectrum is attributed to a filter change in the fluorimeter during the measurement. The Raman scattering from toluene around 420-460nm is not shown as part of the emission spectrum. Emission was collected using excitation at 389 nm, band passes of 5 nm (both excitation and emission), integration time = 1.00 s, number of detector accumulations = 20, number of repetitions = 1 (time between repetitions = 0 s), and the full emission spectrum (420-800 nm) was collected on a CCD detection with a resolution of 1 nm (detector binning = 2 pixels). Excitation was measured by monitoring emission at 590 nm (resolution of 1 nm, detector binning = 2 pixels), with band passes of 10 nm (both excitation and emission), integration time = 1.00 s, number of detector accumulations = 1, number of repetitions = 1 (time between repetitions = 0 s), whilst sweeping excitation between 250 and 570 nm (excitation step increment = 1 nm).

S3.2.2 Excitation-Emission data for 1-Eu 34.6μM in toluene

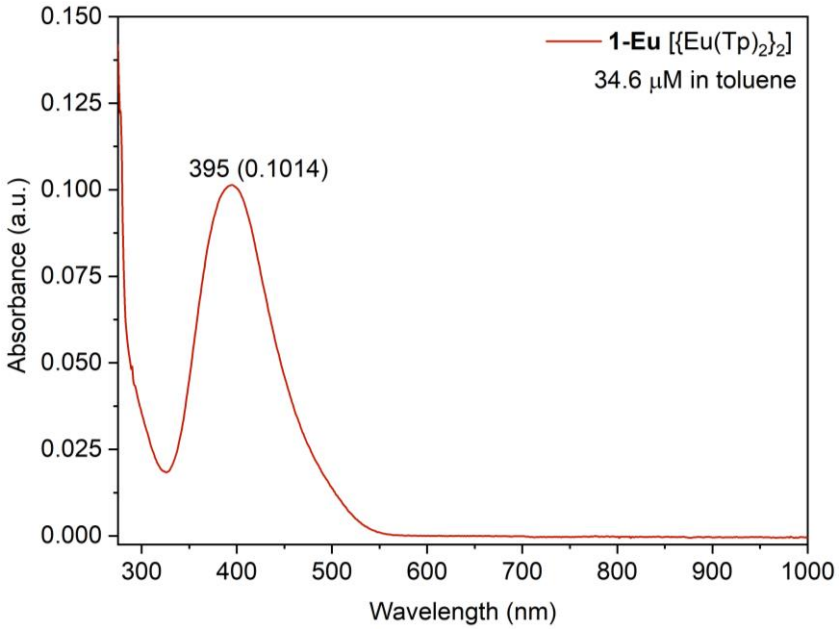

Figure S 59. UV-vis-NIR spectrum of [{Eu(Tp)$_2$}$_2$] **1-Eu**, recorded in toluene (34.6 μM), showing the absorbance (in arbitrary units).

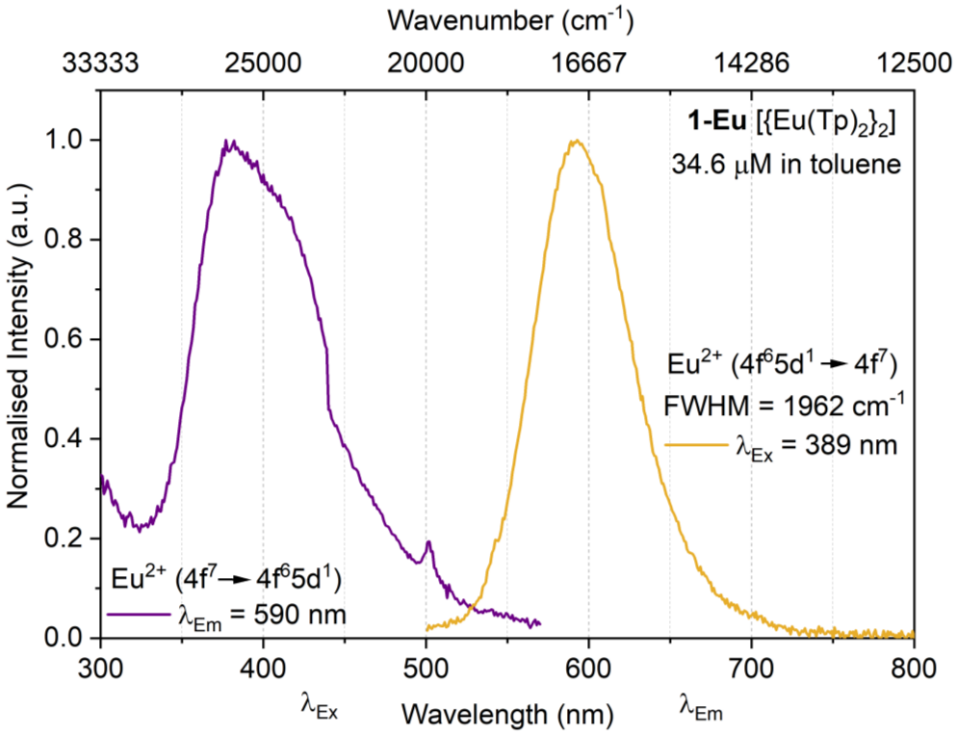

Figure S 60. Excitation (LHS, λ_{Em} = 590 nm) and emission (RHS, λ_{Ex} = 389 nm) spectra of [{Eu(Tp)$_2$}$_2$] **1-Eu**, recorded in toluene (34.6 μM). The steep gradient change around 440 nm in the excitation spectrum is attributed to a filter change in the fluorimeter during the measurement. The Raman scattering from toluene around 420-460nm is not shown as part of the emission spectrum. Emission was collected using excitation at 389 nm, band passes of 5 nm (both excitation and emission), integration time = 1.00 s, number of detector accumulations = 40, number of repetitions = 1 (time between repetitions = 0 s), and the full emission spectrum (420-800 nm) was collected on a CCD detection with a resolution of 1 nm (detector binning = 2 pixels). Excitation was measured by monitoring emission at 590 nm (resolution of 1 nm, detector binning = 2 pixels), with band passes of 5 nm (both excitation and emission), integration time = 1.00 s, number of detector accumulations = 10, number of repetitions = 1 (time between repetitions = 0 s), whilst sweeping excitation between 250 and 570 nm (excitation step increment = 1 nm).

S3.2.3 Excitation-Emission matrix (EEM) data for 1-Eu

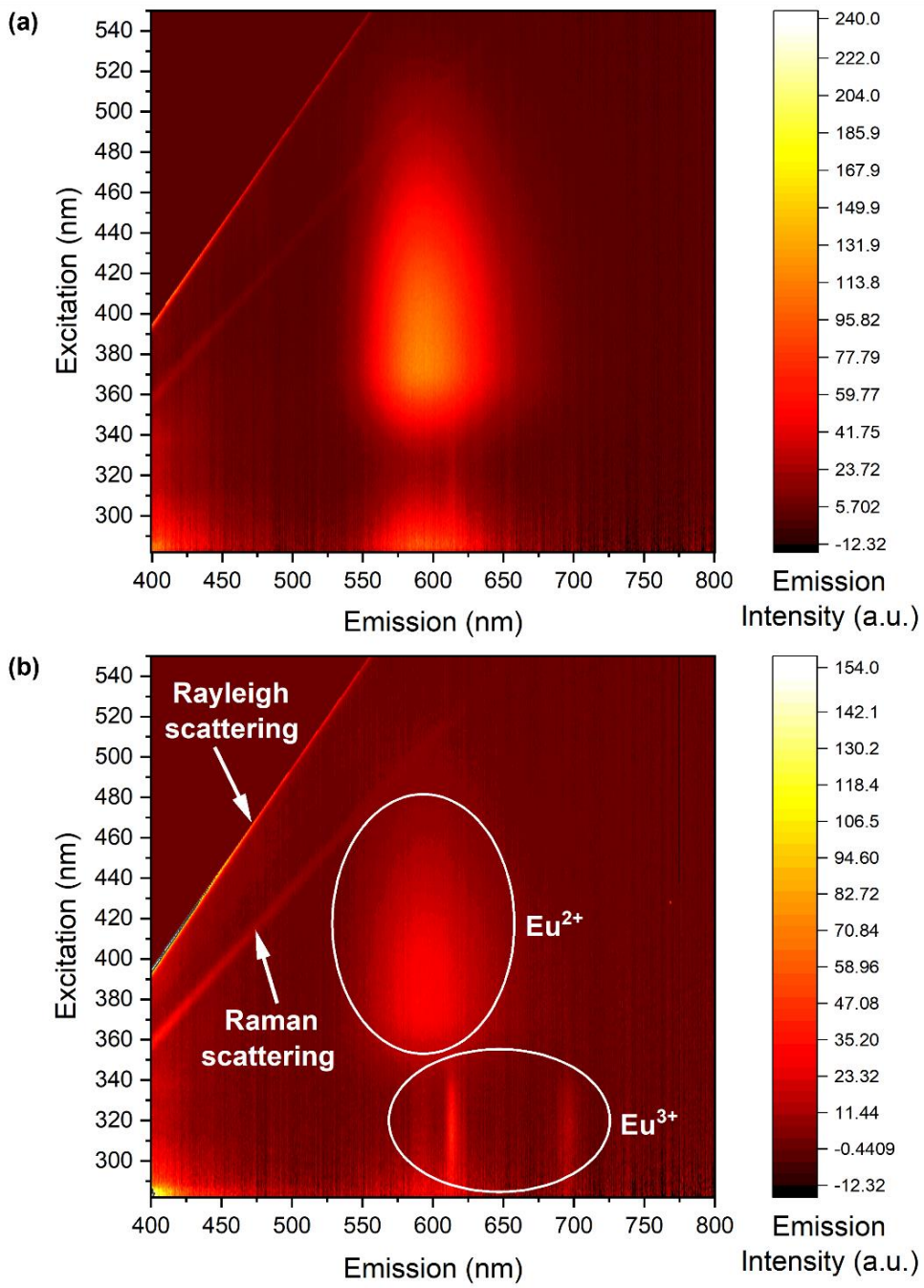

Figure S 61. Contour maps of the excitation-emission matrix (EEM) of [{Eu(Tp)$_2$}$_2$] **1-Eu** in toluene (a) 0.17 mM and (b) 34.6 μM. All data have been treated to mask the Rayleigh scattering of the excitation light (by using a bandpass sum width of 5 nm). Slight traces of Rayleigh and Raman scattering are observed, indicated by the two diagonal lines from the lower left to the upper right of both images, highlighted in (b). The regions showing Eu^{2+} and Eu^{3+} emissions are highlighted in (b), and it is of note that the Eu^{3+} emission in the low concentrated sample (34.6 μM) arises from moisture-mediated decomposition of **1-Eu** due to very small (< 2 ppm) residual water levels in the anhydrous solvent. A colour scale has been included in both cases for the emission intensities (in arbitrary units), with the yellow in the colour scale representing higher intensity and the dark orange/red representing lower intensity. The EEM data were obtained using the following parameters: Emission was collected on a CCD detector in the range of 400-800 nm with a resolution of 0.5 nm (detector binning = 1 pixel), whilst sweeping the excitation light between 250 and 550 nm, using band passes of 5 nm (both excitation and emission), integration time = 0.50 s, number of detector accumulations = 1, number of repetitions = 1 (time between repetitions = 0 s), excitation range step increment = 1 nm.

S4 Single-crystal X-Ray diffraction (SCXRD) data

CIFs for all structures reported here have been deposited with the CCDC and are available free of charge. The CCDC numbers and selected crystallographic details for all structures are given in **Table 5**. Views of crystal structures are shown below, with selected atom labels; hydrogen atoms are omitted for clarity, carbon atoms of Tp displayed in wireframe and displacement ellipsoids for all other atoms are drawn at 50% probability level. Selected metrics are given in **Table 4**. Specific details for individual structures are provided in the figure captions.

Computing details: (a) Data collection and data reduction: *APEX3* Ver. 2016.9-0;[4] (b) Cell refinement: *SAINT* V8.37A;[4] (c) Program(s) used to solve structure: *SHELXT*;[5] (d) Program(s) used to refine structure: *SHELXL* 2018/3;[5] (e) Molecular graphics: Olex2 1.5;[6] (f) Software used to prepare material for publication: Olex2 1.5,[6] Mercury.[7]

Table 4. Selected metrics for the [{Eu(Tp)$_2$}$_2$] **1-Eu**, [Yb(Tp)$_2$] **1-Yb**, [Ln(Tp)$_2$(LB)$_x$] **1-Ln(LB)$_x$** (Ln = Eu, Yb; LB = neutral Lewis bases THF, DME, Ph$_3$PO) and **2-Y** complexes.

Complex	Ln–O bond lengths (Å)	Ln–N(Tp) bond lengths (Å)	P=O bond lengths (Å)	B(Tp)-Ln-B(Tp) angles (°)	X-Ln-X angles (°)
1-Eu	-	κ^3-Tp: 2.591(3)-2.692(3); μ-κ^1-Tp: Eu1–N7 2.636(3), Eu1–N9' 2.815(3), Eu1–N11' 2.704(3); Eu–pz$_{centroid}$(Tp) 2.790	-	124.1-128.5	-
1-Eu(THF)$_2$ (with lattice THF)	Eu–O(THF) 2.683(6)	2.647(8)-2.743(10)	-	128.0	89.8(3) (O of two THF)
1-Eu(THF)$_2$ (without lattice THF)	Eu–O(THF) 2.6361(13)	2.6438(14)-2.7696(14)	-	154.17	126.86(6) (O of two THF)
1-Eu(OPPh$_3$)$_2$	Eu–O(OPPh$_3$) 2.530(6)-2.630(7)	2.686(7)-2.807(7)	1.477(6)-1.487(6)	132.4, 140.9	85.1(2), 87.0(2) (O of two OPPh$_3$)
1-Yb	-	2.455(9)-2.519(9)	-	166.7, 168.9	-
1-Yb(THF)	Yb–O(THF) 2.494(2)	2.481(2)-2.595(2)	-	165.25	-
1-Yb(DME)	Yb–O(DME) 2.559(3)-2.614(3)	2.496(3)-2.629(3)	-	127.63, 132.0	63.26(9)-63.66(10) (two O of DME)
1-Yb(OPPh$_3$)	Yb–O(OPPh$_3$) 2.381(3)	2.524(4)-2.616(3)	1.486(3)	140.6	-
2-Y	Y–O(OTf) 2.331(7)-2.351(6)	2.425(9)-2.524(8)	-	132.8-134.8	76.7(2)-79.6(2) (O of two OTf)

Table 5. Crystallographic data for complexes [{Eu(Tp)$_2$}$_2$] **1-Eu**, [Yb(Tp)$_2$] **1-Yb**, [Eu(Tp)$_2$(THF)$_2$] **1-Eu(THF)$_2$** (two solvates), [Yb(Tp)$_2$(THF)] **1-Yb(THF)**, [Yb(Tp)$_2$(DME)] **1-Yb(DME)**, [Ln(Tp)$_2$(OPPh$_3$)$_n$] **1-Ln(OPPh$_3$)$_n$** (Ln = Eu, n = 2; Yb, n = 1), [Y(Tp)$_2$(μ-OTf)$_2$K(18-crown-6)] **2-Y**, and the separated ion pair [K(2.2.2-cryptand)][Al(NON^{Dipp})].

CCDC No.	**2161063**	**2161064**	**2161065**
Parameter	**1-Eu**	**1-Eu(THF)$_2$** (with lattice THF)	**1-Eu(THF)$_2$** (without lattice THF)
Formula	$C_{36}H_{40}B_4Eu_2N_{24}\cdot 3(C_7H_8)$	$C_{26}H_{36}B_2EuN_{12}O_2\cdot C_4H_8O$	$C_{26}H_{36}B_2EuN_{12}O_2$
*F*w	1432.48	794.35	722.25
Colour and shape	Tablet, yellow	Block, yellow	Block, yellow
Dimensions (mm)	0.13 × 0.06 × 0.02	0.13 × 0.06 × 0.03	0.16 × 0.13 × 0.06
Crystal System	Triclinic	Orthorhombic	Monoclinic
Space group	$P\bar{1}$	$Cmc2_1$	$C2/c$
a (Å)	10.8751(4)	14.5364(6)	10.2076(4)
b (Å)	12.1292(5)	16.0680(6)	15.3147(6)
c (Å)	13.2669(4)	15.1359(8)	20.1892(8)
α (°)	81.942(1)	90	90
β (°)	68.671(1)	90	97.534(1)
γ (°)	73.751(1)	90	90
V (Å^3)	1563.57(10)	3535.3(3)	3128.9(2)
Z	1	4	4
D_x (Mg m^{-3})	1.521	1.492	1.533
No. of reflections measured	27534	16321	26061
No. of independent reflections	7742	4511	3887
No. of reflections with $I > 2\sigma(I)$	6832	3015	3690
R_{int}	0.056	0.084	0.053
R ($F^2 > 2\sigma(F^2)$)	0.039	0.045	0.019
$wR(F^2)$	0.086	0.093	0.046
S	1.08	0.99	1.09
CCDC No.	**2161066**	**2195976**	**2161067**
Parameter	**1-Eu(OPPh$_3$)$_2$**	**1-Yb**	**1-Yb(THF)**
Formula	$C_{54}H_{50}B_2EuN_{12}O_2P_2$ + (solvent)*	$C_{18}H_{20}B_2N_{12}Yb$	$C_{22}H_{28}B_2N_{12}YbO$
*F*w	1134.58	599.12	671.22
Colour and shape	Tablet, yellow	Plate, red	Tablet, red
Dimensions (mm)	0.19 × 0.16 × 0.04	0.12 × 0.09 × 0.02	0.18 × 0.12 × 0.04
Crystal System	Triclinic	Orthorhombic	Monoclinic

Space group	$P\bar{1}$	$P2_12_12$	$P2_1/n$
a (Å)	12.4734(15)	14.2463(8)	8.8930(2)
b (Å)	22.587(3)	12.1041(6)	21.3773(6)
c (Å)	23.443(3)	13.4211(6)	14.6247(4)
α (°)	74.834(4)	90	90
β (°)	89.184(4)	90	104.066(1)
γ (°)	78.004(4)	90	90
V (Å^3)	6230.0(14)	2314.3(2)	2696.91(12)
Z	4	4	4
D_x (Mg m^{-3})	1.210	1.719	1.653
No. of reflections measured	91857	14658	29355
No. of independent reflections	25181	5520	6681
No. of reflections with $I > 2\sigma(I)$	13263	3326	5787
R_{int}	0.212	0.062	0.036
R ($F^2 > 2\sigma(F^2)$)	0.091	0.049	0.023
$wR(F^2)$	0.215	0.107	0.055
S	1.00	1.05	1.06
CCDC No.	**2161068**	**2161069**	**2161070**
Parameter	**1-Yb(OPPh$_3$)**	**1-Yb(DME)**	**2-Y**
Formula	$C_{36}H_{35}B_2N_{12}OPYb$	$C_{22}H_{30}B_2N_{12}O_2Yb\cdot0.25(C_{18}H_{40}F_6K_2O_{14}S_2)$	$C_{32}H_{44}B_2F_6KN_{12}O_{12}S_2Y\cdot1.5(C_7H_8)$
*F*w	877.39	873.44	1254.74
Colour and shape	Rod, red	Tablet, red	Block, yellow
Dimensions (mm)	0.24 × 0.02 × 0.01	0.19 × 0.18 × 0.06	0.11 × 0.08 × 0.07
Crystal System	Triclinic	Triclinic	Triclinic
Space group	$P\bar{1}$	$P\bar{1}$	$P\bar{1}$
a (Å)	11.7840(4)	11.4074(6)	17.124(3)
b (Å)	12.0768(4)	11.9061(6)	18.094(3)
c (Å)	14.8349(5)	27.7046(15)	19.856(3)
α (°)	73.445 (1)	90.550(2)	89.056(7)
β (°)	83.841(1)	95.543(2)	69.647(6)
γ (°)	65.654(1)	99.885(2)	76.348(6)
V (Å^3)	1843.60(11)	3688.3(3)	5590.7(16)
Z	2	4	4
D_x (Mg m^{-3})	1.581	1.573	1.491

No. of reflections measured	52538	74067	100588
No. of independent reflections	9157	18091	22692
No. of reflections with $I > 2\sigma(I)$	7065	16743	9848
R_{int}	0.098	0.037	0.236
R ($F^2 > 2\sigma(F^2)$)	0.042	0.033	0.104
$wR(F^2)$	0.086	0.080	0.316
S	1.03	1.12	1.03
CCDC No.		**2161071**	
Parameter		**[K(2.2.2-cryptand)][Al(NON^{Dipp})] K-Al-SIP**	
Formula		$C_{18}H_{36}KN_2O_6 \cdot C_{28}H_{46}AlN_2OSi_2$	
Fw		925.41	
Colour and shape		Block, yellow	
Dimensions (mm)		0.21 × 0.16 × 0.10	
Crystal System		Monoclinic	
Space group		*C*2/*c*	
a (Å)		19.1041(15)	
b (Å)		16.1012(15)	
c (Å)		19.415(2)	
α (°)		90	
β (°)		116.588(3)	
γ (°)		90	
V (Å^3)		5340.5(9)	
Z		4	
D_x (Mg m^{-3})		1.151	
No. of reflections measured		33752	
No. of independent reflections		6647	
No. of reflections with $I > 2\sigma(I)$		5552	
R_{int}		0.044	
R ($F^2 > 2\sigma(F^2)$)		0.058	
$wR(F^2)$		0.160	
S		1.10	

*SQUEEZE in PLATON was used to determine and account for poorly defined lattice solvent electron density.

S4.1 [{Eu(Tp)$_2$}$_2$] 1-Eu

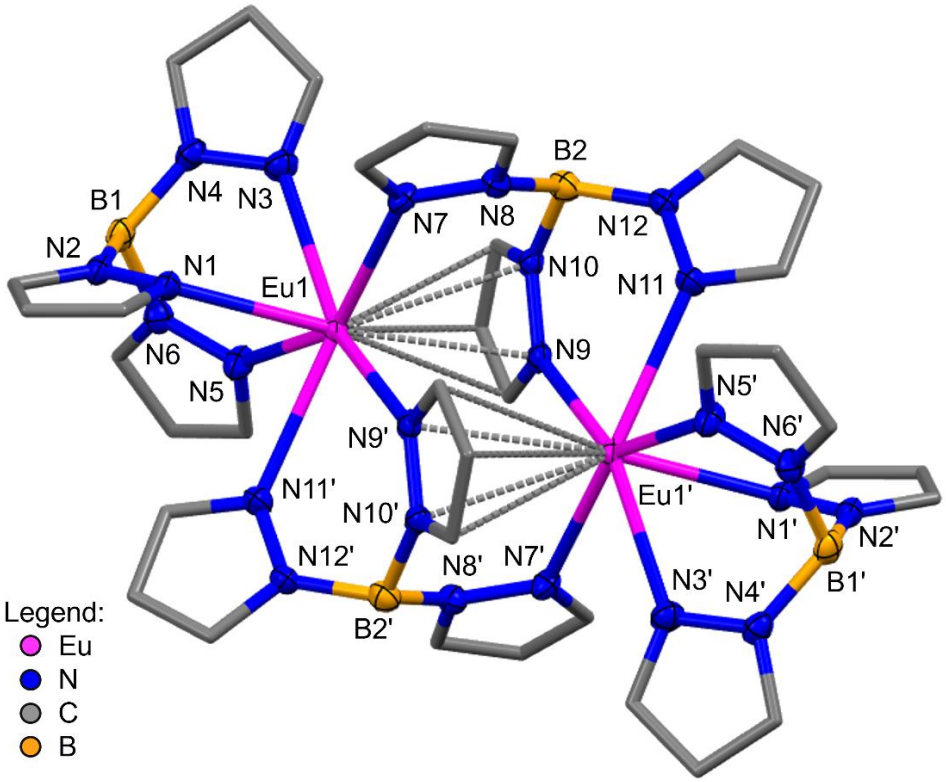

Figure S 62. Molecular structure of **1-Eu**. The dimeric molecule crystallises across an inversion centre with one crystallographically independent Eu site and inversion symmetry completing the dimer. The asymmetric unit contains 0.5 dimer plus 1.5 molecules of toluene, one in a general position and a 0.5 occupied molecule disordered across a second inversion centre; 'prime' atom labels denote symmetry equivalent (1-x, 2-y, 1-z). The lattice toluene is omitted for clarity.

S4.2 [Eu(Tp)$_2$(THF)$_2$] 1-Eu(THF)$_2$ (with and without lattice THF)

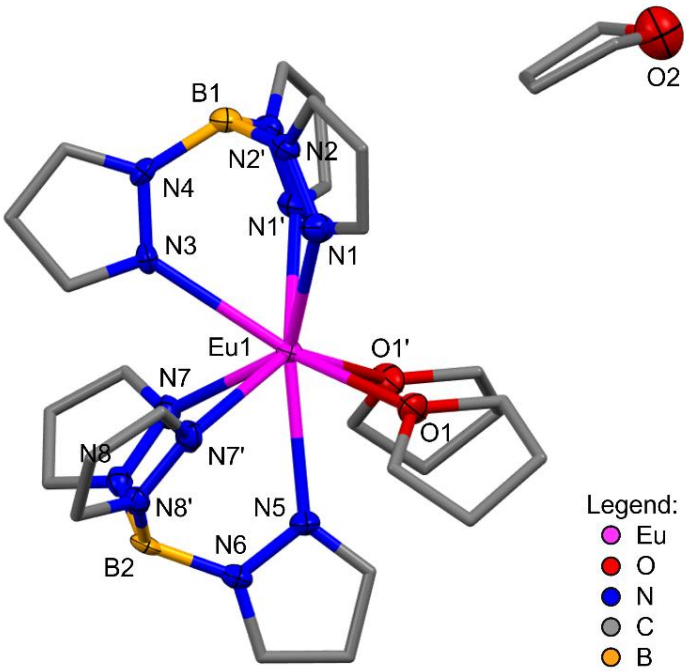

Figure S 63. Molecular structure of **1-Eu(THF)$_2$** (in the presence of lattice THF). The molecule crystallises with the Eu atom lying in a mirror plane, as do one of the pyrazolyl rings of each of the Tp ligands. The asymmetric unit contains 0.5 molecule (2 half Tp ligands, Eu and one coordinated THF) and 0.5 lattice THF molecule; 'prime' atom labels denote symmetry equivalent (-x, y, z).

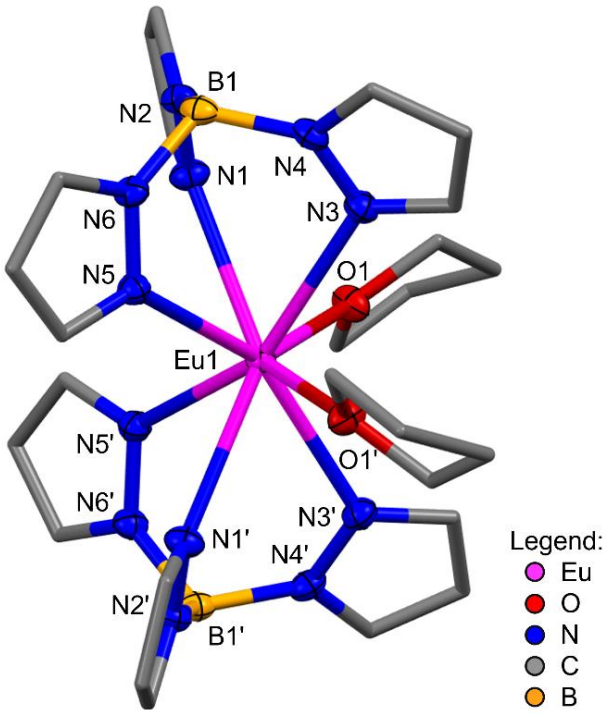

Figure S 64. Molecular structure of **1-Eu(THF)$_2$** (in the absence of lattice THF). The molecule crystallises with the Eu lying on a 2-fold rotation axis and the asymmetric unit contains one Tp and one THF; 'prime' atom labels denote symmetry equivalent (1-x, y, 1.5-z). Disorder present in the THF adduct was modelled over 2 partially occupied sites (0.7:0.3), with the minor component omitted for clarity.

S4.3 [Eu(Tp)$_2$(OPPh3)$_2$] 1-Eu(OPPh$_3$)$_2$

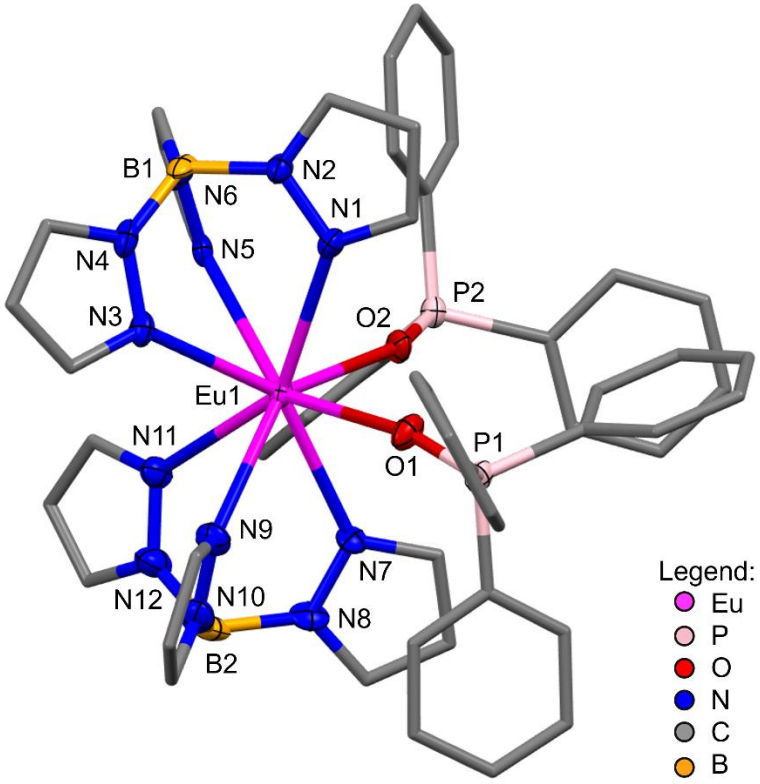

Figure S 65. Molecular structure of **1-Eu(OPPh$_3$)$_2$** showing one of the two crystallographically independent molecules. SQUEEZE was used to calculate and account for some regions of poorly defined solvent; 415 electrons per unit cell which in this case corresponds to 2 molecules of toluene per Eu.

S4.4 [Yb(Tp)$_2$] 1-Yb

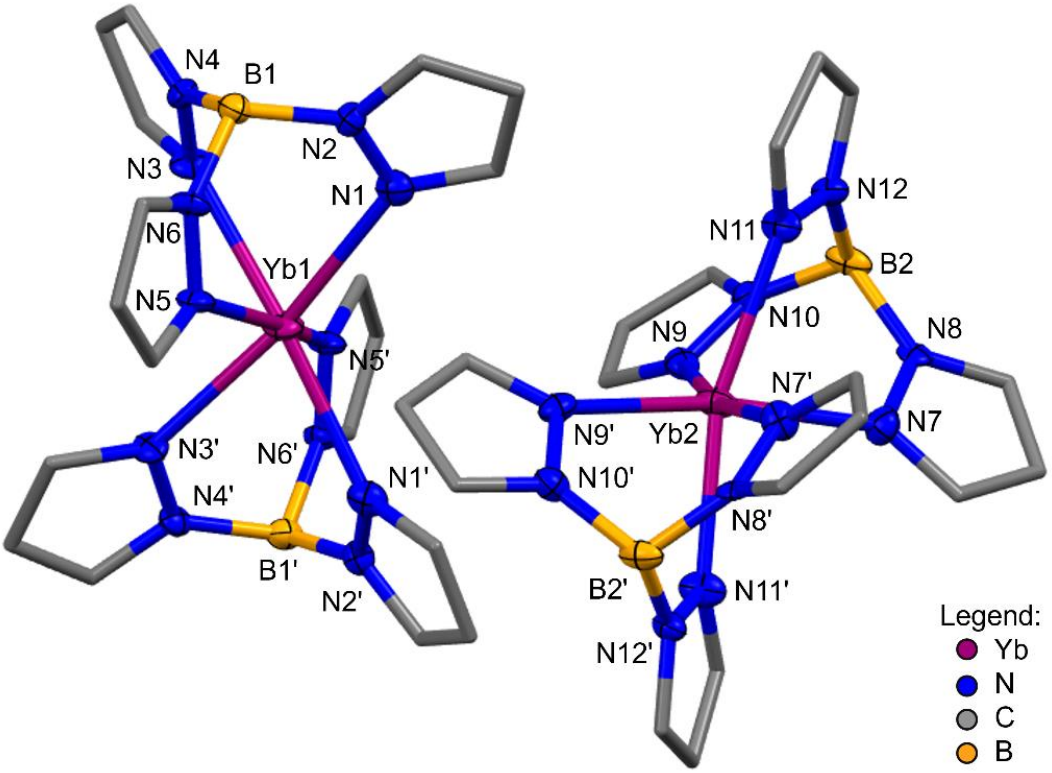

Figure S 66. Molecular structure of **1-Yb**. The asymmetric unit contains 2 crystallographically independent Yb sites which both lie on a 2-fold rotation axis, each with one independent Tp ligand and the coordination is completed with the symmetry equivalent Tp; 'prime' atom labels denote symmetry equivalent (-x, -y, z).

S4.5 [Yb(Tp)$_2$(THF)] 1-Yb(THF)

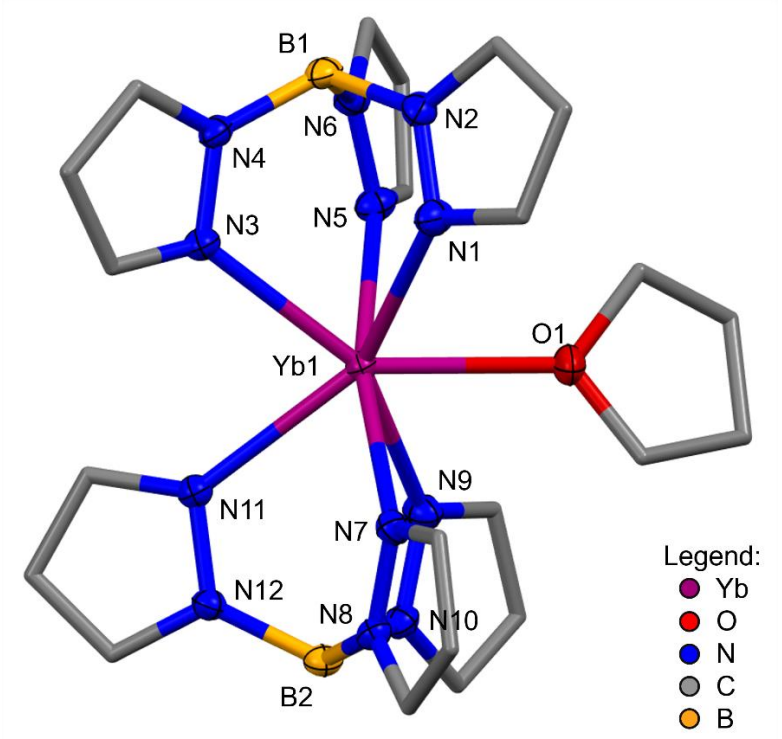

Figure S 67. Molecular structure of **1-Yb(THF)**.

S4.6 [Yb(Tp)$_2$(DME)] 1-Yb(DME)

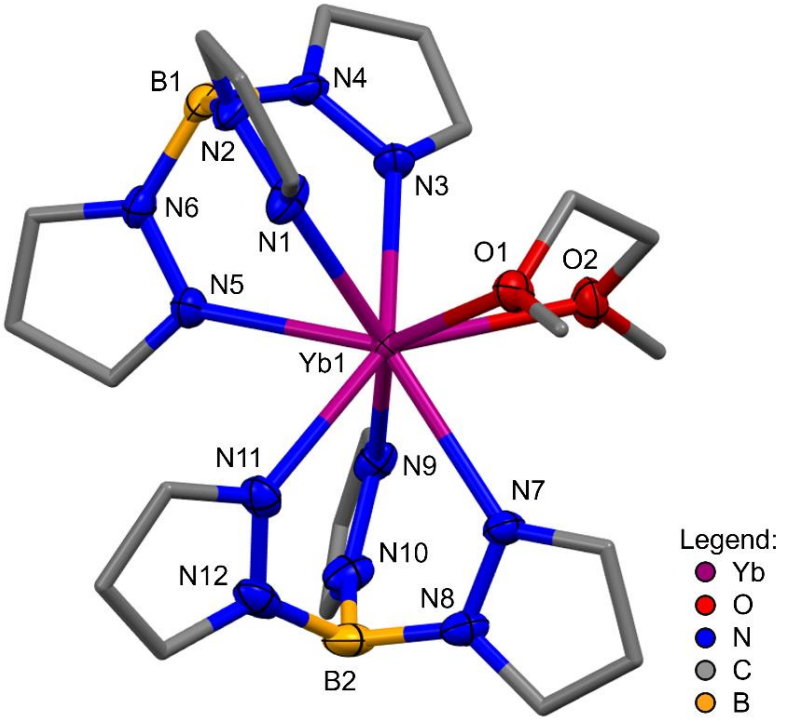

Figure S 68. Molecular structure of **1-Yb(DME)**, showing one of the two independent molecules of **1-Yb(DME)** in the asymmetric unit, which also contains 0.5[{(DME)$_2$K(μ-OTf)}$_2$] which lies across an inversion centre and is omitted for clarity. Disorder is present in the one of the Yb-coordinated DME, one of the K-coordinated DME and one OTf and was modelled over 2 partially occupied sites in each case.

S4.7 [Yb(Tp)$_2$(OPPh$_3$)] 1-Yb(OPPh$_3$)

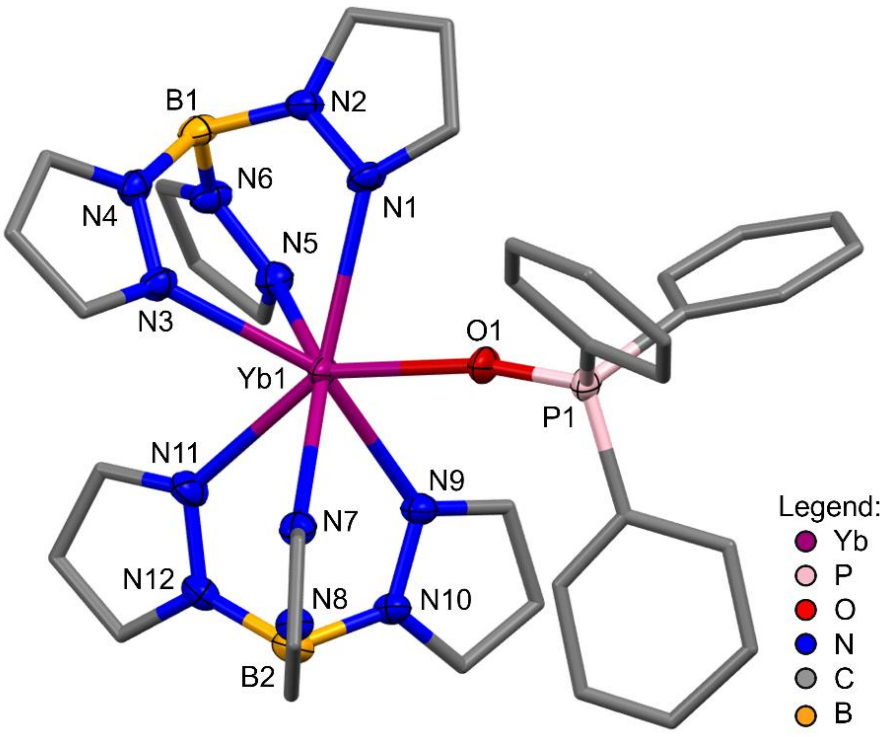

Figure S 69. Molecular structure of **1-Yb(OPPh$_3$)**. Disorder present in one phenyl ring of the Ph$_3$PO was modelled over 2 partially occupied sites (occupancies 0.525:0.475), only one of which is shown.

S4.8 [Y(Tp)$_2$(μ-OTf)$_2$K(18-crown-6)] 2-Y

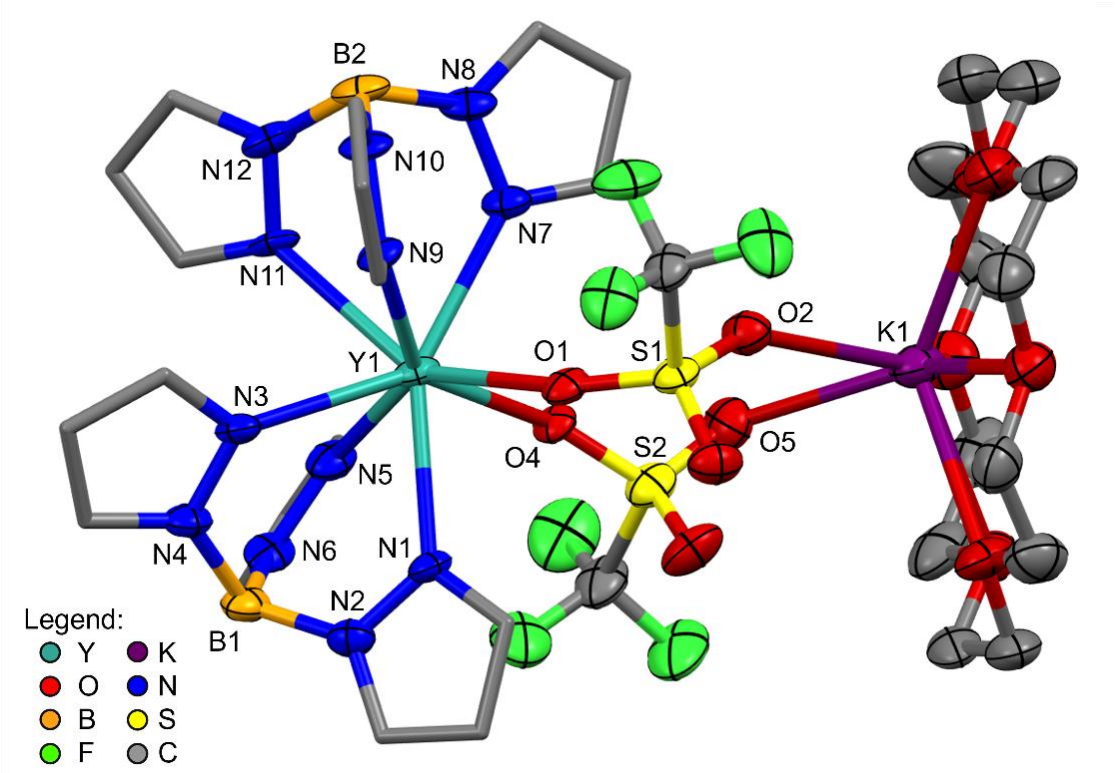

Figure S 70. Molecular structure of **2-Y**, showing one of the two crystallographically independent molecules, the second and lattice solvent are omitted for clarity. The asymmetric unit contains two [Y(Tp)$_2$(μ-OTf)$_2$K(18-crown-6)] molecules and 3 molecules of toluene. 2 of the 3 toluene molecules showed disorder and were modelled over 2 partially occupied sites.

S4.9 [K(2.2.2-cryptand)][Al(NON^{Dipp})] K-Al-SIP

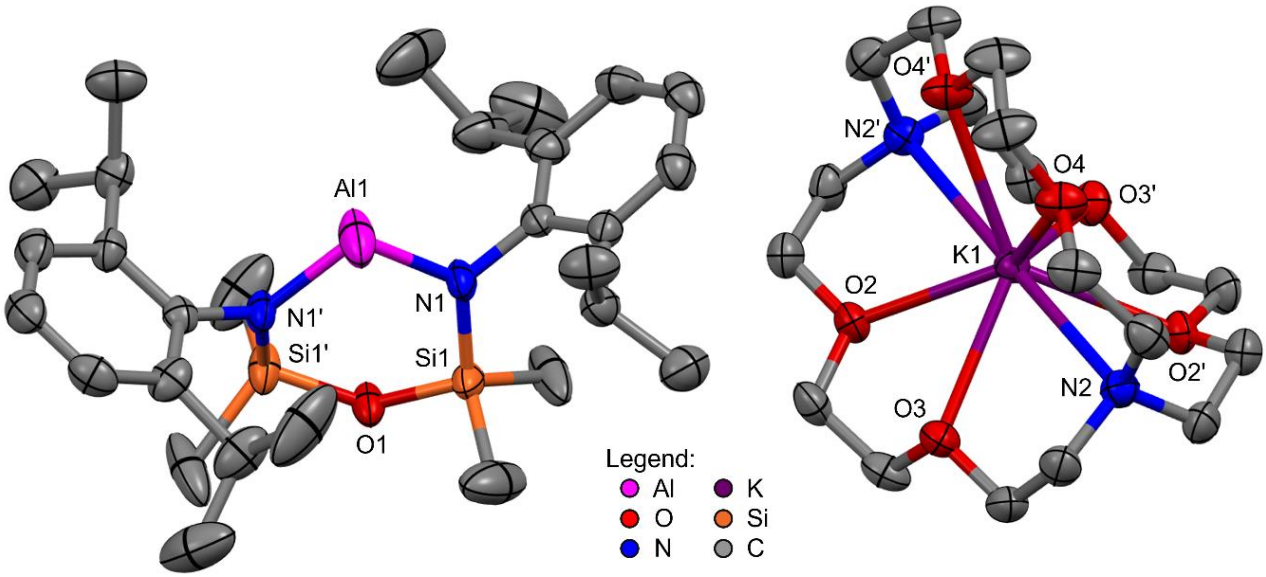

Figure S 71. Molecular structure of [K(2.2.2-cryptand)][Al(NON^{Dipp})] **K-Al-SIP** (NON^{Dipp} = {O(SiMe$_2$N(2,6-^{i}Pr$_2$-C$_6$H$_3$))$_2$}$^{2-}$). The asymmetric unit contains 0.5 of both the K(2.2.2-cryptand) and Al(NON^{Dipp}) with the K lying on a 2-fold rotation axis and application of this symmetry completes the molecules; 'prime' atom labels denote symmetry equivalent (K: 2-x, y, 1.5-z) and (Al: 1-x, y, 1.5-z). The Al(I) ion is disordered across the 2-fold axis and one of the ^{i}Pr groups of [Al(NON^{Dipp})] shows disorder and has been modelled over two 0.5 occupied sites, one of which is omitted for clarity in both cases.

C. References

1. T. Chowdhury, S. J. Horsewill, C. Wilson and J. H. Farnaby, *Aust. J. Chem.*, 2022, **75**, 660-675.
2. R. J. Schwamm, M. D. Anker, M. Lein and M. P. Coles, *Angew. Chem. Int. Ed.*, 2019, **58**, 1489-1493.
3. D. F. Evans, *J. Chem. Soc. (Resumed)*, 1959, 2003-2005.
4. Bruker AXS Inc.: Madison, WI, 2016.
5. G. Sheldrick, *Acta Crystallogr. C*, 2015, **71**, 3-8.
6. O. V. Dolomanov, L. J. Bourhis, R. J. Gildea, J. A. K. Howard and H. Puschmann, *J. Appl. Crystallogr.*, 2009, **42**, 339-341.
7. C. F. Macrae, I. Sovago, S. J. Cottrell, P. T. A. Galek, P. McCabe, E. Pidcock, M. Platings, G. P. Shields, J. S. Stevens, M. Towler and P. A. Wood, *J. Appl. Crystallogr.*, 2020, **53**, 226-235.